Investigation of Seniority Conservation in the $N = 50$ Isotones using Lifetime Measurements

Inaugural-Dissertation

zur
Erlangung des Doktorgrades
der Mathematisch-Naturwissenschaftlichen Fakultät
der Universität zu Köln

vorgelegt von

Mario Ley
aus Haan

angenommen im Jahr 2025

Abstract

In this doctoral thesis, new experimental findings for lifetimes of excited states in the $N = 50$ isotones ^{91}Nb, ^{92}Mo, ^{93}Tc, ^{94}Ru, and ^{95}Rh are presented. The new data are the result of three experimental campaigns conducted at the Institute for Nuclear Physics at the University of Cologne employing the well established γ-γ fast-timing method using a hybrid setup of cerium-doped lanthanum bromide scintillation and high-purity germanium detectors. The nuclei were produced in fusion-evaporation reactions using the Cologne 10 MV FN Tandem accelerator and the emitted γ rays were detected using the HORUS spectrometer of the institute.

The newly acquired data are compared with known experimental values from the literature and with shell-model calculation results. The data are also discussed in the context of potential signatures of partial seniority conservation versus an abrupt breakdown of seniority. The lifetime of the 4_1^+ state in ^{92}Mo was measured with high precision to determine the $B(E2; 4_1^+ \rightarrow 2_1^+)$ transition strength with sufficiently low uncertainty. In particular this lifetime measurement allows to use the $B(E2)$ values from the entire yrast $8_1^+ \rightarrow 6_1^+ \rightarrow 4_1^+ \rightarrow 2_1^+ \rightarrow 0_{\text{gs}}^+$ cascade to extract state-dependent effective charges with high accuracy. These effective charges are then applied within a single-j approximation to predict $B(E2)$ transition strengths for the $(9/2)^3$, $(9/2)^4$, and $(9/2)^5$ systems in the $\pi 1g_{9/2}$ shell, corresponding to the nuclei ^{93}Tc, ^{94}Ru, and ^{95}Rh, respectively. Furthermore, this ansatz enabled the extraction of admixture coefficients for the mixing of states with the same angular momentum but different seniority, by minimizing the deviation between the theoretical predictions based on the single-j approach and the experimental data.

Contents

1 Introduction **3**
1.1 Pairing and Seniority 4
1.2 Seniority in the $j = 9/2$ System 7
1.3 The $\pi 1g_{9/2}$ Orbital in the Neutron deficient $N = 50$ Isotones 9
1.4 Single-j Approximation and State-dependent effective Charges 10
1.5 Lifetime Measurements using the Fast-Timing Method 12
1.6 Experimental Details 15

2 Lifetime measurements in ^{92}Mo: Investigation of seniority conservation in the $N = 50$ isotones **17**

3 Lifetime measurement in ^{94}Ru and ^{93}Tc to investigate seniority conservation in the $N = 50$ isotones **31**

4 Lifetime measurement in ^{95}Rh and ^{95}Ru: Investigation of seniority conservation in the $N = 50$ isotones **41**

5 Summary and Conclusion **53**

6 Outlook **59**

Bibliography **63**

List of Figures **73**

List of publications **75**

Contribution **79**

1 | Introduction

Nuclear structure physics deals with the arrangement and dynamics of protons and neutrons within the atomic nucleus and the resulting properties. Describing nuclear structure is challenging because nuclei are complex, many-body quantum systems that are governed by the strong nuclear force, which is still not fully understood from first principles [1]. Since solving the Schrödinger equation for such systems is computationally not feasible for most nuclei, approximate models must be used, each with its limitations. Collective models like the interacting boson model are most useful to describe nuclei far away from shell closures that often have many valence nucleons [2]. The nuclear shell model on the other side, is especially useful in regions where nuclear structure is dominated by the motion of individual nucleons in well-defined orbitals. This is typically the case for nuclei near magic numbers with only few valence nucleons outside a closed shell. The region of $N = 50$ isotones below ^{100}Sn is of great interest in nuclear physics, as it provides a unique testing ground for nuclear shell model predictions near the doubly magic nucleus ^{100}Sn ($Z = 50$, $N = 50$). One key element to study the nuclear structure is the measurement of lifetimes of excited nuclear states. The lifetime of an excited state reflects how long a nucleus on average remains in that state before decaying, typically by γ-ray emission, to a lower energy level. These measurements provide direct insight into the transition probabilities between nuclear states, which are sensitive to the underlying configuration and interactions between protons and neutrons. Precise measurements to gain data for the lifetimes of excited states help to determine key nuclear structure properties such as the reduced transition strengths $B(\sigma\lambda)$, which give insights to nuclear deformation and collectivity. Comparing these measurables with theoretical predictions, allows validation or refinement of nuclear models and thus further improves our understanding of the nuclear structure. Recently, the region of the $N = 50$ isotones between ^{90}Zr ($Z = 40$) and the doubly magic nucleus ^{100}Sn ($Z = 50$) became subject of new experimental studies regarding the conservation of seniority for the low-lying excited spectrum, generated predominantly from valence configurations in the $\pi 1g_{9/2}$ orbital [3–10]. Advancements in lifetime measurement techniques [11–13], along with the development of radioactive ion beams (RIBs), are significantly enhancing the accessibility of lifetime measurements in this region. While experiments to measure lifetimes of isotones between ^{96}Pd and ^{100}Sn usually require RIB facillities [4–6, 9, 10, 14], the nuclei from ^{90}Zr to ^{95}Rh are also accessible through stable beam experiments using fusion-evaporation reactions. In the scope of this work, the results of three experimental campaigns conducted to measure the lifetimes of low-lying states in the $N = 50$ isotones ^{92}Mo, ^{93}Tc, ^{94}Ru, and ^{95}Rh are presented. Due to the isomers present in these nuclei, lifetime measurements using Doppler-shift based methods become very difficult, especially when populating the nuclei within fusion-evaporation reactions. Since the fast-timing technique is mostly independent of the presence of isomers, it was the applied method in all three experimental campaigns.

1.1 Pairing and Seniority

The concept of seniority is a remarkably simple yet powerful tool in the study of the complex many-body system of the atomic nucleus. The idea was first introduced by Giulio Racah in the context of atomic physics for the coupling of electrons in an l shell [15]. Although initially developed for atomic systems, it was found to be more useful in nuclear physics [16, 17], where jj coupling between two nucleons plays a more significant role than LS coupling. The concept is especially applicable to describe semi-magic nuclei, where only one type of valence nucleons are present within a single-j orbital, while the other type fills a major shell, which can be regarded as inert core that does less likely contribute to excitations of the low-lying spectrum. For such a system of n identical valence particles, with the same angular momentum j, that do interact through a pairing force, the quantum number seniority v is defined as the number of particles that do not pairwise couple to angular momentum $J = 0$ [15]. The low-lying spectrum can then be constructed by coupling of the remaining unpaired nucleons as schematically shown in Fig. 1(a). Because the pairs that couple to $J = 0$ are not contributing to the excitation matrix

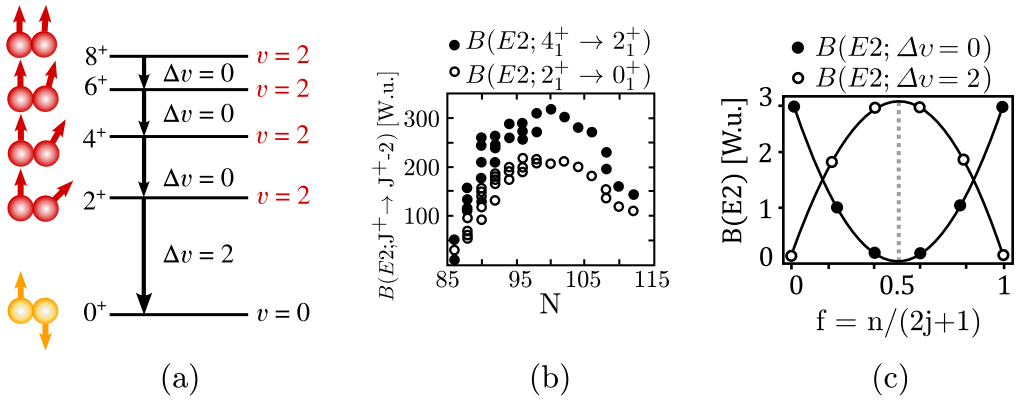

Figure 1: (a) A schematic level scheme for the $(j = 9/2)^2$ configuration in a single-j shell is shown for the two valence nucleon system. The energy levels are labeled with the seniority quantum number v. The change in seniority Δv is indicated for each transition. The figure is based on Fig. 1 from Ref. [18]. (b) Selection of experimental yrast $B(E2)$ strengths for the $62 \leq Z \leq 74$ mid-shell region. According to Ref. [19] few nuclei with known low-lying intruder states are omitted for better clarity. (c) Schematic illustration of the characteristic pattern in $B(E2)$ strengths for $\Delta v = 0$ and $\Delta v = 2$ as a function of fractional orbital filling $f = n/(2j + 1)$. Figure (b) and (c) are based on Fig. 3 from Ref. [19].

elements between configurations in j^n, the system can be reduced to those in j^v, which can lead to a significant simplification of the many body problem, since the low-lying states of nuclei near closed shells typically have low seniority [19]. The classification of nuclear states according to their seniority leads to distinct spectroscopic features. One example is the energy spectrum of the low-lying states. In nuclei where seniority is a proper quantum number the spectrum of states with the same seniority (v multiplet) is independent of the particle number [20], leading to a constancy of their excitation energy along the shell. This is particularly evident in the

excitation energy of the 2_1^+ state in even-even nuclei. By contrast, the increased collectivity in open-shell nuclei typically results in a progressive decrease of the 2_1^+ excitation energy [1]. Another important observable is the characteristic trend in electric quadrupole transition probabilities $B(E2)$ as the valence shell is progressively filled. In general, transition probabilities, like the $B(E2)$ strength, provide valuable insights into the nature of nuclear collectivity and how it evolves with the number of neutrons and/or protons. In almost all even-even nuclei, the $B(E2)$ values connecting the lowest yrast states exhibit a simple and systematic pattern that generally increases with the number of valence nucleons and with the spin, leading to a parabolic trend across a major shell [19]. Figure 1(b) shows the trend of experimental values for the quadrupole-transition propabilites of different nuclei with $62 \leq Z \leq 74$ along a major shell. They maximize towards the mid-shell and the $B(E2; 4_1^+ \rightarrow 2_1^+)$ are about $\sim$1.5 times the $B(E2; 2_1^+ \rightarrow 0_1^+)$ [21]. This is because the number of possible configurations to create a state usually increases with the number of valence nucleons, leading to enhanced collectivity in most cases, as reflected in the high $B(E2)$ strengths [1]. A strongly deviating behavior can be seen in the previously mentioned regions near closed shells where seniority is a good quantum number. The seniority changing transitions $\Delta v \neq 0$ also show the parabolic trend peaking when the single-j orbit is half filled. The seniority conserving transitions $\Delta v = 0$ within a seniority multiplet show an inverted parabola, where the $B(E2)$ strengths are strongly suppressed towards the mid-shell, leading to the formation of seniority isomers [22, 23]. The seniority isomers are a special case of spin isomers, where the transition is hindered because of seniority selection rules, although the difference ΔJ between the angular momenta of the initial and final states is modest [24]. The seniority selection rules for transition matrix elements follow from the unitary symplectic algebra USp$(2j+1)$ [16], that is associated with the conservation of the seniority quantum number in a single-j orbital. The two following selection rules are derived in Refs. [22, 23]. For E2 transitions between states with the same seniority $\Delta v = 0$ one finds

$$\langle j^n v J' || \hat{T}(E2) || j^n v J \rangle = \left(\frac{2j+1-2n}{2j+1-2v} \right) \langle j^v v J' || \hat{T}(E2) || j^v v J \rangle \ , \tag{1.1}$$

and for E2 transitions that change seniority $\Delta v = 2$

$$\langle j^n v - 2\, J' || \hat{T}(E2) || j^n v J \rangle = \sqrt{\frac{(n-v+2)(2j+3-n-v)}{2(2j+3-2v)}} \langle j^v v - 2\, J' || \hat{T}(E2) || j^v v J \rangle \ . \tag{1.2}$$

Plotting the squared prefactor of the matrix element from Eq. 1.1 for given j and v against the number of valence nucleons n yields a convex parabola like the one shown in Fig.1 (c). Doing the same with the prefactor from Eq. 1.2 yields a concave parabola similar to Fig.1 (c). The two selection rules explain the different pattern in $B(E2)$ strengths for $\Delta v = 0$ and $\Delta v = 2$ transitions along the filling $f = n/(2j+1)$ of the shell and the formation of seniority isomers towards mid-shell. As shown in Fig. 2, the pronounced parabolic pattern associated with good seniority is observed in a couple of regions on the nuclear chart. Although such pattern can be observed for a variety of j orbitals, seniority is only strictly conserved for nucleons occupying

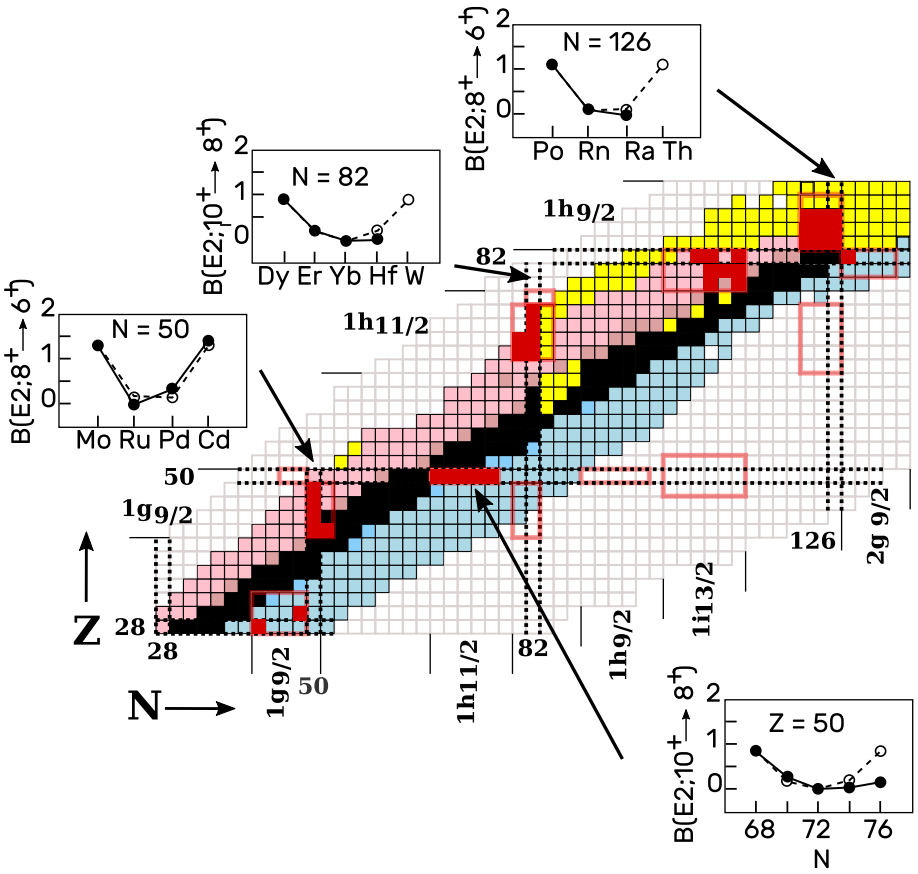

Figure 2: Partial nuclear chart for even-even nuclei, showing regions proposed to exhibit good seniority in red (known data), framed light red (assuming normal magic numbers). Calculations assuming pure seniority (open circles), normalized to the leftmost point in each case. The $B(E2)$ data shown in the insets are given in Weisskopf units. Figure adopted from Ref. [19], modified and colorized. It is worth noting that Ref. [19] dates back to 2004, and more recent experimental data have become available since then. In the inset for $N = 50$ the $B(E2)$ in ^{98}Cd is updated with the current literature value from Ref. [25].

orbitals with $j \leq 7/2$ [26, 27]. For higher-j orbitals, such as $j = 9/2$, seniority is generally an approximate quantum number due to the increased complexity of the residual interactions [19, 24]. Therefore, seniority breaking effects may be observed being admixtures of eigenstates with different seniorities [28].

1.2 Seniority in the $j = 9/2$ System

In general, deviations from good seniority is usually the result of mixing due to a seniority non-conserving interaction like Landau-Zener mixing [29, 30] between close-lying levels or proton-neutron interactions leading to core excitation across the shell gap [3, 19, 31]. However, even when $j \geq 9/2$, it turned out that the strong interaction between nucleons of the same kind conserves seniority to a certain extend, allowing the usage of seniority also for some cases where $j > 7/2$ [24]. This includes also the possibility of partial seniority conservation [20, 28, 32–34] when some eigenstates are mixed in seniority while others remain pure and solvable, which is an example for the concept of partial dynamical symmetry [35, 36]. Since the first shell where seniority violating effects are expected to occur is the $j = 9/2$ system, it has recently received particular interest for experimental studies, especially with regard to the effect of partial seniority conservation [4, 5, 7–10, 37–40]. In this context, two cases are particularly interesting for this work. The mid-shell nucleus, where the $j = 9/2$ orbital is half filled with five valence nucleons and the case near mid-shell with four or six valence nucleons (four holes) in the $j = 9/2$ orbital. Figure 3 displays the energy spectra for both cases, calculated using a surface delta interaction that conserves seniority [24]. For the mid-shell case it can be shown that states theoretically only mix if $\Delta v = 0, \pm 4$, as long as the interaction between the nucleons is of two-body character [20, 24, 41]. In Ref. [42] this mixing rule is also explained as a consequence of the geometric Berry phase [43] associated with the particle-hole conjugation. The mixing rule has important implications for the system of five identical valence nucleons in a $j = 9/2$ orbital $(9/2)^5$. As can be seen in Fig. 3(a), most states with an angular momentum J differ only by $\Delta v = \pm 2$ in seniority and therefore would not mix. The only exception are the $J = 9/2$ ground state with seniority $v = 1$ and an excited state $J = 9/2$ with $v = 5$ that possibly can mix, but because the states have a rather large energy difference one would expect that the mixing remains rather small [24]. Therefore, it is reasonable to expect that seniority is also preserved well at mid-shell in the $j = 9/2$ system. In the case of four or six (four holes) identical valence nucleons in the $j = 9/2$ orbital, the previously mentioned $\Delta v = 0, \pm 4$ rule for the mixing of two states does not apply anymore, since it is only valid for the $(9/2)^5$ mid-shell system. Therefore, mixing of states that differ in seniority by $\Delta v = \pm 2$ becomes possible [24].

However, those states that are unique in angular momentum J have a well-defined seniority quantum number, whereas other states might mix in seniority. One can show that there are two cases, the $J = 4$ and $J = 6$ states with seniority $v = 4$, that still remain pure for any two body interaction [20, 34]. Further examples of this type of partial seniority conservation for fermions confined to a single-j orbital are not known [33].

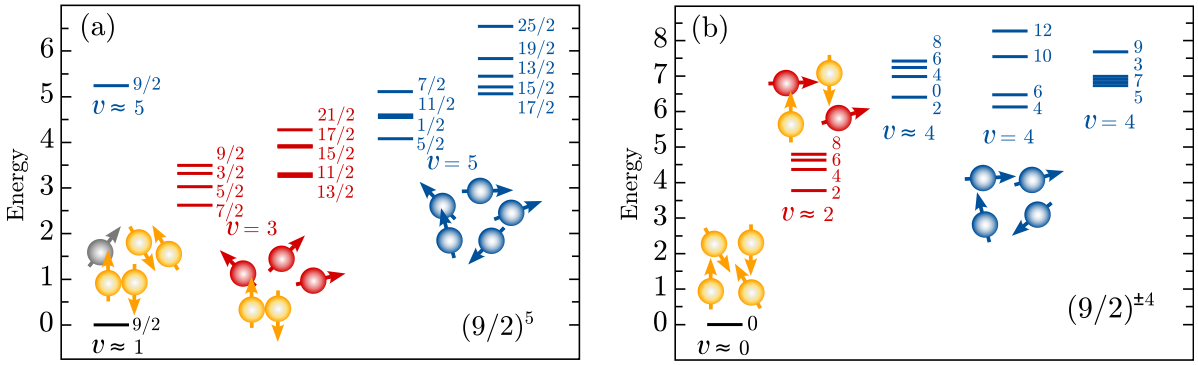

Figure 3: Spectra of identical nucleons in a $j = 9/2$ orbital. The spectrum is obtained with a surface delta interaction that conserves seniority. States are labelled by their angular momentum J and further characterized by seniority v, where black denotes the lowest possible v in the respective system, blue the highest possible v and red in between. Nucleons that couple pairwise to $J = 0$ are depicted in yellow. Energies are in units of the isovector interaction strength. Solvable states with a well-defined seniority quantum number r are indicated with $v = r$ in contrast to those labelled with $v \approx r$. (a) The optained energy spectrum for the $(j = 9/2)^5$ system. (b) The optained energy spectrum for the $(j = 9/2)^{\pm 4}$ system. Both figures are adopted from Ref. [24] and modified.

There are a couple of regions on the nuclear chart which are suitable for studying $j = 9/2$ systems. One notable example is the region around the doubly magic ^{208}Pb, where two $j = 9/2$ orbitals are present, the $\pi 1h_{9/2}$, proton orbital above the doubly magic ^{208}Pb and the $2\nu g_{9/2}$, neutron orbital in lead isotopes east of ^{208}Pb. The $N = 126$ even-even nuclei in the $\pi 1h_{9/2}$ region exhibit characteristic 8^+_1 seniority isomers [44–47], which appear to persist even in certain non semi-magic nuclei with neutron holes below the $N = 126$ shell closure. This effect is likely driven by the differences in the principal quantum number ΔN and orbital angular momentum Δl between the respective proton and neutron orbitals, leading to a reduced radial overlap of their wave functions and, consequently, a weak proton-neutron interaction. [48, 49]. However, new measurements in the region showed signs of collectivity for the low-lying spectrum [50, 51].

Recently, lifetimes of the lower-lying excited states in the $N = 126$ isotones have been measured [38, 39, 52, 53]. The data for lifetimes of lowest-lying yrast states in ^{212}Rn, ^{213}Fr, ^{214}Ra, and ^{215}Ac is currently still incomplete [54]. The 8^+_1 isomers are also systematically observed for the $\nu 2g_{9/2}$, neutron orbital in $^{210-216}$Pb isotopes east of ^{208}Pb [55]. Furthermore, an isomeric nature of the $21/2^+_1$, state in the $(9/2)^5$ mid-shell nucleus ^{213}Pb was recently confirmed [42]. This isomere was expected due to the hindrance originating from the $\Delta v = 2$ E2 transition selection rule Eq. 1.2 and the $\Delta v = \pm 4$ mixing rule at mid-shell, which is interpreted as a manifestation of the Berry phase connecting particle-hole conjugation and seniority conservation [42].

Another interesting case are the Ni isotopes between ^{68}Ni and the doubly magic ^{78}Ni, where neutrons (holes) occupy the $\nu 1g_{9/2}$ shell. An isomeric state with 8^+ has been observed in ^{70}Ni and ^{76}Ni [56, 57]. In the four-valence particle system ^{72}Ni, a level has been tentatively assigned $J = 8$, but its half-life is below 20 ns [58, 59], which is rather short compared to the 8^+ isomers in the

other isotopes. No 8^+ isomeric state has been identified in the four-hole system ^{74}Ni so far [54]. This disappearance of the 8^+ seniority isomerism in the $(9/2)^4$ and $(9/2)^6$ can be explained due to a lowering of the 6^+ level with $\upsilon = 4$ below the 8^+ level with $\upsilon = 2$, allowing for a large $B(E2)$ strength which destroys the isomerism [40, 60, 61]. A very similar case, but with protons occupying the same orbitals, is the $\pi 1g_{9/2}$ orbital in the neutron deficient $N = 50$ isotones. It can therefore be viewed as the valence mirror symmetric [62, 63] partner of the previous mentioned $\nu 1g_{9/2}$ region in the Ni isotopes. Since the $\pi 1g_{9/2}$ region is the main subject of this thesis it is discussed in more detail in the next section.

1.3 The $\pi 1g_{9/2}$ Orbital in the Neutron deficient $N = 50$ Isotones

The $\pi 1g_{9/2}$ orbital is situated below the doubly-magic nucleus ^{100}Sn ($N = Z = 50$) and the $Z = 40$ sub-shell closure. In Fig. 4 the shell structure for protons is shown for the region. Although $Z = 40$ is not a magic number in the traditional nuclear shell model, the $Z = 40$ sub-shell closure in ^{90}Zr ($N = 50$, $Z = 40$) separates the $\pi(p_{1/2}, f_{5/2})$ orbitals from the $\pi 1g_{9/2}$ orbital to a certain degree [1]. When looking at the signs of seniority conservation, the behavior of the 8^+ isomers is different compared to the situation in the above mentioned valence mirror symmetric case in the Ni isotopes. In contrast, the 8^+ isomers in the $(9/2)^4$ and $(9/2)^6$ nuclei, namely ^{94}Ru and ^{96}Pd are preserved. The systematic trend of $B(E2; 8_1^+ \rightarrow 6_1^+)$ strengths along the $\pi 1g_{9/2}$ shell follows the expected seniority pattern [64–67], although the symmetry around midshell is distorted, which is explained due to a $p_{1/2}$ pair scattered to $1g_{9/2}$ giving rise to premature filling of the orbit, as pointed out in Ref [31]. For the lower-lying excited states, signs of significant deviations from the regular seniority pattern were reported in [3], namely the increased $B(E2; 6_1^+ \rightarrow 4_1^+)$ in ^{96}Pd and an unexpected high lower limit for the $B(E2; 4_1^+ \rightarrow 2_1^+)$ in ^{94}Ru. To reproduce the discrepancies within a large-scale shell model calculation, particle-hole cross-shell excitations were added in Ref. [3] and the model space was expanded below $N = 50$. For the mid-shell nucleus ^{95}Rh a relatively short lifetime for the $21/2_1^+$ state was measured [68–70] and therefore an increased $B(E2)$ results. Since one would expect a strong inhibited $B(E2)$ at mid-shell, this can be seen as a hint for deviations from the pure single-j seniority. In 2022, new experimental results on the lifetimes of low-lying states in ^{90}Zr, ^{92}Mo, and ^{94}Ru were published [4, 5]. In particular, the lifetime of the 4_1^+ state in ^{94}Ru was measured using two different techniques. At the Facility for Antiproton and Ion Research (FAIR), the fast-timing technique yielded a lifetime of 32(11) ps [5], while at the Grand Accélérateur d'Ions Lourds (GANIL), the Recoil Distance Doppler-Shift (RDDS) method was applied, resulting in a significantly longer lifetime of 87(8) ps [4]. The notable discrepancy between these two measurements has raised questions about whether seniority is partially conserved or broken in this nuclear system. In 2024, also new data for the ^{95}Rh mid-shell nucleus was published [9]. The experiment was conducted at FAIR and employed the fast-timing technique, yielding the previously unknown lifetime of the $13/2_1^+$ state, as well as an upper limit for the lifetime of the $17/2_1^+$ state. Interestingly, the $13/2_1^+$ lifetime was much longer than expected from theoretical calculations. The upper limit for the $17/2_1^+$

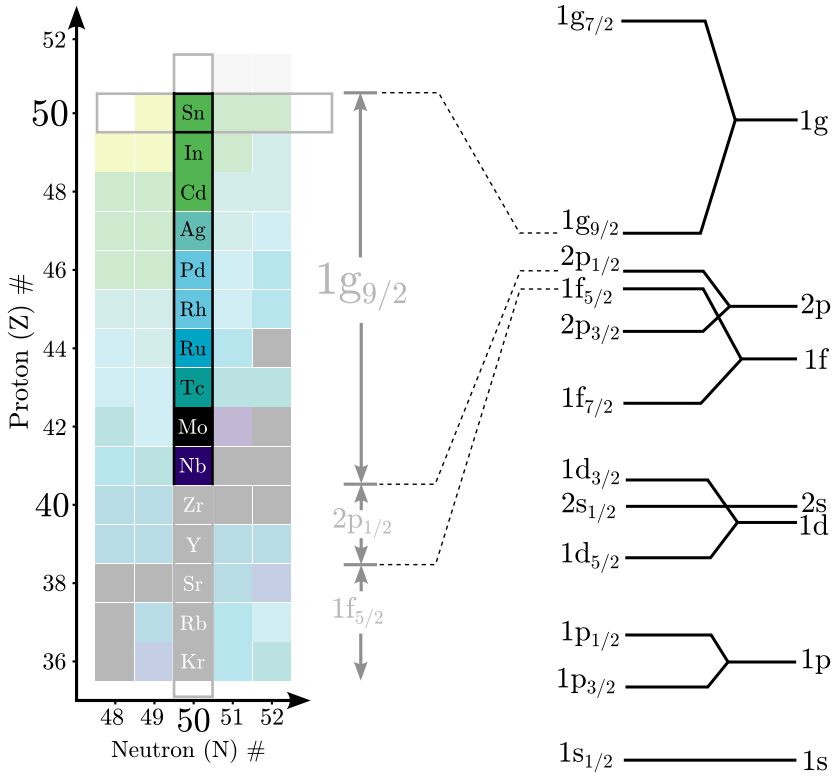

Figure 4: The region of the $N = 50$ isotones between ^{90}Zr and the doubly-magic ^{100}Sn. The shell structure is shown on the right, showing the neighboring orbitals. The major shell closure at $Z = 50$, which separates the $\pi 1g_{9/2}$ from the $\pi 1g_{7/2}$ orbital, and the partial shell closure at $Z = 40$, which separates the $\pi 1g_{9/2}$ from the $\pi 2p_{1/2}$ orbital to a certain extent.

lifetime on the other hand was much higher to be consistent with seniority conservation, leading to the picture of a sudden breakdown of seniority in the mid-shell nucleus ^{95}Rh. In Ref. [9] it is also pointed out, that reproducing the data would require theory to make major revision of the nucleon-nucleon interactions in models or the inclusion of three-body forces. Since the picture of a partial conservation of seniority versus a sudden breaking is not conclusive, one goal of the experimental campaigns, presented in this thesis, is to verify the findings from Refs. [4, 5, 9] and clarify the issue of discrepancies in the experimental data. A further motivation is subject of the following chapter.

1.4 Single-j Approximation and State-dependent effective Charges

One of the key advantages of a shell-model description restricted to a single-j orbital is the applicability of analytical predictions, which can be directly compared with experimentally observed nuclear properties. For example, as described in Ref. [23] there is a relation between the energy spectra of nuclei with two valence nucleons in a j orbital (j^2 system) and the respective system of three valence nucleons j^3. Similar relations between the electric quadrupole strength

$B(E2)$ in the j^2 and j^n systems can be derived in general. Such relations become analytical if seniority is conserved and therefore deviations from the analytical relations may provide important information on the question of seniority conservation [7, 38]. Since the complete derivation is complex, only the relevant results are shown here. A more detailed explanation can be found in Ref. [7], which is Chapter 2 of this work and in the appendix of Ref. [38]. In the single-j approach the $B(E2)$ transition probabilities in the $8_1^+ \to 6_1^+ \to 4_1^+ \to 2_1^+ \to 0_{\text{gs}}^+$ sequence of the j^2 two-nucleon system obey the purely geometric rule

$$B(E2; J \to J-2) = \frac{15(2j+1-J)(2j+2-J)(2j+J)(2j+1+J)(J-1)J}{128\pi j^2(j+1)^2(2J-1)(2J+1)} \left(N+\frac{3}{2}\right)^2 b^4 e_{\text{eff}}^2, \tag{1.3}$$

with N being the major oscillator quantum number associated with the j orbital, b the oscillator length parameter that can be derived from the mass number A [71, 72], and e_{eff} the effective charge of the nucleon. Purely geometric means in that context, that the relation Eq. 1.3 depends only on the angular momenta involved and not on the interaction between the nucleons. The effective charge e_{eff} has to be obtained from experimental data like the quadrupole moment of the ground state in the one valence nucleon system. If the $B(E2)$ strength in the j^2 two-nucleon system cannot be reproduced using a constant effective charge, an alternative ansatz is the use of state-dependent effective charges $\tilde{e}_{\text{eff}}$ instead. As pointed out in [38], using a relation between $\tilde{e}_{\text{eff}}(J,J)$ and $\tilde{e}_{\text{eff}}(J,J-2)$ they can be derived from the experimental $B(E2)$ data of the whole $8_1^+ \to 6_1^+ \to 4_1^+ \to 2_1^+ \to 0_{\text{gs}}^+$ sequence and subsequently propagated from the j^2 system to the j^n systems. The matrix elements of the one-body operator with state-dependent effective charges can be expressed as

$$\langle j^n \upsilon_{\text{f}} J_{\text{f}} || \, \hat{T}_1'(E2) \, || j^n \upsilon_{\text{i}} J_{\text{i}} \rangle = \sum_{J=2,4,\ldots}^{2j-1} f_J(j^n \upsilon_{\text{i}} J_{\text{i}} \upsilon_{\text{i}} J_{\text{f}}) \tilde{e}_{\text{eff}}(J, J-2) \,, \tag{1.4}$$

with $f_J(j^n \upsilon_{\text{i}} J_{\text{i}} \upsilon_{\text{i}} J_{\text{f}})$ being numerical coefficients that can be derived for any n and appropriate j [73]. This ansatz was already applied for the case of ^{210}Po and ^{211}At with protons in the $\pi 1h_{9/2}$ orbital above the doubly magic ^{208}Pb [38, 39], and also for the case of ^{134}Te and ^{135}I with protons in the $\pi 1g_{7/2}$ orbital above the doubly magic ^{132}Sn [74]. Finally, the analytic formula for the transition matix elements Eq. 1.4 allows to predict also $B(E2)$ strengths for transitions between states constructed as a mixture of two states with the same angular momentum J but different seniorities a and b. By assuming ad hoc mixing

$$|J^\pi\rangle = \alpha \, |J^\pi_{\upsilon=a}\rangle + \beta \, |J^\pi_{\upsilon=b}\rangle \,, \tag{1.5}$$

one can derive the admixture parameters (α, β) by minimizing the χ^2 function with respect to the experimentally observed $B(E2)$ strengths. This procedure can provide insights into the constructive or destructive interference between the two components.

1.5 Lifetime Measurements using the Fast-Timing Method

The fast-timing method is a well-established technique used to measure mean lifetimes of excited nuclear states. Using fast cerium-doped lanthanum bromide (LaBr) scintillators the method is sensitive particularly in the picosecond to nanosecond range [12, 75]. The technique relies on the measurement of time differences between events that indicate the population and depopulation of a respective nuclear state. There are different types of observable events that can serve as such indicators. Most commonly the detection of feeding and decaying γ rays of the state, but also β-particles, conversion electrons, X-rays, etc. can be used. In this work it is done by detecting time differences between coincident γ-ray emissions from a nuclear de-excitation cascade. In Fig. 5(a) a minimal example for a modern fast-timing setup is shown. It consists of two LaBr detectors and a fast 500 MHz digitizer to record energy and time information from the detector signals. The time stamp information is determined with picosecond precision using the onboard constant fraction discriminator (CFD) algorithm [13, 76]. Due to the limited time resolution of a given setup, the spectrum of time differences is always a convolution of the exponential decay term with the so called prompt response function (PRF), which is the time distribution one would obtain if the lifetime was insignificantly small. The PRF is a Gaussian-like distribution and its shape is dependent on the energies of the detected feeding and decaying γ rays. For an idealized case of no background contributions the formula for the resulting time distribution $D(t)$ is given by

$$D(t) = \frac{\mathcal{N}}{\tau} \int_{\infty}^{t} P(t' - t_0) \times e^{-\frac{1}{\tau}(t-t')} dt' \quad , \tag{1.6}$$

where τ is the mean lifetime of the state, $P(t - t_0)$ is the above mentioned PRF, and $\mathcal{N}$ a normalization factor. Depending on the time resolution of the setup and the lifetime of the state of interest, two main techniques are used to obtain the lifetime from the time-difference spectrum. If the lifetime is significantly larger than the time resolution of the setup, the lifetime can be obtained by fitting the exponential tail of the distribution. This is shown schematically in Fig. 5(c). If the lifetime is in the order of the time resolution of the setup or below, the exponential term causes the distribution $D(t)$ only to deform asymmetrically and to shift relative to the position of the pure PRF. In this case the centroid-shift method is used [77]. The centroid of a given time distribution is mathematically defined as its first moment

$$C(D) = \frac{\int t D(t) dt}{\int D(t) dt} \quad , \tag{1.7}$$

and can be interpreted as its center of gravity. Because the PRF is dependent on the energies of the feeding (E_{feeder}) and decaying (E_{decay}) transitions, it has a non-negligible influence on the obtained centroid. The energy dependence of the PRF is called the γ-γ time walk (TW), and to correct for its influence, it must be calibrated for each experimental detector setup using well-known calibration standards. The lifetime can be deduced from the following equation

$$C = \tau + TW(E_{\text{feeder}}, E_{\text{decay}}) \, . \tag{1.8}$$

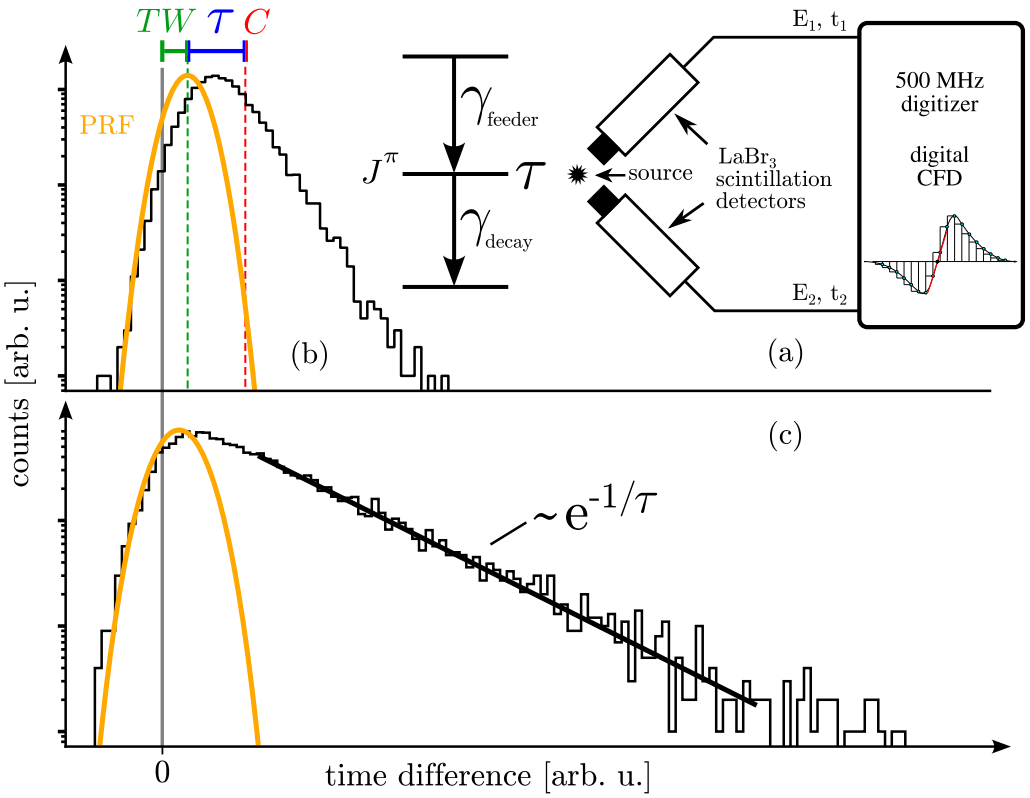

Figure 5: Schematic drawings to explain the fast-timing method. (a) The minimal example for a digital fast-timing setup using two LaBr detectors and fast digitizers with digital CFDs to determine timestamps for each individual detector signal. (b) The concept of the centroid-shift method for the measurement of lifetimes smaller or in the range of the time resolution of the setup. The centroid C (red) of the time distribution can be decomposed into the two components time walk (green) and lifetime (blue), allowing the measurement of lifetimes when the time walk is known. The prompt response function is shown in yellow. (c) The determination of lifetimes by fitting the exponential tail of the time distribution for lifetimes that are significantly longer than the time resolution of the setup.

In Fig. 5(b) the different components involved in the centroid-shift method are schematically shown. For a setup of more than two LaBr detectors the method can be extended analog to the generalized centroid-shift method (GCD) with a superimposed time walk for the whole setup [13, 78, 79]. The time-walk calibration is usually conducted using a ^{152}Eu source, because it covers an energy range from 40-1408 keV and the lifetimes of excited states in the daughter nuclei ^{152}Sm and ^{152}Gd are known with high accuracy [80, 81]. Additional sources like ^{133}Ba or ^{226}Ra can be added to cover a wider energy range and increase the coverage of data points [82, 83]. Figure 6 shows an example for the fit to calibrate the γ-γ time walk using combined data from ^{152}Eu, ^{133}Ba, ^{226}Ra sources as well as in beam data from ^{92}Mo populated in the ^{93}Nb(p,2n)^{92}Mo reaction. A time walk of less than 20 ps for the energy range between 244 and 1510 keV can be achieved by selecting suitable parameters for the digital CFD, which is described more detailed in Ref. [13].

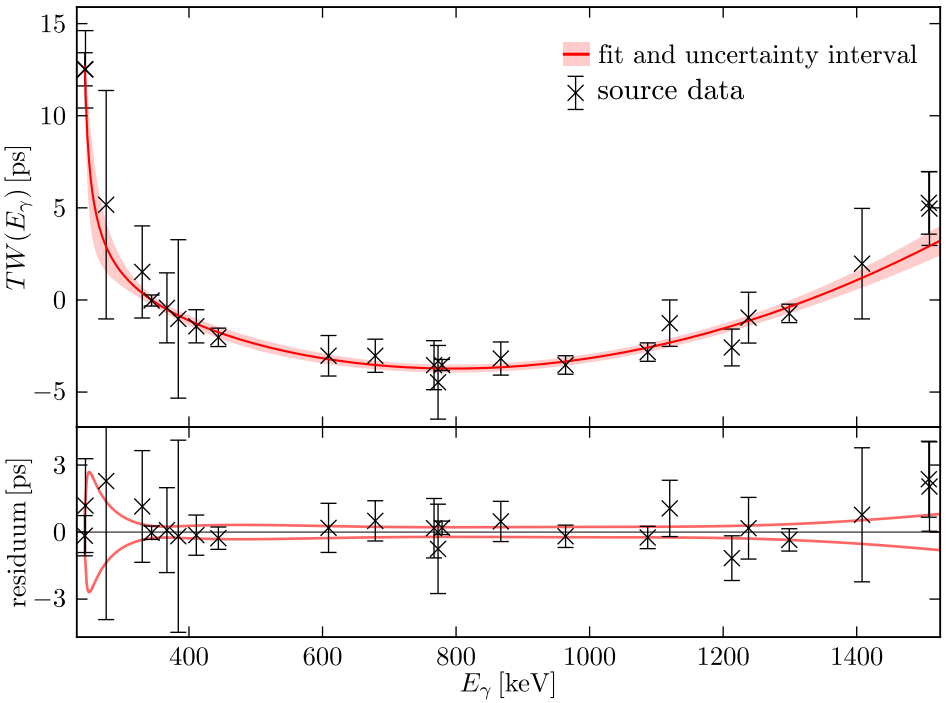

Figure 6: Calibrated mean time-walk characteristic of the detector setup of the HORUS spectrometer in the fast-timing configuration. The data points shown are from ^{152}Eu, ^{133}Ba, ^{226}Ra sources and from ^{92}Mo populated in-beam using the ^{93}Nb(p,2n)^{92}Mo reaction. The lower panel shows the residual of the fit and the 1σ uncertainty interval. The data was recorded during the experiments from April 2023, which is described in more detail in Ref. [8].

Table 1.1: Estimated reaction cross sections σ for the fusion-evaporation reactions at given beam energies used during the experiments. The cross sections were calculated using the program *cascade* [84].

reaction	energy [MeV]	estimated σ [mb]	beam time [d]
^{90}Zr(α, $2n$)^{92}Mo	27	1050	4
^{93}Nb(p, $2n$)^{92}Mo	18	800	1
^{90}Zr(^{6}Li, $3n$)^{93}Tc	33	410	4
^{92}Mo(α, $2n$)^{94}Ru	27	500	4
^{92}Mo(^{6}Li, $3n$)^{95}Rh	36	60	12

1.6 Experimental Details

The experiments presented in this thesis were all conducted at the Institute for Nuclear Physics at the University of Cologne. In the time period from March 2022 to December 2024, three experimental campaigns have been conducted to measure lifetimes of excited states in different $N = 50$ nuclei, namely ^{92}Mo, ^{93}Tc, ^{94}Ru, and ^{95}Rh. Additionally, an enhanced upper limit for a lifetime in ^{91}Nb and lifetimes of excited states in ^{95}Ru have been measured. The excited nuclei were produced using a variety of suitable fusion-evaporation reactions. Prior to each experiment, estimates for the respective reaction cross sections were calculated using the program *cascade* [84] in order to optimize the respective experiment. The particle beam for each experiment was provided by the Cologne 10 MV FN Tandem accelerator. The sputter source and the duoplasmatron (^{4}He beam) were used to produce the negative ions. In Table 1.1 the reaction cross sections at given beam energies according to *cascasde* are summarized for the reactions used for the experiments. The γ rays emitted by the excited nuclei were detected using the HORUS (High efficiency Observatory for γ Ray Unique Spectroscopy) spectrometer [85, 86] in the fast-timing configuration, consisting of a hybrid setup of eight high-purity germanium (HPGe) detectors and up to ten $1.5'' \times 1.5''$ cerium-doped lanthanum bromide detectors with Hamamatsu R13435 photomultiplier tubes (PMTs) [87]. The high energy resolution of the HPGe detectors allows precise selection of distinct coincident transitions and hence enables a fast-timing analysis in triple coincidences. Without the precise HPGe gates it was not possible to analyze the in-beam data for most of the fusion-evaporation reactions. The LaBr detectors were shielded either passively or actively against neighboring detectors to avoid inter-detector Compton scattering. This leads to a reduction of the Compton background in general, but is also particularly important to avoid crosstalk effects between detectors, that can strongly affect the time-difference spectra, due to the time of flight for scattered γ rays between two adjacent detectors. An effect that also leads to the appearance of ghost peaks within the LaBr-LaBr coincidence spectra [89, 90]. Six of the LaBr detectors were actively shielded with bismuth germanium oxide (BGO) anti-Compton shields and the remaining were shielded using lead sheathings. In Ref. [90] the application of the

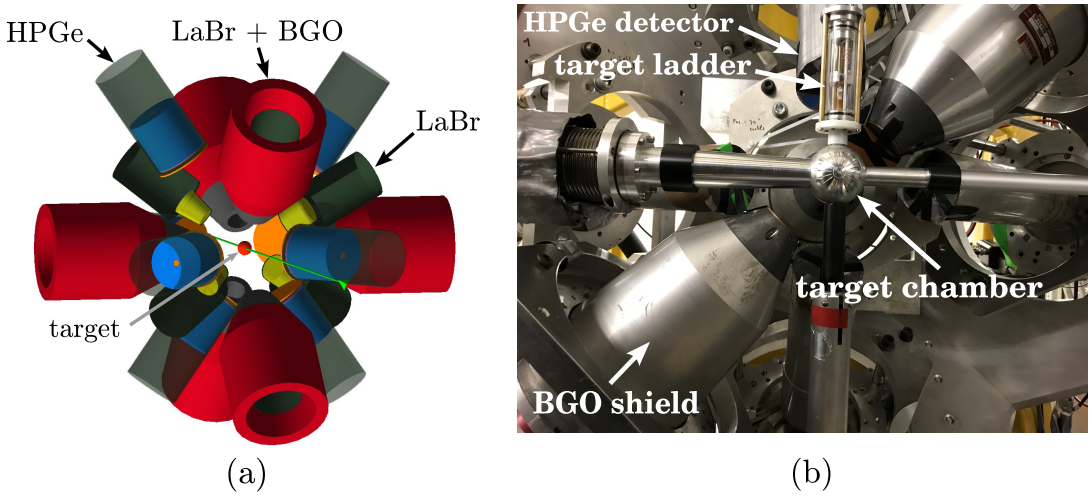

Figure 7: The HORUS spectrometer [85] in the fast-timing configuration. (a) Schematic drawing of the setup, showing the positions of germanium (HPGe), LaBr detectors and LaBr detecors with BGO shields for active Compton suppression. The beam axis is shown in green and the target is shown as red dot in the center. The figure is adopted from [88]. (b) Actual photograph of the HORUS spectrometer showing the above described detectors and the target ladder on top of the target chamber. The beam direction is from right to left in (a) and (b).

HORUS BGO shields in combination with LaBr detectors is discussed in detail. Figure 7 shows the hybrid setup of LaBr and HPGe detectors mounted at the HORUS spectrometer. For each experiment, the possibility of cross talk from opposing detectors was examined. This is especially important when energies in the proximity of the ∼200 keV backscatter peaks are involved. A corresponding analysis, which excluded opposing LaBr detector pairs, revealed no significant deviations relative to the analysis without excluded detector pairs. The signals from the LaBr detectors were recorded with a V1730 [76] fast-sampling digitizer from CAEN S.p.A., which has a sampling rate of 500 MHz and an analog-to-digital converter (ADC) resolution of 14 bits. This module includes real-time interpolating digital CFDs, providing timestamp determination for the fast LaBr detector signals with an accuracy down to picoseconds [13, 76]. The signals from the HPGe detectors were processed using V1782 digitizers, synchronized with the V1730 digitizers. The data acquisition and control software *CoMPASS* [91] was used for the recording. More detailed information on the data acquisition system is given in Refs. [92, 93]. The raw data was sorted using the software *ftSOCO*, an expanded version of the sorting code *SOCO-v2* to include also digital fast timing [93–95].

2 | Publication I: Lifetime measurements in ^{92}Mo: Investigation of seniority conservation in the $N = 50$ isotones

Lifetime measurements in ^{92}Mo: Investigation of seniority conservation in the $N = 50$ isotones

M. Ley,* L. Knafla, J. Jolie, A. Esmaylzadeh, A. Harter, A. Blazhev, C. Fransen, A. Pfeil, and J.-M. Régis
Institut für Kernphysik, Universität zu Köln, D-50937 Köln, Germany

P. Van Isacker
Grand Accélérateur National d'Ions Lourds, CEA/DRF–CNRS/IN2P3, Bvd Henri Becquerel, F-14076 Caen, France

(Received 11 September 2023; accepted 9 November 2023; published 22 December 2023)

Excited states in the yrast and negative parity bands in ^{92}Mo were populated in two different experiments using the ^{90}Zr$(\alpha, 2n)^{92}$Mo and ^{93}Nb$(p, 2n)^{92}$Mo fusion-evaporation reactions at the Cologne FN Tandem accelerator and measured using a hybrid setup of high purity germanium and lanthanum bromide detectors. Lifetimes of the excited 2_1^+, 4_1^+, 6_1^+, 8_1^+, 5_1^-, 7_1^-, and 9_1^- states were measured using the γ-γ fast-timing technique. The newly measured lifetime of the 4_1^+ state differs from the recently published value measured using the recoil distance Doppler shift method. Experimental $B(E2)$ strengths of excited states in ^{92}Mo are used to predict theoretical $B(E2)$ values in the $N = 50$ isotones from ^{93}Tc up to ^{95}Rh using semiempirical calculations in the single-j orbital $0g_{9/2}$ for the protons.

DOI: 10.1103/PhysRevC.108.064313

I. INTRODUCTION

The semimagic $N = 50$ isotones between ^{90}Zr and the doubly magic ^{100}Sn are of particular interest to test the nuclear shell model (SM) since in this region the valence protons gradually fill the $0g_{9/2}$ orbital above an energetically separated, closed core. Consequently, the low energy nuclear structure in this region can be assumed to originate from the interaction of protons confined to the $0g_{9/2}$ orbital. This implies the use of the concept of seniority to describe the low-spin structure ($J \leqslant 8$) of these nuclei. Seniority was first introduced by Racah to describe pairing interaction of electrons in the atom [1]. For a fermionic system of n identical particles, which all have the same angular momentum j and interact through a pairing force, seniority υ is a conserved quantum number and defined as the number of particles that do not pairwise couple to angular momentum $J = 0$ [1]. In nuclear physics, the validity of seniority symmetry has also been demonstrated for a broader class of empirical nucleon-nucleon interactions [2–5] and is expected to provide a useful description for a variety of regions of the nuclear chart [6]. Seniority is strictly conserved for systems with $j \leqslant 7/2$ [7] but is usually relatively well conserved among identical nucleons, even if $j > 7/2$ [8,9]. Recent studies found indications for a partial seniority conservation [10] as well as seniority-breaking behavior [11–13] for protons in the $0g_{9/2}$ orbital. Seniority conservation and breaking remains a topic of current interest in this region of the nuclear chart.

The single-j approximation applied in this article uses the experimentally determined quadrupole transition strength from the two-nucleon j^2 system (^{92}Mo) to make analytical predictions for the quadrupole transition strength in the j^n systems of the isotonic chain, up to ^{95}Rh. This *ansatz* already proved to be successful in the similar case of protons in the $0h_{9/2}$ orbital in the region above ^{208}Pb [14]. Relations between $B(E2)$ values in the j^2 and j^n systems can be derived in general. Such relations become analytical if seniority is conserved and therefore deviations from the analytical relations may provide important information on the question of seniority conservation.

In order to have an adequate basis for the single-j prediction, lifetimes of the first excited states in ^{92}Mo, especially of the 4_1^+ state, were measured with high precision using the fast-timing method with two independent experiments.

II. EXPERIMENT

The two independent experiments used different nuclear reactions to populate excited states in ^{92}Mo. In the first experiment, the states were populated using a ^{90}Zr$(\alpha, 2n)^{92}$Mo fusion evaporation reaction, it will be referred to as EXP1 in the following. The 5.3 mg/cm^2 thick target of 97.62% enriched ^{90}Zr was irradiated with a beam of 27 MeV α particles provided by the Cologne 10 MV FN Tandem accelerator with an average current of 3 pnA. Due to a clean reaction channel, almost no other nuclei were populated, and hence no major contaminations are visible in the γ-ray spectrum. The setup consisted of eight high purity germanium (Ge) detectors and nine $LaBr_3$(Ce) detectors (hereafter denoted as LaBr). Six of the LaBr detectors were actively shielded with bismuth germanium oxide (BGO) anti-Compton shields. The remaining LaBr detectors were passively shielded against scattered γ rays using lead sheaths. A 500 MHz digitizer, implementing online interpolation constant fraction discrimination (CFD), was used to record time and pulse height information from

*Corresponding author: mley@ikp.uni-koeln.de

the LaBr detectors photomultipliers (PM). A detailed investigation of the digital CFDs for fast-timing experiments is given in Ref. [15].

In the second experiment (EXP2), excited states in ^{92}Mo were populated using a ^{93}Nb$(p, 2n)^{92}$Mo reaction. The target was 5.4 mg/cm^2 of monoisotopic ^{93}Nb and the proton beam had an energy of 18 MeV. In both cases the targets were solid and thick enough to stop all reaction residues. The stopping times are much shorter than the lifetimes measured with the fast-timing technique. Both experiments were performed using the HORUS spectrometer fast-timing configuration [16–19]. Notably, the second experiment was performed almost one year later and the exact positions of the detectors differ between the two configurations. The two data sets yield strictly independent results.

Using the fast-timing method, lifetimes of excited states are deduced by measuring the time difference between the observation of events that indicates the population and depopulation of the state. Here, these events are γ rays populating and depopulating the state of interest. The fast-timing method is sensitive down to the range of picoseconds [20,21]. Lifetimes that are significantly larger than the time resolution of the fast-timing setup can be extracted by fitting the exponential tail of the time spectrum or using the convolution method [20,22]. For lifetimes in the range of the setups time resolution and smaller, the centroid shift method [23] is used. The method is based on measuring the centroid of the time distribution, mathematically also referred to as the first moment, to deduce the lifetime.

To extract the signals time information, a fast 500 MHz digitizer with an implemented real-time interpolating CFD algorithm was used to provide time stamps with picosecond precision [15]. In this way the data are intrinsically symmetrical with regard to the interchange of the start and stop detectors and therefore, an easy creation of symmetrical energy-energy-time-difference cubes for the analysis is possible. In the following, only aspects of the fast-timing method that are relevant to the presented analysis will be discussed. For more details on the fast-timing method in general, please refer to Refs. [21,24] and for the analysis using symmetrical fast-timing cubes as done in this study, please refer to Refs. [15,25].

A time difference spectrum for a given feeder-decay cascade is created by gating on the respective transitions. The lifetime τ results from the spectrum as the shift of the distribution's centroid C, corrected for the energy-dependent γ-γ time walk (TW) of the respective feeder-decay combination

$$C = \tau + TW(E_{\text{feeder}}, E_{\text{decay}}), \quad (1)$$

$$TW(E_{\text{feeder}}, E_{\text{decay}}) = TW(E_{\text{feeder}}) - TW(E_{\text{decay}}). \quad (2)$$

The energy dependence of the time walk was determined experimentally using the standard calibration procedure with a ^{152}Eu source [15,26], which covers a wide range of suitable transition energies and well-known lifetimes of intermediate states. From the measured centroid of the time distribution, for a given feeder-decay cascade with intermediate states in ^{152}Gd or ^{152}Sm with well-known lifetime, the time walk can be derived according to Eq. (1). The lifetimes used within the time walk calibration procedure were taken from Ref. [27] and the lifetime from the 2_1^+ in ^{152}Gd from Ref. [28]. Recently, the lifetime of the first excited 2^+ state in ^{152}Gd was remeasure with high precision, reducing its uncertainty by an order of magnitude [28]. This significantly reduces the uncertainty of the time walk calibration using a ^{152}Eu source as calibration standard. Because the γ-ray energies from the 330–773 keV cascade in ^{92}Mo are almost identical to the 344–779 keV cascade in ^{152}Gd, this optimization of the calibration standard significantly reduced the contribution of the time walk to the uncertainty for the lifetime of the 4_1^+ state in ^{92}Mo. The resulting data points are fitted using the function

$$TW(E_\gamma) = \frac{a}{\sqrt{E_\gamma + b}} + E_\gamma^2\, c + E_\gamma\, d + e. \quad (3)$$

The resulting $TW(E_\gamma)$ curves for EXP1 and EXP2 are shown in Figs. 1 and 2, respectively. For both experiments, the

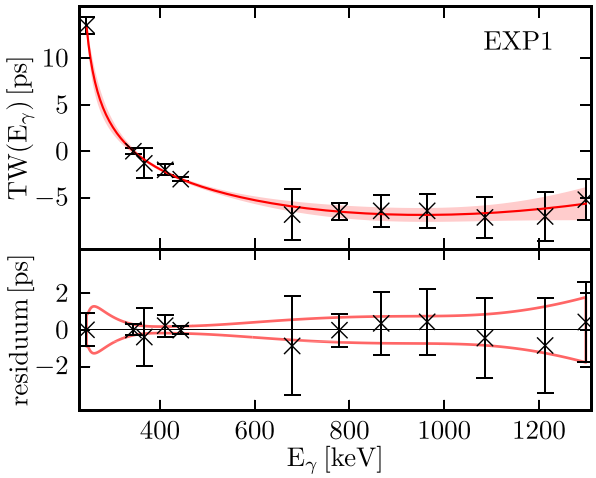

FIG. 1. Calibrated mean time-walk characteristic of the setup used for EXP1 (top). The residuum of the fit and the 1σ uncertainty interval (bottom).

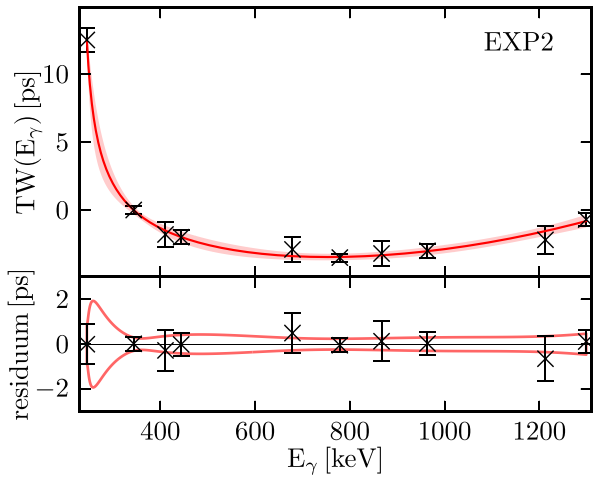

FIG. 2. Calibrated mean time-walk characteristic of the setup used for EXP2 (top). The residuum of the fit and the 1σ uncertainty interval (bottom).

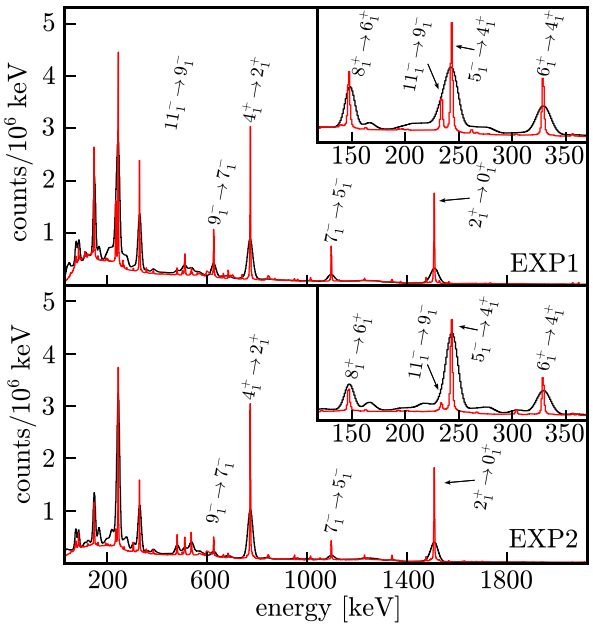

FIG. 3. Coincidence spectra of both experiments for multiplicity three data with Ge-LaBr-LaBr coincidences shown in black and Ge-LaBr-Ge coincidences shown in red. Transitions that were used within the analysis are labeled. The insets show a zoom of the low-energy part.

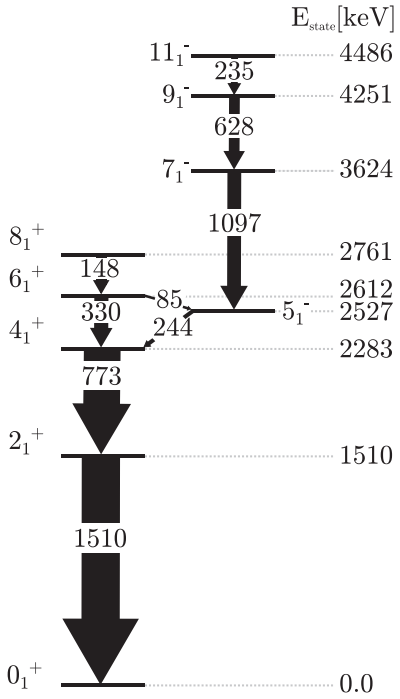

FIG. 4. Partial level scheme showing important states and transitions used within the analysis. The transition energies are given in keV. The arrows thickness approximately emphasize the relative intensities of the transitions observed with the ^{90}Zr$(\alpha, 2n)$^{92}Mo reaction (EXP1). Adopted from Refs. [29,30].

maximum range of the time-walk curves amounts to less than 20 ps in the range between 244 and 1299 keV. Coincidence spectra for both experiments are shown in Fig. 3. The spectra are sorted with the coincidence multiplicity condition of one Ge and two LaBr. In both experiments, no significant peaks from nuclei other than ^{92}Mo are visible. Transitions important within the analysis are labeled and Fig. 4 displays a partial level scheme of ^{92}Mo showing the yrast and negative parity bands.

III. ANALYSIS

The lifetimes were extracted from the data using the centroid shift method or by fitting the exponential tail of the time distribution. As an example the procedure for the latter case is shown in Fig. 5 for the lifetimes of the first excited 6_1^+ and 5_1^- states in ^{92}Mo. The lifetime of the 8_1^+ state was determined in the same way but using Ge-LaBr timing. In the following the focus is on the analysis of the lifetime of the 4_1^+ state in ^{92}Mo, which was performed using the centroid shift method. The analyses of the 2_1^+, 7_1^-, and 9_1^- states were performed analogously. For the lifetime analysis of the 4_1^+ state the data were sorted with a threefold coincidence multiplicity condition. Different conditions on the detector types were tested: triples of one Ge and two LaBr and triples of three LaBr with a narrow coincidence window of 20 ns. Taking into account background corrections, which will be discussed in detail later in the text, led to consistent results in all cases. The adopted analysis was done using a threefold multiplicity condition with exactly one Ge and two LaBr detectors. As an example, Figs. 6 and 7 show the resulting LaBr spectra (black) after setting a Ge and a LaBr gate on the feeder (b) or decay (a) transition. To significantly reduce the influence of random correlated γ rays, an additional timing window was placed for the LaBr-LaBr coincidences within the threefold Ge-LaBr-LaBr coincidences. As shown in Ref. [15], for a well-synchronized LaBr array a coincidence window of less

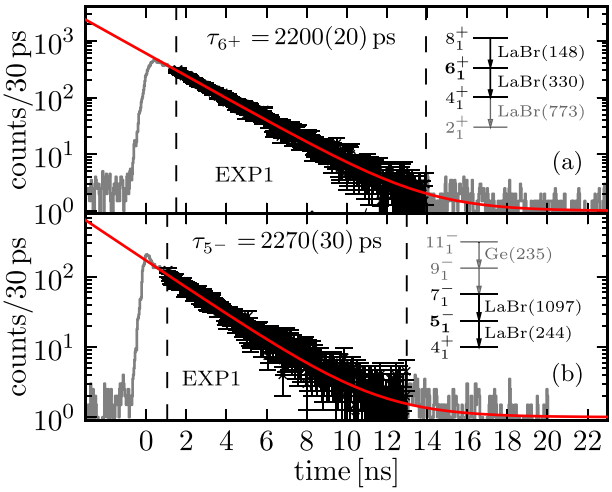

FIG. 5. Time spectra used for the measurement of the lifetime of the 6_1^+ state (a) and for lifetime of the 5_1^- state (b). The procedure is shown for the data from EXP1. The term for the random distributed background was set to a constant value, which was determined via integration and also as parameter from a fit, leading to consistent results. The data from EXP2 was processed in the same way.

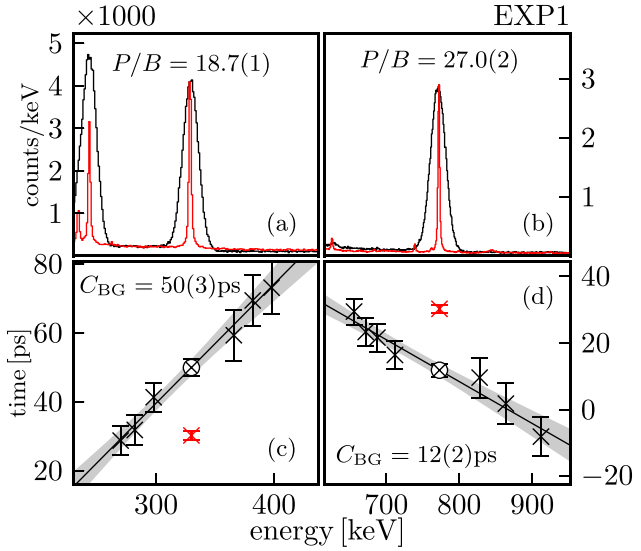

FIG. 6. Background correction procedure for the analysis of the 4_1^+ state measured in EXP1. (a) Resulting spectra after gating on the 773 keV decay transition. (b) Respective spectra after gating on the 330 keV feeder transition. The LaBr spectra are shown in black and corresponding gated Ge spectra for monitoring in red. (c) and (d) The corresponding background interpolation (black), the uncorrected centroid C_{exp} is shown in red, the interpolated centroid C_{BG} is marked with ⊗.

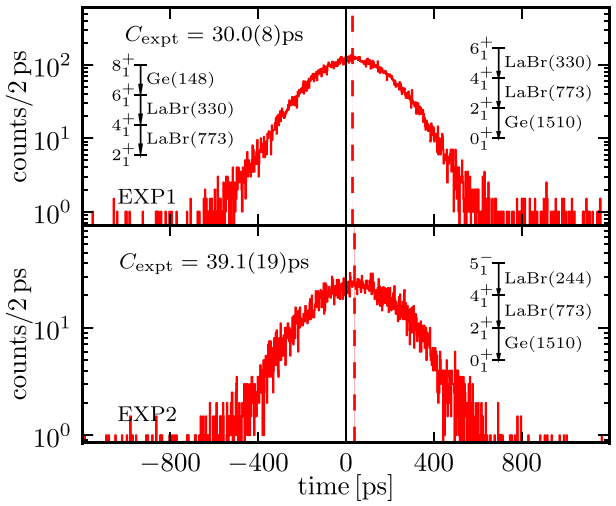

FIG. 8. The resulting time distributions, centroids (dashed lines) and gate information used to measure the 4_1^+ state for EXP1 (top) and EXP2 (bottom). For the upper time distribution, matrices with Ge gates on 148 keV and 1510 keV were added to increase the statistic. Since the multiplicity condition was set to only validate coincidences containing exactly two LaBr hits and one Ge hit the two energy conditions are mutual excluding/exclusive and no risk of double counting exists.

than 10 ns is sufficient for LaBr-LaBr timing. To still gain sufficient coincidences with the Ge detector a large time window of 400 ns was combined with the short LaBr-LaBr timing coincidence window of 10 ns. If such an additional LaBr-LaBr timing window is not applied, the P/B ratios measured in the LaBr spectra will be smaller due to the continuum of random coincidences within the large coincidence window. To verify the absence of contaminating transitions within the broad LaBr peaks, triple events with a coincidence condition for two Ge and one LaBr detectors were built. Using the same gates as before yielded the respective Ge spectra shown in red, which shows no major contamination within the LaBr peaks for the given cascade. The resulting time spectra after setting the second LaBr gate are shown in Fig. 8 together with the resulting centroid of the respective distribution.

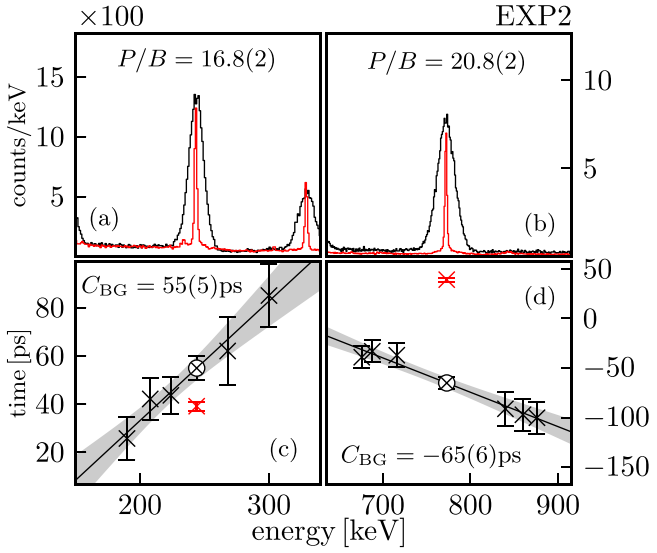

FIG. 7. Background correction procedure for the analysis of the 4_1^+ state measured in EXP2. (a) Resulting spectra after gating on the 773 keV decay transition. (b) Respective spectra after gating on the 244 keV feeder transition. The LaBr spectra are shown in black and corresponding gated Ge spectra for monitoring in red. (c) and (d) The corresponding background interpolation (black), the uncorrected centroid C_{exp} is shown in red, the interpolated centroid C_{BG} is marked with ⊗.

The measured time spectra are always influenced by Compton background beneath the peaks of interest and a background correction procedure was applied. As described in Ref. [26], the centroid of an experimental time-difference distribution is a linear superposition of multiple centroid components and for a proper lifetime determination, the component of the pure peak vs. peak centroid C_{PP} is needed, which was approached by using a background correction procedure as shown in Ref. [26]. The correction is based on Eqs. (4)–(6):

$$C_{PP} = C_{exp} + \tilde{t}_{cor}, \tag{4}$$

$$\tilde{t}_{cor} = \frac{P/B(E_f)\,t_{cor}(E_i) + P/B(E_i)\,t_{cor}(E_f)}{P/B(E_i) + P/B(E_f)}, \tag{5}$$

$$t_{cor} = \frac{C_{exp} - C_{BG}(E)}{P/B(E)}, \tag{6}$$

where C_{BG} is the centroid of the Compton background under the peak and $P/B(E)$ are the respective peak to background ratios. The component C_{BG} is only accessible by interpolating the Compton background in the vicinity of the peak.

TABLE I. Summary of the measured mean lifetimes of the states $J_i^{\pi_i}$ and the respective reduced transition probabilities.

$J_i^{\pi_i} \to J_f^{\pi_f}$	τ_{EXP1} ps	τ_{EXP2} ps	τ_{adopted} ps	Multipolarity	$B(\sigma\lambda; J_i^{\pi_i} \to J_f^{\pi_f})$ adopted	$B(\sigma\lambda; J_i^{\pi_i} \to J_f^{\pi_f})$ literature
$2_1^+ \to 0_1^+$	$\leqslant 3$	$\leqslant 8$	*$\leqslant 3$*	$E2$	$\geqslant 35\ e^2\,\mathrm{fm}^4$	207(12) $e^2\,\mathrm{fm}^4$ [30,31]
$4_1^+ \to 2_1^+$	22.5(11)	23(2)[a]	*22.5(11)*	$E2$	$132^{+7}_{-6}\ e^2\,\mathrm{fm}^4$	84.3(14) $e^2\,\mathrm{fm}^4$ [5]
$6_1^+ \to 4_1^+$	2200(20)	2220(70)	*2200(20)*	$E2$[b]	81(2) $e^2\,\mathrm{fm}^4$	80(3) $e^2\,\mathrm{fm}^4$ [30,32]
$\to 5_1^-$				$E1$[b]	$5.3(6)\times 10^{-5}\ e\,\mathrm{fm}^2$	$5.3(7)\times 10^{-5}\ e\,\mathrm{fm}^2$ [30]
$8_1^+ \to 6_1^+$	$310(3)\times 10^3$[c]	–	*$310(3)\times 10^3$*	$E2$	28.6(3) $e^2\,\mathrm{fm}^4$	32(1) $e^2\,\mathrm{fm}^4$ [30,33–37]
$5_1^- \to 4_1^+$	2270(30)	2250(60)	*2270(30)*	$E1$[d]	$\geqslant 1.88(3)\times 10^{-5}\ e\,\mathrm{fm}^2$	$1.91(5)\times 10^{-5}\ e\,\mathrm{fm}^2$ [30,38]
				$M2$[d]	$\leqslant 93\ \mu N^2\,\mathrm{fm}^4$	$\leqslant 98\ \mu N^2\,\mathrm{fm}^4$ [30]
$7_1^- \to 5_1^-$	$\leqslant 5$	$\leqslant 7$	*$\leqslant 5$*	$E2$	$\geqslant 101\ e^2\,\mathrm{fm}^4$	–
$9_1^- \to 7_1^-$	37(11)	29(7)	*31(6)*[e]	$E2$	$271^{+65}_{-44}\ e^2\,\mathrm{fm}^4$	–

[a]Averaged value from feeder-decay cascades 244–773 and 330–773 calculated using a Monte Carlo method.
[b]The branching ratio for the 6_1^+ level was derived using the intensities from Ref. [29].
[c]Determined using Ge-LaBr timing.
[d]Mixing ratio $\delta \leqslant 0.05$ from Ref. [39].
[e]Weighted average from EXP1 and EXP2.

The interpolation of the Compton background is shown in Figs. 6 and 7 (bottom). The results for both experiments are listed in Table I alongside the respective reduced transition probabilities $B(\sigma\lambda)$, which were calculated using the adopted values for the measured lifetimes, decay energies, and the total conversion coefficient calculated using the program BrIcc [40]. The remeasured values for the lifetimes of the 2_1^+, 6_1^+, 5_1^-, and 8_1^+ state fit well to the current literature values. The lifetime of the 4_1^+ state is in significant disagreement with the recently published literature value $\tau_{\mathrm{RDDS}} = 35.5(6)$ ps [5], measured using the recoil distance Doppler shift method and a radioactive beam.

IV. DISCUSSION

The present experimental work established another case of a nucleus with two valence nucleons in a $j = 9/2$ orbital, in which all $B(E2)$ values in the sequence $8_1^+ \to 6_1^+ \to 4_1^+ \to 2_1^+ \to 0_1^+$ are measured. In a single-j approach the $E2$ transition probabilities in this sequence obey the following rule:

$$B(E2; j^2 J \to j^2 J-2) = \frac{15(2j+1-J)(2j+2-J)(2j+J)(2j+1+J)(J-1)}{128\pi\, j^2(j+1)^2(2J-1)(2J+1)}\left(N+\frac{3}{2}\right)^2 b^4 e_{\mathrm{eff}}^2, \tag{7}$$

where N is the major oscillator quantum number associated with the j orbital and e_{eff} is the effective charge of the nucleon, which usually is taken the same for all $E2$ transitions in a given nucleus. In Eq. (7) also appears the oscillator length parameter b, for which we use the estimate of Blomqvist and Molinari [41] (see also the more recent discussion of Kirson [42]):

$$b = \sqrt{\frac{41.46}{45A^{-1/3} - 25A^{-2/3}}}\ \mathrm{fm}. \tag{8}$$

It should be stressed that the result (7) is purely geometric, that is, it depends only on the angular momenta involved and not on the interaction between the nucleons. In the column labeled '$\hat{T}_1(E2)$' of Table II, the single-j prediction is compared with the $B(E2)$ values measured in ^{92}Mo. The effective charge in the one-body operator $\hat{T}_1(E2)$ is obtained from the quadrupole moment of the $9/2^+$ ground state of ^{91}Nb, with the experimental value and uncertainty $Q(9/2_1^+) = -25(3)\,e\,\mathrm{fm}^2$. With an oscillator length parameter $b \approx 2.18$ fm this implies $e_{\mathrm{eff}} \approx 1.32$. This effective charge is essentially the same as what is obtained from the $B(E2; 8^+ \to 6^+)$ value in ^{92}Mo, $e_{\mathrm{eff}} \approx 1.31$. It is possible to obtain better results for ^{92}Mo by fitting the effective charge to the $n = 1$ and $n = 2$ data but that would be problematic given the discrepant description of the $B(E2)$ values in ^{92}Mo.

It is seen from Table II that there are significant deviations from Eq. (7) for all transitions other than $8_1^+ \to 6_1^+$, in

TABLE II. Experimental and calculated $B(E2)$ values in ^{92}Mo.

υ_i	J_i^π	υ_f	J_f^π	$B(E2; J_i^\pi \to J_f^\pi)$ ($e^2\,\mathrm{fm}^4$) Exp	$\hat{T}_1(E2)$	$\hat{T}_1'(E2)$
2	2_1^+	0	0_1^+	207(12)	89	207(12)
2	4_1^+	2	2_1^+	132^{+7}_{-6}	103	132^{+7}_{-6}
2	6_1^+	2	4_1^+	81(2)	71	81(2)
2	8_1^+	2	6_1^+	28.6(3)	28	28.6(3)

particular for the $2_1^+ \to 0_1^+$ transition. The situation is reminiscent of the one in the $A = 210$ isotopes of lead and polonium but, interestingly, whereas in the latter nuclei the calculated $B(E2; 2_1^+ \to 0_1^+)$ is a factor two larger than the measured value, in ^{92}Mo the single-j prediction is more than a factor two too small.

It is assumed that the correct $B(E2)$ values can be obtained by considering an appropriately large model space, which, when reduced to a manageable model space, gives rise to effective charges. The purpose of the present discussion is not a microscopic derivation of an effective $E2$ operator in nuclei with two valence nucleons but rather the use of effective charges determined from the two-nucleon $E2$ data in nuclei with $n > 2$ valence nucleons.

A. State-dependent effective charges

In this approach, the $E2$ operator remains of one-body character but state-dependent effective charges are taken. To distinguish this operator from the one with a constant effective charge, $\hat{T}_1(E2)$, it is denoted in the following as $\hat{T}_1'(E2)$. The idea is that, if the $B(E2; J \to J-2)$ values in the two-nucleon system cannot be explained with a constant effective charge, these can be made J dependent so as to reproduce the data. These effective charges are subsequently propagated to the n-nucleon systems. In Refs. [14,43,44] this procedure was applied to express $B(E2)$ values in the three-nucleon system in terms of those in the two-nucleon system. This could be achieved analytically under the assumption of conservation of seniority. In this subsection, we outline the procedure for n nucleons for a general interaction in a single-j orbital. In the next subsection analytic results are presented for an interaction that conserves seniority.

The matrix element of a one-body tensor of rank λ between n-body states can be calculated with the following recursive formula [45,46]:

$$\begin{aligned}\langle j^n \alpha' J' \| \hat{T}_1(\lambda) \| j^n \alpha J \rangle &= \frac{n}{n-1}(-)^{j+J}[J][J'] \sum_{\tilde{\alpha} R \tilde{\alpha}' R'} c_{n\alpha J}^{\tilde{\alpha} R} c_{n\alpha' J'}^{\tilde{\alpha}' R'} \\ &\times \begin{Bmatrix} J & J' & \lambda \\ R' & R & j \end{Bmatrix} \langle j^{n-1} \tilde{\alpha}' R' \| \hat{T}_1(\lambda) \| j^{n-1} \tilde{\alpha} R \rangle, \end{aligned} \tag{9}$$

where $[x] \equiv \sqrt{2x+1}$. The label α denotes possible quantum numbers needed to distinguish states of the j^n configuration with the same angular momentum J and $c_{n\alpha J}^{\tilde{\alpha} R}$ is a short-hand notation for the coefficient of fractional parentage $[j^{n-1}(\tilde{\alpha} R) j J | \} j^n \alpha J]$. Usually this recursion relation is applied until one arrives on the right-hand side at a one-nucleon matrix element, i.e., until $n = 2$. Therefore, for the operator $\hat{T}_1(E2)$ with a constant effective charge $e_{\rm eff}$, all $E2$ matrix elements between n-nucleon states can be expressed in terms of

$$\langle j \| \hat{T}_1(E2) \| j \rangle \equiv e_{\rm eff} \langle j \| r^2 Y_2 \| j \rangle = \sqrt{5} \tilde{e}_{\rm eff}, \tag{10}$$

where $\tilde{e}_{\rm eff}$ is proportional to the effective charge, $\tilde{e}_{\rm eff} = f_j(A) e_{\rm eff}$, with

$$f_j(A) = -\left(N + \frac{3}{2}\right) b^2 \left[\frac{(2j-1)(2j+1)(2j+3)}{64\pi j(j+1)}\right]^{1/2}. \tag{11}$$

For the operator $\hat{T}_1'(E2)$, with effective charges that depend on the two-nucleon states $|j^2 J\rangle$, the recursive procedure is halted when one arrives on the right-hand side of Eq. (9) at a *two*-nucleon matrix element

$$\begin{aligned}&\langle j^2 J_{\rm f} \| \hat{T}_1'(E2) \| j^2 J_{\rm i} \rangle \\ &\quad = -\sqrt{20}[J_{\rm f}][J_{\rm i}] \begin{Bmatrix} j & j & 2 \\ J_{\rm f} & J_{\rm i} & j \end{Bmatrix} \tilde{e}_{\rm eff}(J_{\rm i}, J_{\rm f}). \end{aligned} \tag{12}$$

This recursive procedure can only be carried out if all two-nucleon matrix elements, that is, all effective charges $\tilde{e}_{\rm eff}(J_{\rm i}, J_{\rm f})$, are known. If these are to be obtained from measured $E2$ data, that is unlikely to be possible since it would require the knowledge of the 'moment' effective charges $\tilde{e}_{\rm eff}(J_{\rm i}, J_{\rm f})$ with $J_{\rm i} = J_{\rm f}$. A possible strategy to circumvent this problem was outlined in Ref. [14] and leads to the following relation between $\tilde{e}_{\rm eff}(J, J)$ and $\tilde{e}_{\rm eff}(J, J-2)$:

$$\frac{\tilde{e}_{\rm eff}(J,J)}{\tilde{e}_{\rm eff}(J,J-2)} = \frac{[J]}{[J-2]} \begin{Bmatrix} j & j & 2 \\ J & J & j \end{Bmatrix} \begin{Bmatrix} j & j & 2 \\ J-2 & J & j \end{Bmatrix}^{-1}, \tag{13}$$

which allows to deduce all required effective charges from the $B(E2; J \to J-2)$ values in the nucleus with two nucleons in the valence space.

B. Analytic results for seniority-conserving interactions

As shown many years ago by de-Shalit and Talmi [45,46], the interaction between identical nucleons conserves seniority to a good approximation. With this assumption it is possible to derive analytic results for the matrix elements of $\hat{T}_1'(E2)$ between all states in a single-j orbital as long as $j \leqslant 9/2$, that is, if all states are uniquely defined by their angular momentum and seniority. The matrix elements of the one-body operator with state-dependent effective charges can be written in generic form as

$$\begin{aligned}&\langle j^n \upsilon_{\rm f} J_{\rm f} \| \hat{T}_1'(E2) \| j^n \upsilon_{\rm i} J_{\rm i} \rangle \\ &\quad = \sum_{J=2,4,\ldots}^{2j-1} f_J(j^n \upsilon_{\rm i} J_{\rm i} \upsilon_{\rm f} J_{\rm f}) \tilde{e}_{\rm eff}(J, J-2), \end{aligned} \tag{14}$$

where $f_J(j^n \upsilon_{\rm i} J_{\rm i} \upsilon_{\rm f} J_{\rm f})$ are numerical coefficients. Similar results relating the $B(E2)$ values in $n = 3$ and $n = 2$ nuclei were derived in Refs. [14,43] for $j = 7/2, 9/2$. The coefficients $f_J(j^n \upsilon_{\rm i} J_{\rm i} \upsilon_{\rm f} J_{\rm f})$ can be derived for any n and are available on request [47].

C. Application to $N = 50$ isotones

We apply the method outlined in the previous subsections to $N = 50$ isotones, making use of the complete set of $B(E2)$ values for the sequence $8_1^+ \to 6_1^+ \to 4_1^+ \to 2_1^+ \to 0_1^+$ measured in ^{92}Mo in order to fix an effective $E2$ operator. Similarly, an effective Hamiltonian appropriate for the $0g_{9/2}$ orbital can be derived from energy spectra. The two-body interaction matrix elements are taken from ^{92}Mo and from ^{98}Cd, corresponding to two valence particles and two valence

TABLE III. Experimental and calculated $B(E2)$ values in ^{93}Tc.

				$B(E2; J_i^\pi \to J_f^\pi)$ (e^2 fm^4)		
υ_i	J_i^π	υ_f	J_f^π	Exp	$\hat{T}_1(E2)$	$\hat{T}_1'(E2)$
3	$3/2_1^+$	3	$5/2_1^+$	–	212	256^{+7}_{-6}
3	$3/2_1^+$	3	$7/2_1^+$	–	31	35(1)
3	$5/2_1^+$	3	$7/2_1^+$	–	17	$9.0^{+1.3}_{-1.1}$
3	$5/2_1^+$	1	$9/2_1^+$	–	93	156(6)
3	$7/2_1^+$	1	$9/2_1^+$	–	178	278^{+9}_{-8}
3	$9/2_2^+$	3	$5/2_1^+$	–	23	32(1)
3	$9/2_2^+$	3	$7/2_1^+$	–	20	26(2)
3	$9/2_2^+$	1	$9/2_1^+$	–	11	16.0(5)
3	$9/2_2^+$	3	$11/2_1^+$	–	85	99(1)
3	$9/2_2^+$	3	$13/2_1^+$	–	3.3	4.8(3)
3	$11/2^+$	3	$7/2_1^+$	–	39	63(2)
3	$11/2_1^+$	1	$9/2_1^+$	–	59	87(3)
3	$11/2_1^+$	3	$13/2_1^+$	–	102	132(3)
3	$13/2_1^+$	1	$9/2_1^+$	–	102	166(6)
3	$15/2_1^+$	3	$11/2_1^+$	–	52	62(1)
3	$15/2_1^+$	3	$13/2_1^+$	–	16	$17.7^{+0.4}_{-0.3}$
3	$17/2_1^+$	3	$13/2_1^+$	88(18)[a]	99	114(3)
3	$17/2_1^+$	3	$15/2_1^+$	–	30	30.1(5)
3	$21/2_1^+$	3	$17/2_1^+$	73(5)[b]	57	61(1)

[a]From Ref. [48].
[b]From Ref. [49].

TABLE IV. Experimental and calculated $B(E2)$ values in ^{94}Ru.

				$B(E2; J_i^\pi \to J_f^\pi)$ (e^2 fm^4)		
υ_i	J_i^π	υ_f	J_f^π	Exp	$\hat{T}_1(E2)$	$\hat{T}_1'(E2)$
4	0_2^+	2	2_1^+	–	30	37(1)
4	0_2^+	4	2_2^+	–	128	164(4)
2	2_1^+	0	0_1^+	165(80)[a]	136	186(4)
4	2_2^+	0	0_1^+	–	7×10^{-6}	$0.07^{+0.06}_{-0.03}$
4	3_1^+	2	2_1^+	–	9×10^{-6}	$0.04^{+0.03}_{-0.02}$
4	3_1^+	4	2_2^+	–	66	79(1)
4	3_1^+	2	4_1^+	–	55	73(2)
4	3_1^+	4	4_2^+	–	12	14(1)
2	4_1^+	2	2_1^+	38(3)[a], 103(24)[b]	12	7.8(7)
2	4_1^+	4	2_2^+	–	25	35(1)
4	4_2^+	2	2_1^+	–	165	224(5)
4	4_2^+	4	2_2^+	–	9.5	15(1)
4	5_1^+	4	3_1^+	–	16	22(1)
4	5_1^+	2	4_1^+	–	124	173(4)
4	5_1^+	4	4_2^+	–	8.3	$5.4^{+0.4}_{-0.3}$
4	5_1^+	2	6_1^+	–	26	38(1)
4	5_1^+	4	6_2^+	–	16	23(1)
2	6_1^+	2	4_1^+	3.0(2)[b]	8.0	$3.9^{+0.5}_{-0.4}$
2	6_1^+	4	4_2^+	–	60	80(2)
4	6_2^+	2	4_1^+	–	25	36(1)
4	6_2^+	4	4_2^+	–	107	130^{+3}_{-2}
2	8_1^+	2	6_1^+	0.09(1)[b]	3.2	1.0(2)
2	8_1^+	4	6_2^+	–	98	137(3)
4	8_2^+	2	6_1^+	–	61	82(2)
4	8_2^+	4	6_2^+	–	21	27(1)
4	10_1^+	2	8_1^+	–	105	147(3)
4	10_1^+	4	8_2^+	–	22	23.3(4)

[a]From Ref. [5].
[b]From Ref. [13].

holes in $0g_{9/2}$, respectively, and an interpolated interaction is taken for intermediate $N = 50$ isotones. This procedure breaks particle-hole symmetry in the $0g_{9/2}$ orbital, akin to the effect of a three-body interaction. However, the interaction remains of two-body character and exhibits selection rules associated with the partial conservation of seniority, in particular in the midshell nucleus ^{95}Rh.

In the following we compare the results obtained with the operator $\hat{T}_1(E2)$ with a constant effective charge with those of the operator $\hat{T}_1'(E2)$ with state-dependent effective charges, and with the data when available. The input data depend on the assumed character of the $E2$ operator, as is explained below.

Results obtained with the two different $E2$ operators are summarised in Tables II–V for ^{92}Mo, ^{93}Tc, ^{94}Ru, and ^{95}Rh, respectively. Note that the method allows to estimate the uncertainty on a given $B(E2)$ value. For example, in the calculation with the operator $\hat{T}_1'(E2)$, one obtains information on how the uncertainties on the experimental values in the $n = 2$ nucleus ^{92}Mo propagate into the results for nuclei with $n > 2$.

We now comment on the results obtained with the two $E2$ operators.

1. The E2 operator with a constant effective charge

The effective charge derived from the quadrupole moment of the ground state of ^{91}Nb, $e_{\text{eff}} = 1.32(16)$, is assumed to be normally, and therefore symmetrically, distributed around a central value. As a result all calculated $B(E2)$ values have asymmetric uncertainties—a property of the squared normal distribution. In this example it leads to an upper uncertainty of about 27% and a lower uncertainty that is somewhat smaller, 22%, uncertainties not indicated in the column labeled '$\hat{T}_1(E2)$' of Tables II to V.

Although calculations have been performed with a general two-body interaction, which in principle can break seniority symmetry for a $j = 9/2$ orbital, it is found that the υ quantum number is conserved to a very good approximation and for many states this conservation of seniority is rigorously valid. Specifically, in the midshell nucleus ^{95}Rh no mixing can occur between levels that differ by $\Delta\upsilon = 2$ [7,51] and therefore all levels carry an exact seniority quantum number with the exception of $9/2_1^+$, which is dominantly $\upsilon = 1$ but does carry a small $\upsilon = 5$ component, and $9/2_3^+$, which is orthogonal to it.

TABLE V. Experimental and calculated $B(E2)$ values in ^{95}Rh.

				$B(E2; J_i^\pi \to J_f^\pi)$ (e^2 fm^4)		
υ_i	J_i^π	υ_f	J_f^π	Exp	$\hat{T}_1(E2)$	$\hat{T}_1'(E2)$
5	$1/2_1^+$	3	$3/2_1^+$	–	161	205(4)
5	$1/2_1^+$	1	$5/2_1^+$	–	0	$0.98^{+0.24}_{-0.21}$
5	$1/2_1^+$	3	$5/2_2^+$	–	231	294(5)
3	$3/2_1^+$	1	$5/2_1^+$	–	10	13.1(2)
3	$3/2_1^+$	3	$5/2_2^+$	–	0	$1.5^{+0.5}_{-0.4}$
3	$3/2_1^+$	3	$7/2_1^+$	–	0	$0.61^{+0.24}_{-0.17}$
1	$5/2_1^+$	3	$7/2_1^+$	–	328	417^{+8}_{-7}
1	$5/2_1^+$	1	$9/2_1^+$	–	0	$0.04^{+0.03}_{-0.02}$
3	$5/2_2^+$	1	$5/2_1^+$	–	205	260(5)
3	$5/2_2^+$	3	$7/2_1^+$	–	0	$0.78^{+0.16}_{-0.14}$
3	$5/2_2^+$	1	$9/2_1^+$	–	125	159(3)
3	$7/2_1^+$	1	$9/2_1^+$	–	238	303^{+6}_{-5}
3	$11/2_1^+$	3	$7/2_1^+$	–	0	$0.02^{+0.03}_{-0.01}$
3	$11/2_1^+$	1	$9/2_1^+$	–	78	100(2)
5	$11/2_2^+$	3	$7/2_1^+$	–	97	123(2)
5	$11/2_2^+$	1	$9/2_1^+$	–	0	$0.05^{+0.04}_{-0.02}$
3	$13/2_1^+$	1	$9/2_1^+$	–	137	174(3)
3	$13/2_1^+$	3	$11/2_1^+$	–	0	$0.38^{+0.07}_{-0.06}$
3	$15/2_1^+$	3	$13/2_1^+$	–	0	<0.02
5	$15/2_2^+$	3	$13/2_1^+$	–	15	18.9(3)
3	$17/2_1^+$	3	$13/2_1^+$	–	0	$0.87^{+0.22}_{-0.19}$
3	$17/2_1^+$	3	$15/2_1^+$	–	0	$0.36^{+0.06}_{-0.05}$
5	$17/2_2^+$	3	$13/2_1^+$	–	168	213(4)
5	$17/2_2^+$	3	$15/2_1^+$	–	62	79(1)
3	$21/2_1^+$	3	$17/2_1^+$	24(2)[a]	0	1.0(2)
3	$21/2_1^+$	5	$17/2_2^+$	113(13)[a]	138	176(3)
5	$25/2_1^+$	3	$21/2_1^+$	–	86	109(2)

[a]From Ref. [50].

In ^{94}Ru, 4_2^+ and 2_2^+ are solvable states and carry exact $\upsilon = 4$ for any two-body interaction [52–54]. Furthermore, the usual selection rules hold for the one-body operator $\hat{T}_1(E2)$, namely the seniorities of the initial and final states cannot differ by more than 2, $\Delta\upsilon \leqslant 2$, and $E2$ transitions with $\Delta\upsilon = 0$ are suppressed toward, and exactly forbidden in, the middle of the orbital. As a result many $E2$ transitions in ^{95}Rh are therefore characterized by an exact '0' in the column '$\hat{T}_1(E2)$' of Table V. In the $n = 4$ nucleus ^{94}Ru the $\Delta\upsilon = 0$ $E2$ transitions are not exactly zero but rather suppressed. The only $\Delta\upsilon = 4$ transition in this nucleus is between 2_2^+ and 0_1^+, which is forbidden if seniority is conserved. The calculated result for the $2_2^+ \to 0_1^+$ transition in Table IV indicates that a very small breaking of seniority occurs in ^{94}Ru. Another transition with a tiny $B(E2)$ value is $3_1^+ \to 2_1^+$. The latter transition is forbidden if seniority is conserved due to a summation property of coefficients of fractional parentage.

2. *The E2 operator with state-dependent effective charges*

The state-dependent effective charges needed to reproduce the $B(E2; J \to J-2)$ values in ^{92}Mo are $e_{\rm eff}(J, J-2) = 1.99(6)$, 1.48(4), 1.39(2), and 1.31(1) for $J = 2$, 4, 6, and 8, respectively. These are obtained from $\tilde{e}_{\rm eff}(J, J-2) = f_j(A) e_{\rm eff}(J, J-2)$, where $f_j(A)$ is the proportionality factor defined in Eq. (11), together with the expressions

$$
\begin{aligned}
B(E2; 2_{\upsilon=2}^+ \to 0_{\upsilon=0}^+) &= \tfrac{2}{5}\tilde{e}_{\rm eff}(2,0)^2,\\
B(E2; 4_{\upsilon=2}^+ \to 2_{\upsilon=2}^+) &= \tfrac{91}{198}\tilde{e}_{\rm eff}(4,2)^2,\\
B(E2; 6_{\upsilon=2}^+ \to 4_{\upsilon=2}^+) &= \tfrac{500}{1573}\tilde{e}_{\rm eff}(6,4)^2,\\
B(E2; 8_{\upsilon=2}^+ \to 6_{\upsilon=2}^+) &= \tfrac{7}{55}\tilde{e}_{\rm eff}(8,6)^2. \qquad (15)
\end{aligned}
$$

The different values of the effective charge could also be an indication that there is more collectivity in the lowest transition, which could come from components with more than one $g_{9/2}$ pair, effectively coming from the excitations from $p_{1/2}$ [11,12] leading to mixing of configurations with different even number of protons in $g_{9/2}$, especially for the 0_1^+ state.

The $E2$ transition properties of the $N = 50$ isotones calculated with an $E2$ operator with state-dependent effective charges are shown in the column '$\hat{T}_1'(E2)$' of Tables II to V. All $B(E2)$ values in nuclei with $n \geqslant 3$ valence protons in the $0g_{9/2}$ orbital are expressed in terms of the two-nucleon effective charges $\tilde{e}_{\rm eff}(J, J-2)$ and do not depend on the one-nucleon effective charge $\tilde{e}_{\rm eff}$. Understandably, the effective charges $\tilde{e}_{\rm eff}(J, J-2)$ for $J = 6$ and 8 are close to $\tilde{e}_{\rm eff}$ derived from the quadrupole moment of the ground state of ^{91}Nb but $\tilde{e}_{\rm eff}(2, 0)$ is considerably and $\tilde{e}_{\rm eff}(4, 2)$ somewhat larger than $\tilde{e}_{\rm eff}$. This reflects the deviations for the $B(E2; 2_1^+ \to 0_1^+)$ and $B(E2; 4_1^+ \to 2_1^+)$ values in ^{92}Mo obtained with the operator $\hat{T}_1(E2)$ with a constant effective charge. As a result, most $B(E2)$ values calculated with state-dependent effective charges are larger than the corresponding ones obtained with a single effective charge. However, the differences cannot be represented by a simple scale factor. Generally, the $E2$ transitions between high angular momentum states do not change much while $B(E2)$ values between states of low angular momentum states do.

Two $B(E2)$ values have been measured to date in ^{93}Tc. The $B(E2; 21/2_1^+ \to 17/2_1^+)$ value essentially depends only on the effective charges $\tilde{e}_{\rm eff}(6, 4)$ and $\tilde{e}_{\rm eff}(8, 6)$ (see Table IV of Ref. [14]) and therefore is rather close to the value obtained with the $\hat{T}_1(E2)$ operator with a constant effective charge. The $B(E2; 17/2_1^+ \to 13/2_1^+)$ value depends additionally on the effective charge $\tilde{e}_{\rm eff}(4, 2)$, which leads to an increase compared with the result obtained with $\hat{T}_1(E2)$.

To obtain an understanding of the results for the nucleus ^{94}Ru in Table IV, we note that, under the assumption of seniority conservation, the relevant expressions for the $B(E2)$ values of the $6_1^+ \to 4_1^+$ and $8_1^+ \to 6_1^+$ transitions can be

derived from the matrix elements

$$\langle j^4 4^+_{\upsilon=2} \| \hat{T}'_1(E2) \| j^4 6^+_{\upsilon=2} \rangle = \sqrt{\frac{1}{5}} \left(-\frac{40}{33} \tilde{e}_{\rm eff}(2,0) + \frac{24220}{51909} \tilde{e}_{\rm eff}(4,2) + \frac{90422}{51909} \tilde{e}_{\rm eff}(6,4) + \frac{816}{1573} \tilde{e}_{\rm eff}(8,6) \right),$$

$$\langle j^4 6^+_{\upsilon=2} \| \hat{T}'_1(E2) \| j^4 8^+_{\upsilon=2} \rangle = \sqrt{\frac{119}{55}} \left(-\frac{526}{1485} \tilde{e}_{\rm eff}(2,0) + \frac{21046}{70785} \tilde{e}_{\rm eff}(4,2) - \frac{31604}{1061775} \tilde{e}_{\rm eff}(6,4) + \frac{13513}{32175} \tilde{e}_{\rm eff}(8,6) \right). \quad (16)$$

The calculated $B(E2)$ values in ^{94}Ru are obtained by inserting the state-dependent effective charges obtained from ^{92}Mo. Compared with the calculation with a constant effective charge a somewhat better agreement with the measured $B(E2)$ values is found but the improvement is marginal.

On the other hand, a disagreement is seen to occur for the $4^+_1 \to 2^+_1$ transition in ^{94}Ru. While the two experimental $B(E2; 4^+_1 \to 2^+_1)$ values are discrepant, both are significantly larger than the theoretical prediction. To obtain an understanding of this disagreement, it is essential to consider two 4^+ levels, which for four particles or four holes in a $j = 9/2$ orbital occur close in energy. For a one-body $E2$ operator with a constant effective charge the $B(E2)$ values in a $j = 9/2$ orbital, under the assumption of conservation of seniority, are

$$B(E2; 4^+_{\upsilon=2} \to 2^+_{\upsilon=2}) = \tfrac{91}{1782} \tilde{e}^2_{\rm eff},$$
$$B(E2; 4^+_{\upsilon=4} \to 2^+_{\upsilon=2}) = \tfrac{34000}{46629} \tilde{e}^2_{\rm eff}. \quad (17)$$

In ^{94}Ru (as well as ^{96}Pd) the dominant component of the 4^+_1 (4^+_2) state has seniority $\upsilon = 2$ ($\upsilon = 4$). Given that the $\Delta\upsilon = 2$ transition is ∼14 times faster than the one with $\Delta\upsilon = 0$, a small admixture of $\upsilon = 4$ in the 4^+_1 state can considerably alter the $B(E2; 4^+_1 \to 2^+_1)$ value. However, as has been shown in Refs. [52,53], the $4^+_{\upsilon=4}$ state is solvable for *any* interaction in a $j = 9/2$ orbital, which means that it cannot mix with other 4^+ states. A proper description of the $4^+_1 \to 2^+_1$ transition in ^{94}Ru and ^{96}Pd therefore necessarily must involve components outside the $0g_{9/2}$ orbital.

The use of a one-body $E2$ operator with state-dependent effective charges does not alter this conclusion. Under the assumption of seniority conservation, the matrix elements of the operator $\hat{T}'_1(E2)$ for $4^+ \to 2^+$ transitions in ^{94}Ru are

$$\langle j^4 2^+_{\upsilon=2} \| \hat{T}'_1(E2) \| j^4 4^+_{\upsilon=2} \rangle = \sqrt{\frac{7}{286}} \left(\frac{442}{165} \tilde{e}_{\rm eff}(2,0) - \frac{2369}{605} \tilde{e}_{\rm eff}(4,2) - \frac{12392}{9075} \tilde{e}_{\rm eff}(6,4) - \frac{476}{275} \tilde{e}_{\rm eff}(8,6) \right),$$

$$\langle j^4 2^+_{\upsilon=2} \| \hat{T}'_1(E2) \| j^4 4^+_{\upsilon=4} \rangle = \sqrt{\frac{85}{5181}} \left(\frac{446}{99} \tilde{e}_{\rm eff}(2,0) + \frac{1828}{363} \tilde{e}_{\rm eff}(4,2) + \frac{18802}{5445} \tilde{e}_{\rm eff}(6,4) + \frac{1156}{165} \tilde{e}_{\rm eff}(8,6) \right). \quad (18)$$

If one makes the association $4^+_1 = 4^+_{\upsilon=2}$ and $2^+_1 = 2^+_{\upsilon=2}$, one finds, with the effective charges obtained in ^{92}Mo, $B(E2; 4^+_1 \to 2^+_1) = 7.8(7)\ e^2\,{\rm fm}^4$, more than an order of magnitude smaller than observed in ^{94}Ru. In fact, with state-dependent effective charges the disagreement increases as compared to the result obtained with a constant effective charge.

While a single-j calculation cannot reproduce the observed $4^+_1 \to 2^+_1$ $E2$ transition in ^{94}Ru, at least not with reasonable effective charges, it can give insight into the problem by assuming an ad hoc mixed structure of the 4^+_1 state,

$$|4^+_1\rangle = \alpha_4 |4^+_{\upsilon=2}\rangle + \beta_4 |4^+_{\upsilon=4}\rangle \quad (19)$$

with $\alpha_4^2 + \beta_4^2 = 1$. A large $B(E2; 4^+_1 \to 2^+_1)$ value, as in ^{94}Ru, is obtained through a constructive interference between the two components, which happens if α_4 and β_4 have the opposite sign. The corresponding transition in ^{96}Pd is much slower [$B(E2; 4^+_1 \to 2^+_1) = 3.8(4)\ e^2\,{\rm fm}^4$] because of destructive interference: the $\Delta\upsilon = 0$ matrix elements change sign under particle-hole conjugation while those with $\Delta\upsilon = 2$ do not. This is the essence of the argument presented in Ref. [13], which therefore can be understood from a simple perspective.

It should be emphasized that, due to the dominance of the $\Delta\upsilon = 2$ over the $\Delta\upsilon = 0$ $E2$ transitions in ^{94}Ru, results are extremely dependent on the admixture β_4. In addition, since $6^+_{\upsilon=4}$ is also a solvable state [52,53], the same type of mixing should be assumed for the 6^+_1 state,

$$|6^+_1\rangle = \alpha_6 |6^+_{\upsilon=2}\rangle + \beta_6 |6^+_{\upsilon=4}\rangle \quad (20)$$

with $\alpha_6^2 + \beta_6^2 = 1$. The three $E2$ transitions, $4^+_1 \to 2^+_1$, $6^+_1 \to 4^+_1$ and $8^+_1 \to 6^+_1$, depend on the 4^+ or 6^+ mixing, or on both. The $B(E2)$ values between the mixed 4^+ and 6^+ states can be calculated with the help of Eqs. (16) and (18) together

with

$$\langle j^4 4^+_{\upsilon=4} \| \hat{T}'_1(E2) \| j^4 6^+_{\upsilon=2} \rangle = \sqrt{\frac{238}{6123}} \left(\frac{9256}{5445} \tilde{e}_{\text{eff}}(2,0) + \frac{66608}{19965} \tilde{e}_{\text{eff}}(4,2) + \frac{371744}{299475} \tilde{e}_{\text{eff}}(6,4) + \frac{28832}{9075} \tilde{e}_{\text{eff}}(8,6) \right),$$

$$\langle j^4 4^+_{\upsilon=2} \| \hat{T}'_1(E2) \| j^4 6^+_{\upsilon=4} \rangle = \sqrt{\frac{2261}{843}} \left(-\frac{1372}{5445} \tilde{e}_{\text{eff}}(2,0) + \frac{3352}{259545} \tilde{e}_{\text{eff}}(4,2) - \frac{160228}{778635} \tilde{e}_{\text{eff}}(6,4) - \frac{6664}{23595} \tilde{e}_{\text{eff}}(8,6) \right),$$

$$\langle j^4 4^+_{\upsilon=4} \| \hat{T}'_1(E2) \| j^4 6^+_{\upsilon=4} \rangle = \sqrt{\frac{2470}{44117}} \left(\frac{952}{1089} \tilde{e}_{\text{eff}}(2,0) + \frac{1149253}{311454} \tilde{e}_{\text{eff}}(4,2) + \frac{18704}{11979} \tilde{e}_{\text{eff}}(6,4) + \frac{6881}{1573} \tilde{e}_{\text{eff}}(8,6) \right),$$

$$\langle j^4 6^+_{\upsilon=4} \| \hat{T}'_1(E2) \| j^4 8^+_{\upsilon=2} \rangle = \sqrt{\frac{19}{9273}} \left(\frac{556}{33} \tilde{e}_{\text{eff}}(2,0) + \frac{12104}{1573} \tilde{e}_{\text{eff}}(4,2) + \frac{315992}{23595} \tilde{e}_{\text{eff}}(6,4) + \frac{15776}{715} \tilde{e}_{\text{eff}}(8,6) \right). \quad (21)$$

With the state-dependent effective charges fixed from ^{92}Mo all experimental $E2$ transitions in ^{94}Ru can be exactly reproduced with the admixtures $(\alpha_4, \beta_4) = (0.854, -0.520)$ and $(\alpha_6, \beta_6) = (0.994, -0.111)$ if the the experimental $B(E2; 4^+_1 \to 2^+_1)$ value of 103(24) is adopted. If the experimental $B(E2; 4^+_1 \to 2^+_1)$ value is taken as 38(3), reasonable agreement is obtained with the admixtures $(\alpha_4, \beta_4) = (0.980, -0.204)$ and $(\alpha_6, \beta_6) = (0.994, -0.113)$. It can therefore be concluded that the currently known $E2$ data in ^{94}Ru are consistent with moderate to strong seniority mixing of the 4^+ levels and 6^+ states that are rather pure in seniority.

Also for ^{95}Rh the known $B(E2)$ values for the states of interest are scarce (see Table V) due to the fact that only the lifetime of the $21/2^+_1$ state is known, yielding $B(E2)$ values to the first two $17/2^+$ states. The prediction for the seniority forbidden transition to the first $17/2^+$ state is clearly not in agreement with the experimental findings. Also here a mixing between both states could be considered provided more is known on the decay of both $17/2^+$ states.

V. CONCLUSION

Lifetimes of excited states in ^{92}Mo were measured using the γ-γ fast-timing technique in two independent experiments. The lifetime of the first excited 4^+ state was measured with high accuracy. The experimental $B(E2)$ values calculated with the measured lifetimes were used to obtain state dependent effective charges for the single-j calculation with $j = 9/2$. Comparing the predicted $B(E2)$ values for ^{93}Tc with the scarce experimental data, one finds that the single-j prediction qualitatively reproduces the experimental data within 3σ of the experimental uncertainties. The discrepancy from the $B(E2)$ for $B(E2; 4^+_1 \to 2^+_1)$ in ^{94}Ru to the experimental value is quantitatively discussed in terms of an ad hoc mixing between $\upsilon = 2$ and $\upsilon = 4$ states, with the result that in this way the experimental data in ^{94}Ru is exactly reproduced using state-dependent effective charges. Since the data on lifetimes in ^{93}Tc, ^{94}Ru, and ^{95}Rh is yet to be completed, further experiments are planned to probe the results from the single-j calculation.

ACKNOWLEDGMENTS

We acknowledge the Deutsche Forschungsgemeinschaft (DFG) for the upgrade of the used germanium detectors under Grant No. INST 216/988-1 FUGG. M.L. acknowledges the financial support of the DFG under Grant No. JOL 391/18-1. J.J. acknowledges support by GANIL for an extended stay there. Support of the University of Cologne in operating the Tandem accelerator is acknowledged.

[1] G. Racah, Phys. Rev. **63**, 367 (1943).
[2] R. Gross and A. Frenkel, Nucl. Phys. A **267**, 85 (1976).
[3] L. Coraggio *et al.*, J. Phys. G: Nucl. Part. Phys. **26**, 1697 (2000).
[4] J. Blomqvist and L. Rydström, Phys. Scr. **31**, 31 (1985).
[5] R. M. Pérez-Vidal *et al.*, Phys. Rev. Lett. **129**, 112501 (2022).
[6] J. J. Ressler *et al.*, Phys. Rev. C **69**, 034317 (2004).
[7] R. D. Lawson, *Theory of the Nuclear Shell Model* (Clarendon Press, Oxford, 1980).
[8] D. J. Rowe and G. Rosensteel, Phys. Rev. Lett. **87**, 172501 (2001).
[9] G. Rosensteel and D. J. Rowe, Phys. Rev. C **67**, 014303 (2003).
[10] E. Caurier, M. Rejmund, and H. Grawe, Phys. Rev. C **67**, 054310 (2003).
[11] H. Grawe, in *The Euroschool Lectures on Physics with Exotic Beams, Vol. I*, edited by J. Al-Khalili and E. Roeckl (Springer, Berlin/Heidelberg, 2004), pp. 33–75.
[12] H. Mach *et al.*, Phys. Rev. C **95**, 014313 (2017).
[13] B. Das *et al.*, Phys. Rev. C **105**, L031304 (2022).
[14] V. Karayonchev *et al.*, Phys. Rev. C **99**, 024326 (2019).
[15] A. Harter *et al.*, Nucl. Instrum. Methods Phys. Res. A **1053**, 168356 (2023).
[16] V. Karayonchev *et al.*, Phys. Rev. C **95**, 034316 (2017).
[17] A. Harter *et al.*, Phys. Rev. C **106**, 024326 (2022).
[18] L. Knafla *et al.*, Phys. Rev. C **102**, 044310 (2020).
[19] M. Stoyanova *et al.*, Phys. Rev. C **100**, 064304 (2019).
[20] H. Mach *et al.*, Nucl. Instrum. Methods Phys. Res. A **280**, 49 (1989).
[21] J.-M. Régis *et al.*, Nucl. Instrum. Methods Phys. Res. A **622**, 83 (2010).
[22] B. Olsen and L. Boström, Nucl. Instrum. Methods **44**, 65 (1966).
[23] Z. Bay, Phys. Rev. **77**, 419 (1950).

[24] J.-M. Régis *et al.*, Nucl. Instrum. Methods Phys. Res. A **726**, 191 (2013).
[25] J.-M. Régis *et al.*, Nucl. Instrum. Methods Phys. Res. A **897**, 38 (2018).
[26] J.-M. Régis *et al.*, Nucl. Instrum. Methods Phys. Res. A **823**, 72 (2016).
[27] M. Martin, Nucl. Data Sheets **114**, 1497 (2013).
[28] L. Knafla *et al.*, Nucl. Instrum. Methods Phys. Res. A **1052**, 168279 (2023).
[29] T. Numao *et al.*, Nucl. Phys. A **305**, 163 (1978).
[30] C. M. Baglin, Nucl. Data Sheets **113**, 2187 (2012).
[31] F. R. Metzger, Phys. Rev. C **15**, 193 (1977).
[32] C. Gil, J. Phys. Soc. Jpn. **34**, 575 (1973).
[33] K. E. G. Löbner, Nucl. Phys. **58**, 49 (1964).
[34] O. Häusser *et al.*, Nucl. Phys. A **293**, 248 (1977).
[35] C. Lederer *et al.*, Nucl. Phys. A **169**, 449 (1971).
[36] L. Hannappel *et al.*, Nucl. Instrum. Methods **167**, 289 (1979).
[37] A. Ádám *et al.*, Nucl. Phys. A **180**, 587 (1972).
[38] S. Cochavi *et al.*, Phys. Rev. C **3**, 1352 (1971).
[39] L. I. Govor *et al.*, Phys. At. Nucl. **73**, 1289 (2010).
[40] T. Kibédi *et al.*, Nucl. Instrum. Methods Phys. Res. A **589**, 202 (2008).
[41] J. Blomqvist and A. Molinari, Nucl. Phys. A **106**, 545 (1968).
[42] M. W. Kirson, Nucl. Phys. A **781**, 350 (2007).
[43] P. Spagnoletti *et al.*, Phys. Rev. C **95**, 021302(R) (2017).
[44] V. Karayonchev *et al.*, Phys. Rev. C **106**, 044321 (2022).
[45] A. de Shalit and I. Talmi, *Nuclear Shell Theory* (Academic Press, New York, 1963).
[46] I. Talmi, *Simple Models of Complex Nuclei: The Shell Model and Interacting Boson Model* (Harwood, Chur, 1993).
[47] P. Van Isacker (unpublished).
[48] C. Broude *et al.*, Z. Phys. A **336**, 133 (1990).
[49] C. M. Baglin, Nucl. Data Sheets **112**, 1163 (2011).
[50] S. Basu, G. Mukherjee, and A. Sonzogni, Nucl. Data Sheets **111**, 2555 (2010).
[51] J. J. Valiente-Dobón *et al.*, Phys. Lett. B **816**, 136183 (2021).
[52] A. Escuderos and L. Zamick, Phys. Rev. C **73**, 044302 (2006).
[53] P. Van Isacker and S. Heinze, Phys. Rev. Lett. **100**, 052501 (2008).
[54] Y. Qian and C. Qi, Phys. Rev. C **98**, 061303(R) (2018).

3 | Publication II:
Lifetime measurement in ^{94}Ru and ^{93}Tc to investigate seniority conservation in the $N = 50$ isotones

Lifetime measurement in ^{94}Ru and ^{93}Tc to investigate seniority conservation in the $N = 50$ isotones

M. Ley,* J. Jolie, L. Knafla, A. Blazhev, A. Esmaylzadeh, C. Fransen, A. Pfeil, and J.-M. Régis
Institut für Kernphysik, Universität zu Köln, D-50937 Köln, Germany

P. Van Isacker
Grand Accélérateur National d'Ions Lourds, CEA/DRF–CNRS/IN2P3, Boulevard Henri Becquerel, F-14076 Caen, France

(Received 3 June 2024; accepted 14 August 2024; published 18 September 2024)

Low-lying excited states in ^{93}Tc and ^{94}Ru were populated using the two fusion-evaporation reactions ^{90}Zr(^{6}Li, $3n$)^{93}Tc and ^{92}Mo(α, $2n$)^{94}Ru at the Cologne FN Tandem accelerator and their lifetimes were measured using a hybrid setup of high-purity germanium and fast cerium doped lanthanum bromide detectors for γ-γ fast-timing. The measured lifetimes fill gaps in the experimental data for electromagnetic transition probabilities $B(\sigma\lambda)$ along the $N = 50$ isotonic chain and provide more insight for ambiguous cases, such as the lifetime of the 4_1^+ state in ^{94}Ru. The experimental data are compared with theoretical $B(E2)$ values from a single-j approximation, with state-dependent effective charges derived from ^{92}Mo and with the results from shell-model calculations performed using the SR88MHJM interaction in the $\pi(1p_{1/2},\ 0g_{9/2})$ model space.

DOI: 10.1103/PhysRevC.110.034320

I. INTRODUCTION

The region of semimagic $N = 50$ isotones between ^{90}Zr and ^{100}Sn has become of particular interest to studies regarding the question of seniority conservation [1–5]. For a fermionic system of n identical particles with angular momentum j, seniority υ is defined as the number of particles that do not pairwise couple to angular momentum $J = 0$ [6]. Since seniority is only strictly conserved for shells with $j \leqslant 7/2$ [7], the first shell where seniority-violating effects can occur is $0g_{9/2}$. Between ^{90}Zr and ^{100}Sn the $0g_{9/2}$ orbit gradually fills with protons, while distortions from the $1p_{1/2}$ orbit may be assumed to be small. However, experimental findings indicated a breakdown of seniority as a good quantum number in ^{94}Ru and ^{96}Pd, which can be attributed to cross-shell proton-hole excitation leading to significant mixing of $\upsilon = 2$ and $\upsilon = 4$ states [5]. Recently, the shorter lifetimes of the low-lying states in the region became accessible in experiments applying the fast-timing method with $LaBr_3$(Ce) detectors [8,9] or the recoil distance Doppler shift method [10].

In a previous work [9], experimentally determined transition probabilities from the complete yrast cascade $8_1^+ \rightarrow 6_1^+ \rightarrow 4_1^+ \rightarrow 2_1^+$ in ^{92}Mo were used to extract state-dependent effective charges, which were used in a semiempirical single-j approximation to predict theoretical electromagnetic quadrupole ($E2$) transition probabilities for the nuclei ^{93}Tc, ^{94}Ru, and ^{95}Rh. This ansatz was successfully applied in a similar case of protons in the $0h_{9/2}$ orbital in the trans-lead region [11]. However, experimental results showed a deviation from the expected seniority pattern of $B(E2)$ values in ^{94}Ru when approaching the half-filled $0g_{9/2}$ orbital [5,8–10]. This deviation was explained by the mixing between seniority $\upsilon = 2$ and $\upsilon = 4$ states [8,12].

Since the analytical predictions from the single-j approximation assume seniority conservation, they cannot reproduce all transition probabilities in ^{94}Ru, but they do allow us to derive *ad hoc* admixtures for the mixing of the respective $\upsilon = 2$ and $\upsilon = 4$ states, to fit the experimental data. The aim of this work is to provide more experimental data on the electromagnetic transition probabilities in ^{94}Ru and ^{93}Tc to fill gaps and try to clarify ambiguous cases, especially for the lifetime of the 4_1^+ state in ^{94}Ru. Additionally, the limit for the lifetime of the $17/2_1^+$ state in ^{91}Nb was improved.

II. EXPERIMENT

Two nuclear reactions were used to populate excited states in ^{93}Tc and ^{94}Ru. The first was the ^{92}Mo(α, $2n$)^{94}Ru fusion-evaporation reaction. A 5.5 mg/cm^2 thick target of 99.93% highly enriched ^{92}Mo was irradiated with a beam of 27 MeV α particles provided by the Cologne 10 MV FN Tandem accelerator with an average current of 3 pnA. The second was the ^{90}Zr(^{6}Li, $3n$)^{93}Tc fusion-evaporation reaction, using a 5.3 mg/cm^2 thick target of 97.62% enriched ^{90}Zr and a ^{6}Li beam with an energy of 33 MeV and an average current of 1 pnA. In both cases the targets were thick enough to stop all reaction residues and the stopping times were much shorter than the lifetimes measured with the fast-timing technique. The experiment was performed using the HORUS spectrometer in the fast-timing configuration [13–16]. The detector setup consisted of eight high-purity germanium detectors and ten cerium-doped lanthanum bromide detectors (hereafter referred to as Ge and LaBr). Six of the LaBr detectors were actively shielded with bismuth germanium oxide (BGO) anti-Compton shields. The remaining LaBr

*Contact author: mley@ikp.uni-koeln.de

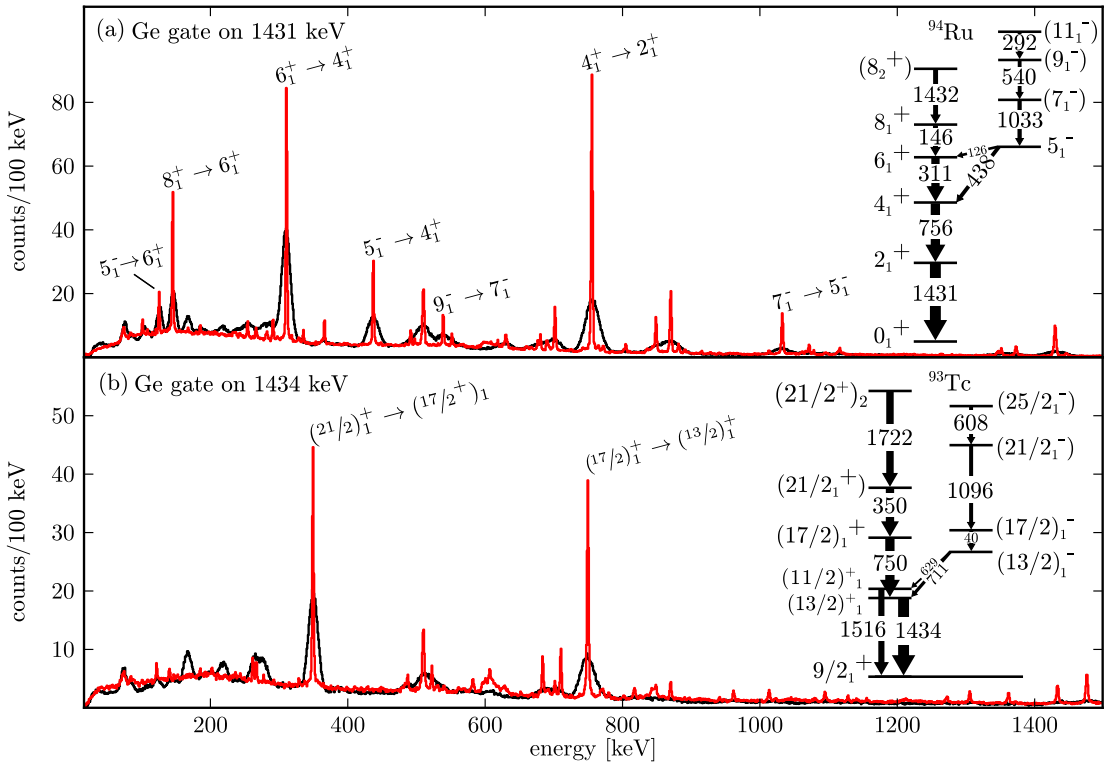

FIG. 1. Coincidence spectra and partial level schemes for ^{94}Ru (a) and ^{93}Tc (b) showing important states and transitions used in the analysis. The transition energies in the level schemes are given in keV. The black spectra display Ge-LaBr-LaBr coincidences with a Ge cleaning gate on a suitable ground state transition and the red spectra show Ge-Ge-LaBr coincidences with the same Ge cleaning gates. In (a) the Ge gate was set on the 1431 keV and in (b) on the 1434 keV transition. Level scheme partially adopted from Refs. [18,19].

detectors were passively shielded against scattered γ rays using lead sheaths. To record time and pulse height information from the LaBr detectors' photomultiplier tubes, a 500 MHz digitizer, implementing online interpolation constant fraction discrimination (CFD), was used. The use of this digitizer for fast-timing application was extensively studied in Ref. [17]. Figure 1 displays projections of triple-γ coincidences from the Ge and LaBr detector setup for the ^{92}Mo$(\alpha, 2n)^{94}$Ru and the ^{90}Zr$(^{6}$Li$, 3n)^{93}$Tc reaction alongside the respective low-energy level schemes for ^{94}Ru and ^{93}Tc. The lifetimes were measured using the fast-timing method, which is based on the direct measurement of the time difference between the population and depopulation of an excited state. In this case, it is done by measuring the time difference between the feeding and decaying γ rays. This allows the measurement of lifetimes down to the range of picoseconds [20,21]. For a detailed description of the analysis procedure using the fast-timing method with a similar setup, please refer to Ref. [9], and for the fast-timing method in general please refer to Refs. [17,21–23]. If the lifetime is much longer than the time resolution of the detector setup, the lifetime is obtained by fitting the exponential tail of the time distribution. An example is shown in Fig. 3(b). Shorter lifetimes are determined using the centroid shift method [24], where the lifetime is deduced from the first moment of the time distribution. The centroid of a time difference spectrum from a particular feeding-decay cascade consists of the lifetime and the energy-dependent γ-γ time walk (TW) of the setup

$$C = \tau + TW(E_{\text{feeder}}, E_{\text{decay}}), \quad (1)$$

$$TW(E_{\text{feeder}}, E_{\text{decay}}) = TW(E_{\text{feeder}}) - TW(E_{\text{decay}}). \quad (2)$$

To obtain the lifetime, the energy dependence of the time walk has to be calibrated by measuring well-known calibration standards. In order to have an optimal coverage of energies, several sources were measured before the experiment. A ^{152}Eu source was used to cover the mid-energy range from 244 to 1299 keV and a ^{133}Ba source was used for the mid-to-low-energy part [25]. To measure lifetimes in both nuclei, a reliable time-walk calibration for energies up to 1434 keV in ^{94}Ru and 1516 keV in ^{93}Tc was required. Since the ^{152}Eu source is not sufficient for this case, two new potential sources for the time-walk calibration were used. The first one is γ rays from ^{214}Po coming from a standard ^{226}Ra source. The recently measured lifetime of the 2_1^+ in ^{214}Po [26] allows the use of this source for the time-walk calibration in the range of 609–1509 keV. The other standard was an in-beam time-walk calibration using γ rays from the decay of excited states in ^{92}Mo. The γ rays from ^{92}Mo are well suited for this purpose, since their energies 244, 330, 773, and 1510 keV match with the most prominent γ rays from the ^{152}Eu source, but extend the range up to 1510 keV. Furthermore, the relevant lifetimes of the first excited 2^+ and 4^+ are known with sufficiently low uncertainties [9]. The states in ^{92}Mo were populated using the

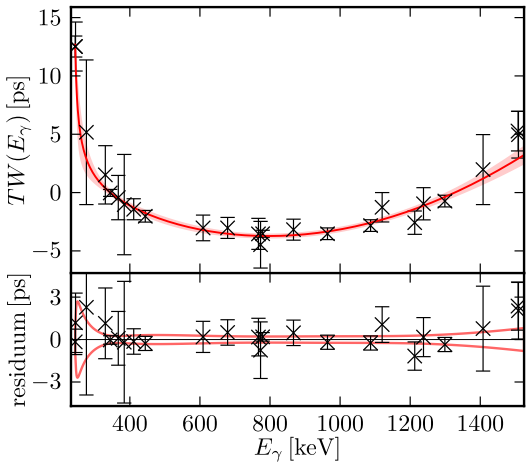

FIG. 2. Calibrated mean time-walk characteristic of the detector setup. Data from ^{152}Eu, ^{133}Ba, ^{226}Ra sources and from ^{92}Mo populated in-beam using the ^{93}Nb$(p, 2n)$ ^{92}Mo reaction. The lower panel shows the residual of the fit and the 1σ uncertainty interval.

^{93}Nb$(p, 2n)$ ^{92}Mo reaction, with a beam energy of 17 MeV and a 5.4 mg/cm^2 thick target of natural Nb. This reaction has some significant advantages in comparison to others. Beam and target are easy to obtain, since natural Nb is monoisotopic. The estimated reaction cross section at this energy is 800 mbarn [27] with no significant other reaction channels, and since ^{92}Mo is stable, the spectrum is free from contamination caused by potential decay products. Because the population of high-spin states is less likely in the reaction, the 244 keV transition in ^{92}Mo is not disturbed by the 235 keV $11^-_1 \rightarrow 9^-_1$ transition. The resulting data points are fitted using the function

$$TW(E_\gamma) = \frac{a}{\sqrt{E_\gamma + b}} + E_\gamma^2\, c + E_\gamma\, d + e. \tag{3}$$

In Fig. 2 the combined time walk from the ^{152}Eu, ^{226}Ra, and ^{133}Ba source measurements and the ^{92}Mo in-beam data is shown for the relevant energy region. The maximum range of the time-walk curve amounts to less than 20 ps in the range between 244 and 1516 keV.

III. ANALYSIS

In the following, the measurement of the first excited 4^+_1 state in ^{94}Ru is shown exemplarily for the analysis procedure using the centroid shift method. If not explicitly marked in Table I, the analysis of further states was performed analogously. Similarly to the procedure in Ref. [9], the analysis was done using a threefold multiplicity condition with exactly two LaBr detectors and one Ge detector within a coincidence window of 400 ns. By requiring an additional coincidence window of 10 ns explicit for the LaBr-LaBr timing the data can be improved and the peak-to-background ratios (P/B) are optimized, because the amount of disturbing random coincidences, which occur in the 400 ns window, are minimized. Figure 3(a) shows the resulting time difference spectrum after gating on the 311 keV feeder and 756 keV decay transitions in the LaBr spectrum combined with a narrow Ge gate on the 1431 keV transition. The time spectrum has almost no random background and the centroid was determined to be 70.7(17) ps. Figures 4(a) and 4(b) display the peak-to-background ratios from feeder and decay transitions. The respective Ge-Ge-LaBr coincidence spectra (red) in Figs. 4(a) and 4(b) confirm the absence of contaminating transitions within the LaBr peaks. To correct the influence of the Compton background beneath the peaks of interest, a background correction procedure was applied, as described in Ref. [25]. The pure peak versus peak centroid C_{PP} is obtained from the uncorrected centroid C_{expt}, the interpolated centroids of the Compton background under the peaks C_{BG}, and the respective peak-to-background ratios $P/B(E)$ using Eqs. (4)–(6):

$$C_{\mathrm{PP}} = C_{\mathrm{expt}} + \tilde{t}_{\mathrm{cor}}, \tag{4}$$

$$\tilde{t}_{\mathrm{cor}} = \frac{P/B(E_d)\, t_{\mathrm{cor}}(E_f) + P/B(E_f)\, t_{\mathrm{cor}}(E_d)}{P/B(E_f) + P/B(E_d)}, \tag{5}$$

$$t_{\mathrm{cor}} = \frac{C_{\mathrm{expt}} - C_{\mathrm{BG}}(E)}{P/B(E)}, \tag{6}$$

with E_f and E_d being the energies of feeder and decay transitions. The P/B from feeder and decay transitions are obtained from the energy projections after gating on the decay or feeder transition, respectively. Since there is currently no way to distinguish between the full energy events and Compton-scattered events with the same energy deposition in the detector, the centroid of the Compton background under the peak C_{BG} cannot be measured directly, but is estimated via interpolation of the peak versus background time response in the proximity of the respective full energy peaks. Figure 4 shows the background correction procedure exemplarily for the 4^+_1 state in ^{94}Ru using the 311–756 keV cascade. In Figs. 4(a) and 4(b) the energy projections for the determination of the P/B are shown. In Figs. 4(c) and 4(d) the interpolation procedure used to obtain the C_{BG} components from feeder and decay transitions are shown. This results in a lifetime of $\tau_{4^+} = 66(2)$ ps, which was also confirmed by using the 438 keV feeding transition from the 5^-_1 state resulting in the lifetime $\tau_{4^+} = 65(4)$ ps. The adopted lifetime is located between the two currently known literature values of 32(11) ps from Ref. [8] and 87(8) ps from Ref. [10].

The results from all measured lifetimes in ^{94}Ru, ^{93}Tc, and ^{91}Nb are listed in Table I. The remeasured lifetimes for the first excited 2^+_1, 6^+_1, and 10^+_1 states match the previous known literature values well within the 1σ uncertainty. The measurement of the first excited 5^-_1 state deviates from the literature value by a factor of almost 2. The lifetime was determined by fitting the exponential slope, which is shown in Fig. 3(b) for the 1033–126 keV cascade. To increase the statistics, matrices with multiple Ge gates have been added, which is analogous to applying a logical OR condition for the Ge gates on the 311, 756, and 1431 keV transitions. The lifetime was also measured using the 1033–438 keV cascade. The two values overlap within a 2σ interval and since they are obtained from strictly independent events the weighted average $\tau_{5^-} = 1240(30)$ ps was chosen as the adopted value. The previously unknown lifetimes of the 7^-_1 and 9^-_1 states were measured to be an upper limit of $\leqslant 5$ ps and 139(8) ps,

TABLE I. Summary of the measured mean lifetimes of states J^π in the $N = 50$ isotones. The italic numbers in the table are used to emphasize adopted values.

Nucleus	State J^π	E_{state} (keV)	Cascade (keV)	Ge gate (keV)	P/B (feeder − decay)	τ_{expt} (ps)	τ_{adopted} (ps)	$\tau_{\text{literature}}$ (ps)
^{94}Ru	2_1^+	1431	756–1431	311	60.1(2) − 67.2(2)	$\leqslant$2	$\leqslant$2	0.8(4) [10]
	4_1^+	2187	311–756 438–756	1431	24.2(2) − 41.8(4) 10.3(3) − 10.4(2)	66(2) 65(4)	*66(2)*[a]	32(11) [8] 87(8) [10]
	6_1^+	2498	146–311	756, 1431[b]	5.58(3) − 7.24(4)	95.5(6) × 10^3[c]	95.5(6) × 10^3	94(3) × 10^3 [18]
	10_1^+	3991	498–1347	1079	12(1) − 11(1)	$\leqslant$13[d]	$\leqslant$13	<5 [28]
	5_1^-	2624	1033–438 1033–126	756, 1431[b] 311, 756, 1431[b]	2.05(5) − 3.05(7) 2.32(5) − 1.96(4)	1170(40)[c] 1300(40)[c]	*1240(30)*[a]	731(67) [28]
	7_1^-	3658	540–1033	438, 756, 1431[b]	5.2(2) − 5.7(2)	$\leqslant$5	$\leqslant$5	–
	9_1^-	4197	292–540	438, 1033[b]	2.42(7) − 3.42(9)	139(8)	*139(8)*	–
	11_1^-	4489	1079–498	1347	4.5(4) − 2.9(2)	900(100)[c]	*900(100)*	1097(50) [28]
^{93}Tc	$(11/2)_1^+$	1516	629–1516	–	2.17(2) − 3.45(2)	2(2)	$\leqslant$4	–
	$(13/2)_1^+$	1434	750–1434	350 –	15.0(4) − 12.8(3) 6.38(4) − 6.85(4)	2(4) 0(1)	$\leqslant$6	<14 × 10^3 [29]
	$(17/2)_1^+$	2185	350–750	1434 –	13.0(3) − 13(2) 5.20(2) − 4.33(2)	30(4) 28(1)	*28(1)*	39(7) [30]
	$(21/2)_1^+$	2535	1722–350	750, 1434[b]	1.31(4) − 4.1(1)	2310(90)[c]	*2310(90)*	2320(80)[a] [31–33]
	$(21/2^-)_1$	3281	608–1096	–	2.84(2) − 3.16(2)	$\leqslant$6	$\leqslant$6	<2 [32]
^{91}Nb	$(17/2)_1^+$	3110	357–819	2291	5.5(4) − 4.5(3)	3(15)[d]	<48	<290 [34]

[a]Weighted average.
[b]Matrices with multiple Ge gates have been added to increase the statistic.
[c]Determined by fitting the exponential slope.
[d]Without background correction.

respectively. The lifetime of the 11_1^- state overlaps with the previously known literature value within a 2σ interval. In ^{93}Tc the previously unknown lifetime of the $(11/2)_1^+$ state was measured to have an upper limit of $\leqslant$ 4 ps and for the $(13/2)_1^+$ state the upper limit was lowered from the previous limit of $<14 \times 10^3$ ps down to $\leqslant$6 ps. The lifetime of the $(17/2)_1^+$ state was measured with LaBr-LaBr-Ge triples and with LaBr-LaBr doubles. The values overlap within the 1σ interval and the result from the LaBr-LaBr doubles is taken as the adopted value. Figure 5 shows the time spectra for the measurements of the $(17/2)_1^+$ and $(13/2)_1^+$ states. The lifetime of the $(21/2)_1^+$ state was measured by fitting the exponential slope and the resulting value confirms the previously known literature value. The lifetime of the $(21/2)_1^-$ state confirms the previously known upper limit.

The ^{90}Zr(^{6}Li, $n\alpha$)^{91}Nb reaction channel was also observed but with a much lower cross section than the $3n$ channel. Therefore, the statistic was only sufficient to measure an upper limit for the $(17/2)_1^+$ state in ^{91}Nb. Due to the low statistic an uncertainty of 3σ was taken for the adopted upper limit.

IV. DISCUSSION

The measured lifetimes are used to calculate the reduced transition probabilities $B(\sigma\lambda)$ for the known transitions. The results for ^{94}Ru, ^{93}Tc, and ^{91}Nb are listed in Table II. The transition energies were taken from Refs. [18,19,36] and the total conversion coefficients were calculated using the program BrIcc [40]. Table II also shows the theoretical predictions from the single-j approximation from Ref. [9]. Two values are given for the single-j approximation. The first one was obtained using a constant effective charge for the one-body transition operator, derived from the quadrupole moment of the $9/2^+$ ground state of ^{91}Nb, and the second is obtained using state-dependent effective charges, derived from fitting the experimental data of the two-nucleon system, namely ^{92}Mo. The values that use a constant effective charge are labeled $T_1(E2)$ and the values that use state-dependent effective charges are labeled $T_1'(E2)$. Also shown in Table II are the results of shell-model calculations performed using the program NuShellX@MSU [41], with the SR88MHJM [1,42] interaction and a $\pi(1p_{1/2}, 0g_{9/2})$ model space for the protons. The

TABLE II. Reduced transition probabilities $B(\sigma\lambda)$ calculated from the adopted experimental values, literature values for experimental $B(\sigma\lambda)$, theoretical predictions from the single-j approximation using a one-body transition operator with constant effective charge $T_1(E2)$ or state-dependent effective charges $T_1'(E2)$, and results from shell-model calculations using a $\pi(1p_{1/2}, 0g_{9/2})$ model space. All $B(E2)$ transition probabilities are given in units of e^2 fm^4 and $B(E1)$ in e^2 fm^2. The branching ratios were derived using intensities from Refs. [18,35,36].

Nucleus	Transition $J_i^{\pi_i} \to J_f^{\pi_f}$	E_γ (keV)	$\sigma\lambda$	$B(\sigma\lambda; J_i^{\pi_i} \to J_f^{\pi_f})$ adopted	$B(\sigma\lambda; J_i^{\pi_i} \to J_f^{\pi_f})$ literature	$B(E2)$ single-j [9] $\hat{T}_1(E2)$ | $\hat{T}_1'(E2)$	Shell-model $B(E2)$ SR88MHJM
^{94}Ru	$2_1^+ \to 0_1^+$	1431	(E2)	$\geqslant$68	165(80) [10]	136 | 186(4)	177
	$4_1^+ \to 2_1^+$	756	(E2)	50(2)	38(3), 103(24) [10], [8]	12 | 7.8(7)	7.4
	$6_1^+ \to 4_1^+$	311	E2	2.85(2)	3.0(2) [8]	8.0 | $3.9^{+0.5}_{-0.4}$	4.6
	$8_1^+ \to 6_1^+$	146	E2	–	0.09(1) [37,38]	3.2 | 1.0(2)	1.5
	$(10)_1^+ \to 8_1^+$	1347	E2	$\geqslant$14	$\geqslant$37[a]	105 | 147(3)	134
	$5_1^- \to 6_1^+$	126	E1	$7.7(3) \times 10^{-5}$	$13.3(15) \times 10^{-5}$ [18]	–	–
	$5_1^- \to 4_1^+$	438	E1	$4.05(12) \times 10^{-6}$	$6.9(8) \times 10^{-6}$ [18]	–	–
	$(7^-)_1 \to 5_1^-$	1033	(E2)	$\geqslant$139[b]	–	–	178
	$(9)_1^- \to (8^+)_2$	267	(E1)	$2.4(2) \times 10^{-5}$[c]	–	–	–
	$(9)_1^- \to (7^-)_1$	540	(E2)	98(6)[b]	–	–	7×10^{-8}
	$(9)_1^- \to 8_1^+$	1553	(E1)	$1.5(1) \times 10^{-7}$[c]	–	–	–
	$(11)_1^- \to (9)_2^-$	151	E2	128^{+25}_{-22}	107(18) [18]	–	182
	$(11)_1^- \to (9)_1^-$	292	E2	134^{+17}_{-13}	111(5) [18]	–	6×10^{-8}
	$(11)_1^- \to (10)_1^+$	498	E1	$3.8(5) \times 10^{-6}$	$3.1(3) \times 10^{-6}$ [18]	–	–
^{93}Tc	$(11/2)_1^+ \to (7/2^+)_1$	836	(E2)	$\geqslant$19	–	39 | 63(2)	39
	$(11/2)_1^+ \to 9/2_1^+$	1516	M1+E2	$\geqslant$24[d]	–	59 | 87(3)	78
	$(13/2)_1^+ \to 9/2_1^+$	1434	E2	$\geqslant$22	$\geqslant$0.009 [35]	102 | 166(6)	140
	$(17/2)_1^+ \to (13/2)_1^+$	750	E2	122(5)	88(18) [30]	99 | 114(3)	99
	$(21/2)_1^+ \to (17/2)_1^+$	350	E2	66(3)	66(2)[e]	57 | 61(1)	57
	$(21/2^-)_1 \to (21/2)_1^+$	745	(E1)	$\geqslant 2.7 \times 10^{-6}$[c]	–	–	–
	$(21/2^-)_1 \to (17/2)_1^-$	1096	E2	$\geqslant$84	$\geqslant$250 [35]	–	136
^{91}Nb	$(17/2)_1^+ \to (15/2^-)_1$	450	(E1)	$\geqslant 2 \times 10^{-6}$[c]	$\geqslant 2 \times 10^{-6}$ [36]	–	–
	$(17/2)_1^+ \to (13/2)_1^+$	819	E2	$\geqslant$50	$\geqslant$7 [36]	–	130

[a]Calculated using upper limit from Ref. [28].
[b]Limit assuming a pure $E2$ transition; this is also taken into account for the $B(\sigma\lambda)$ calculation of further decays from the same state.
[c]Limit assuming a pure $E1$ transition; this is also taken into account for the $B(\sigma\lambda)$ calculation of further decays from the same state.
[d]Mixing ratio $\delta = -16.6^{+21}_{-29}$ from Ref. [39].
[e]Calculated using the weighted average from Table I.

shell-model calculations were performed using the effective proton charge $e^{\pi}_{\text{eff}} = 1.5e$. The choice for the effective charge was motivated by the findings of Ref. [43]. In contrast to the single-j approximation, the shell-model calculations also make predictions for transitions between states of negative parity, though in this shell-model space $E1$ transition strengths cannot be calculated.

A. ^{93}Tc

In the following the theoretical predictions from the single-j and shell-model calculation are compared with the experimental findings. For the $(11/2)_1^+ \to (7/2^+)_1$ and $(11/2)_1^+ \to 9/2_1^+$ transitions the newly measured upper limit for the lifetime of $(11/2)_1^+$ leads to lower limits for the reduced transition probabilities. The theoretical predictions from the single-j and shell-model calculations agree with the experimental limits. For the $(13/2)_1^+ \to 9/2_1^+$ transition the previously known limit of $\geqslant 0.009\ e^2$ fm^4 was significantly enhanced to $\geqslant 22\ e^2$ fm^4 and the theoretical calculations agree with it. Since all theoretical calculations match the limits, it is not possible to make any statement about the pertinence of using state-dependent effective charges. The newly measured

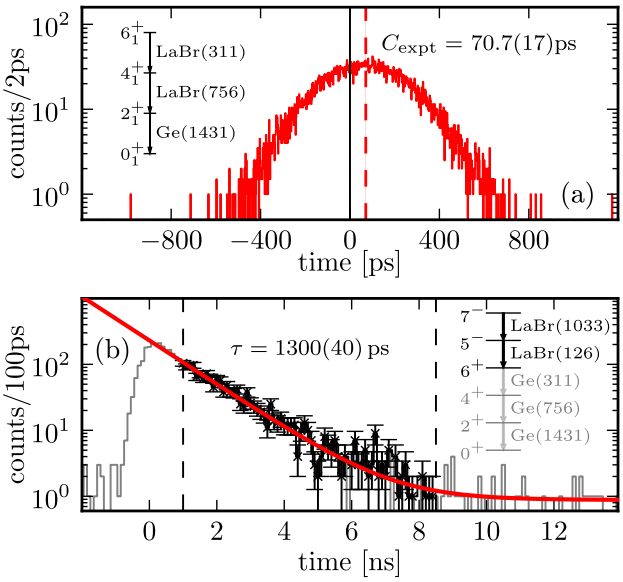

FIG. 3. Time spectra for the lifetime measurement of the 4_1^+ state (a) and for the 5_1^- state (b) in ^{94}Ru. The 4_1^+ state is measured using the centroid shift method using a cleaning Ge gate on the 1431 keV ground state transition and LaBr gates on the 311 keV feeder and 756 keV decay transitions. The centroid of the resulting time spectrum is displayed with a dashed line. The 5_1^- state is measured by fitting the exponential tail. In order to increase the statistics, several Ge cleaning gates with a logical OR condition were used, which is indicated in the level scheme by the gray color.

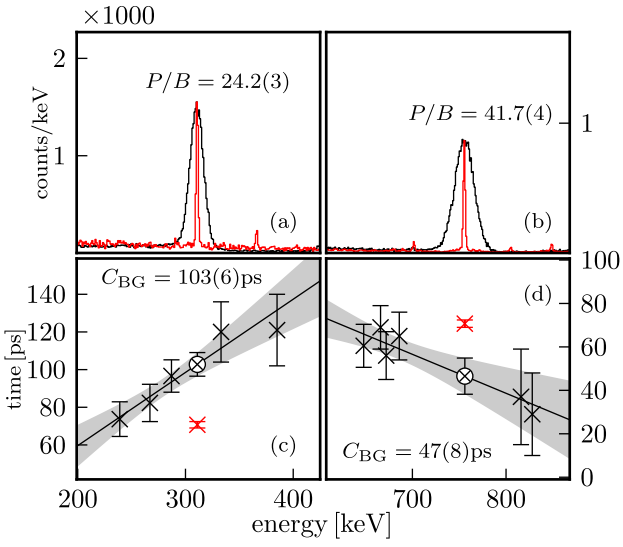

FIG. 4. The background correction procedure for the analysis of the first excited 4_1^+ state in ^{94}Ru. (a) Resulting spectra after gating on the 756 keV decay transition. (b) Respective spectra after gating on the 311 keV feeder transition. The LaBr spectra are shown in black and corresponding gated Ge spectra for monitoring in red. Time response of the Compton background in the proximity of the feeder transition with respect to the decay (c) and vice versa (d). Data from the respective background interpolation (black); the uncorrected centroid C_{expt} is shown in red, and the interpolated centroid C_{BG} is marked with the symbol ⊗.

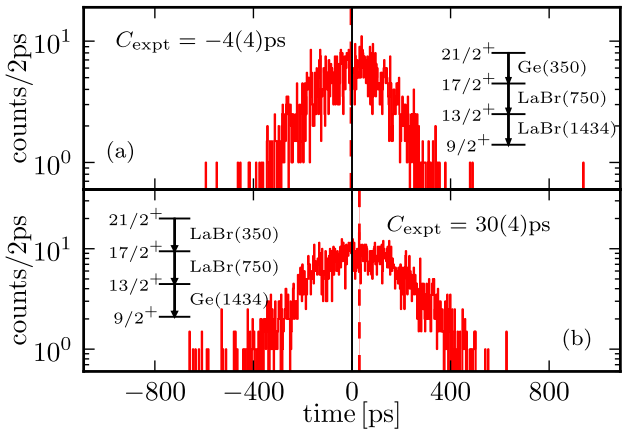

FIG. 5. The resulting time distributions used to measure the lifetimes of the $(13/2)_1^+$ (a) and $(17/2)_1^+$ (b) states. The respective centroid of the distributions is indicated by a dashed line. The reduced level schemes show information on the applied gates.

$B(E2)$ value for the $(17/2)_1^+ \rightarrow (13/2^+)_1$ transition is 122(5) e^2 fm^4, which is consistent with the single-j calculation using state-dependent effective charges. The best prediction for the $(21/2)_1^+ \rightarrow (17/2^+)_1$ transition is obtained for the single-j calculation with state-dependent effective charges. For the $(21/2)_1^- \rightarrow (17/2^-)_1$ transition the shell-model calculation is consistent with the newly measured limit of $\geqslant 84$ e^2 fm^4.

B. ^{94}Ru

The lower limit for the transition probability of the $2_1^+ \rightarrow 0_1^+$ transition is in agreement with the literature value. The theoretical predictions from single-j and shell-model calculations generally agree with the experimental values with some exceptions. Due to the large experimental uncertainty no statement can be made about the choice of different effective charges. The newly measured transition probability of the $4_1^+ \rightarrow 2_1^+$ transition is 50(2) e^2 fm^4. This value is in between the recent experimental findings of 103(24) e^2 fm^4 [8] and 38(3) e^2 fm^4 [10]. The theoretical predictions cannot reproduce any of these experimental values and will be discussed in more detail later in the text. For the $6_1^+ \rightarrow 4_1^+$ the single-j and shell-model calculations only slightly overestimate the measured transition probability. The predicted $B(E2)$ values for the $(10)_1^+ \rightarrow 8_1^+$ and the $(7)_1^- \rightarrow 5_1^-$ transitions are in agreement with the experimental limits. The shell-model transition strengths from $(11)_1^-$ to $(9)_{1,2}^-$ and from $(9)_{1,2}^-$ to 7_1^- are not matching the experimental results. While the $(11)_1^- \rightarrow (9)_1^-$ is calculated to be nearly zero, the $(11)_1^- \rightarrow (9)_2^-$ $E2$ is nearly equal to the sum of the experimental $E2$ strengths from $(11)_1^-$ to $(9)_1^-$ and to $(9)_2^-$. This suggests that the calculated pure configurations of shell-model (SM) $(9)_1^-$ and $(9)_2^-$ should be mixed with roughly equal amounts to reproduce the experimental $(11)_1^-$ to $(9)_{1,2}^-$ strengths. The same conclusion is suggested when comparing the experimentally measured $B(E2)$ for the $(9)_1^- \rightarrow 7_1^-$ state with the SM calculations. The SM $E2$ strength for $(9)_1^-$ to 7_1^- is calculated to be practically zero, while for $(9)_2^-$ to 7_1^- SM predicts $B(E2) = 221$ e^2 fm^4. Again, a mixed SM $(9)_1^-$ state with

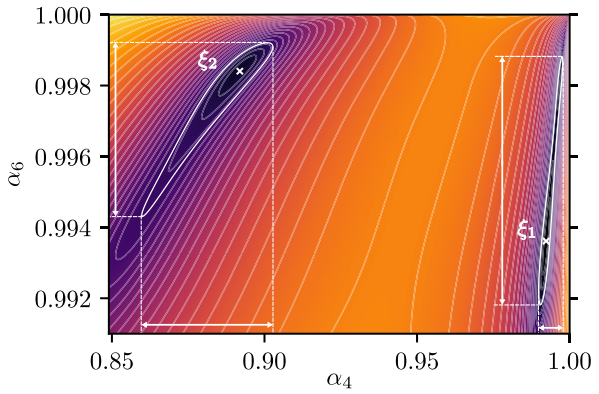

FIG. 6. Surface plot showing the two minima in the χ^2 minimization. For illustrative purposes the heat map color is in logarithmic scale. The minima are marked with crosses. See text for further details.

about half of the original configuration should carry about half of the SM $B(E2)$ strength, i.e., about $B(E2) = 110\ e^2\,\mathrm{fm}^4$, which is nearly equal to the experimentally observed $B(E2) = 98(6)\ e^2\,\mathrm{fm}^4$. As also observed in Refs. [5,8,10] the reduced transition probabilities for the $2_1^+ \to 0_1^+$, $6_1^+ \to 4_1^+$, and $8_1^+ \to 6_1^+$ transitions follow the pattern expected from a single-j system when the proton Fermi level approaches the middle of the $\pi g_{9/2}$ subshell. The seniority-changing transition $2_1^+ \to 0_1^+$ with $\Delta\upsilon = 2$ is relatively enhanced and the $\Delta\upsilon = 0$ transitions are largely suppressed. For the single-j calculation, the best agreement with the experimental data is obtained using state-dependent effective charges and the shell-model calculation with the effective charge $e^{\pi}_{\mathrm{eff}} = 1.5$ produces similar results. The newly measured $B(E2; 4_1^+ \to 2_1^+) = 50(2)\ e^2\,\mathrm{fm}^4$ deviates strongly from the prediction, however. Other experimental findings are $103(24)\ e^2\,\mathrm{fm}^4$ [8] and $38(3)\ e^2\,\mathrm{fm}^4$ [10]. All values are significantly larger than the theoretical predictions in Table II. In Refs. [8,12] this behavior is explained due to mixing of $\upsilon = 2$ and $\upsilon = 4$ states, which is induced by cross-orbital nondiagonal matrix elements of the two-body interaction. The single-j calculation cannot reproduce any of the three experimental $B(E2; 4_1^+ \to 2_1^+)$ values in ^{94}Ru, but it allows us to derive $\upsilon = 2$ and $\upsilon = 4$ admixtures for the 4_1^+ and 6_1^+ states by assuming *ad hoc* mixing:

$$|4_1^+\rangle = \alpha_4|4^+_{\upsilon=2}\rangle + \beta_4|4^+_{\upsilon=4}\rangle,$$
$$|6_1^+\rangle = \alpha_6|6^+_{\upsilon=2}\rangle + \beta_6|6^+_{\upsilon=4}\rangle, \qquad (7)$$

with $\alpha_i^2 + \beta_i^2 = 1$. In Ref. [9] the admixtures (α_i, β_i) are adjusted to minimize a χ^2 cost function, which is the deviation between the calculated and experimental $B(E2)$ values in the $8_1^+ \to 6_1^+ \to 4_1^+ \to 2_1^+$ cascade. Reasonable agreement is obtained when using the previously known $B(E2)$ values [8,10]. Proceeding in the same way using $B(E2; 4_1^+ \to 2_1^+) = 50(2)\ e^2\,\mathrm{fm}^4$ and $B(E2; 6_1^+ \to 4_1^+) = 2.85(2)\ e^2\,\mathrm{fm}^4$, one finds that the χ^2 function has two minima. Figure 6 illustrates the two minima ξ_1 and ξ_2 in the χ^2 plot, with ξ_1 being the minimum with the smallest χ^2. The first minimum ξ_1 is obtained with the admixtures $(\alpha_4, \beta_4) = (0.992, -0.126)$ and $(\alpha_6, \beta_6) = (0.994, -0.113)$, which reproduces the $8_1^+ \to 6_1^+$ and $6_1^+ \to 4_1^+$ transition in good agreement while underestimating the $4_1^+ \to 2_1^+$ transition with $B(E2) = 21^{+2}_{-7}\ e^2\,\mathrm{fm}^4$. The second minimum ξ_2 corresponds to the admixtures $(\alpha_4, \beta_4) = (0.892, -0.452)$ and $(\alpha_6, \beta_6) = (0.998, -0.056)$, which also reproduces the $8_1^+ \to 6_1^+ \to 4_1^+$ transition in good agreement, but overestimates the $4_1^+ \to 2_1^+$ transition with $B(E2) = 86^{+15}_{-5}\ e^2\,\mathrm{fm}^4$. The uncertainties have been estimated by taking the extremal $B(E2)$ when using α_4 and α_6 combinations having a χ^2 lower than $\chi^2_{\mathrm{min}} + \chi^2_{\mathrm{pdf}}$, with χ^2_{pdf} being the χ^2 per degree of freedom. Since for both minima χ^2_{pdf} is larger than 1, this was chosen instead of $\chi^2_{\mathrm{min}} + 1$ to include the external error and thus quality of the fit. In Fig. 6 both $\chi^2_{\mathrm{min}} + \chi^2_{\mathrm{pdf}}$ levels are displayed with the thick contour lines around the minima. In Table III the $B(E2)$ values for both minima are listed together with the results from a large-scale shell model calculation presented in Ref. [5]. One can see that the second minimum ξ_2 of the mixing gives the same $B(E2; 4_1^+ \to 2_1^+)$ as the calculation from Ref. [5]. However, the *ad hoc* mixing cannot reproduce all experimental $B(E2)$ values in the $8_1^+ \to 6_1^+ \to 4_1^+ \to 2_1^+$ cascade simultaneously.

TABLE III. Resulting $B(E2)$ values in units of $e^2\,\mathrm{fm}^4$ for the two minima $\xi_{1,2}$ and results from a large-scale shell model calculation in the $(0g, 1d, 2s)$ proton-neutron model space [5].

Transition	ξ_1	ξ_2	Expt. $B(E2)$	SM $B(E2)$ [5]
$4_1^+ \to 2_1^+$	21^{+2}_{-7}	86^{+15}_{-5}	50(2)	85.2
$6_1^+ \to 4_1^+$	$2.8^{+0.3}_{-0.3}$	$2.8^{+0.4}_{-0.4}$	2.85(2)	17.3
$8_1^+ \to 6_1^+$	$0.11^{+0.14}_{-0.11}$	$0.12^{+0.17}_{-0.12}$	0.09(1)	0.77

V. CONCLUSION

Lifetimes of excited states in ^{94}Ru, ^{93}Tc, and ^{91}Nb were measured and used to calculate reduced transition probabilities. The data are compared with the results from a single-j approximation using state-dependent effective charges obtained from ^{92}Mo and with shell-model calculations in the $\pi(1p_{1/2}, 0g_{9/2})$ space. For ^{93}Tc the theoretical predictions match the experimental findings to a reasonable degree, but the lifetimes of the $(11/2)_1^+$, $(13/2)_1^+$, and $(21/2^-)_1$ states are below the sensitivity limit of the applied fast-timing method. Assuming that the theoretical predictions are approximately adequate, one can make an estimate for the expected lifetimes. For the $(11/2)_1^+$ and $(13/2)_1^+$ states these are of the order of 1 ps, which should be reachable using the Doppler-shift attenuation method. For ^{94}Ru, the lifetime for the $4_1^+ \to 2_1^+$ transition was measured with high statistics and large P/B, leading to a high degree of confidence in the new experimental value. However, since the result is in the middle between two other recent experimental results [8,10], it should be confirmed by another independent experiment to clarify the issue.

ACKNOWLEDGMENTS

We acknowledge the Deutsche Forschungsgemeinschaft (DFG) for the upgrade of the used germanium detectors

under Grant No. INST 216/988-1 FUGG. M.L. acknowledges the financial support of the DFG under Grant No. JOL 391/18-2. A.E. acknowledges the support by the BMBF under Grant No. 05P15PKFNA and the DFG under Grant No. JO 391/20-1. J.J. acknowledges support by GANIL for an extended stay there. Support of the University of Cologne in operating the Tandem accelerator is acknowledged.

[1] T. Faestermann, M. Górska, and H. Grawe, Prog. Part. Nucl. Phys. **69**, 85 (2013).
[2] A. Escuderos and L. Zamick, Phys. Rev. C **73**, 044302 (2006).
[3] P. Van Isacker and S. Heinze, Phys. Rev. Lett. **100**, 052501 (2008).
[4] P. Van Isacker and S. Heinze, Ann. Phys. **349**, 73 (2014).
[5] H. Mach *et al.*, Phys. Rev. C **95**, 014313 (2017).
[6] G. Racah, Phys. Rev. **63**, 367 (1943).
[7] R. Lawson, *Theory of the Nuclear Shell Model* (Clarendon Press, Oxford, 1980).
[8] B. Das *et al.*, Phys. Rev. C **105**, L031304 (2022).
[9] M. Ley *et al.*, Phys. Rev. C **108**, 064313 (2023).
[10] R. M. Pérez-Vidal *et al.*, Phys. Rev. Lett. **129**, 112501 (2022).
[11] V. Karayonchev *et al.*, Phys. Rev. C **99**, 024326 (2019).
[12] C. Qi, Phys. Lett. B **773**, 616 (2017).
[13] V. Karayonchev *et al.*, Phys. Rev. C **95**, 034316 (2017).
[14] A. Harter *et al.*, Phys. Rev. C **106**, 024326 (2022).
[15] L. Knafla *et al.*, Phys. Rev. C **102**, 044310 (2020).
[16] M. Stoyanova *et al.*, Phys. Rev. C **100**, 064304 (2019).
[17] A. Harter *et al.*, Nucl. Instrum. Methods Phys. Res., Sect. A **1053**, 168356 (2023).
[18] D. Abriola and A. Sonzogni, Nucl. Data Sheets **107**, 2423 (2006).
[19] C. M. Baglin, Nucl. Data Sheets **70**, 1 (1993).
[20] H. Mach *et al.*, Nucl. Instrum. Methods Phys. Res., Sect. A **280**, 49 (1989).
[21] J.-M. Régis *et al.*, Nucl. Instrum. Methods Phys. Res., Sect. A **622**, 83 (2010).
[22] J.-M. Régis *et al.*, Nucl. Instrum. Methods Phys. Res., Sect. A **726**, 191 (2013).
[23] J.-M. Régis *et al.*, Nucl. Instrum. Methods Phys. Res., Sect. A **897**, 38 (2018).
[24] Z. Bay, Phys. Rev. **77**, 419 (1950).
[25] J.-M. Régis, A. Esmaylzadeh, J. Jolie, V. Karayonchev, L. Knafla, U. Köster, Y. Kim, and E. Strub, Nucl. Instrum. Methods Phys. Res., Sect. A **955**, 163258 (2020).
[26] A. Esmaylzadeh *et al.*, Phys. Rev. C (to be published).
[27] F. Pühlhofer, Nucl. Phys. A **280**, 267 (1977).
[28] A. Jungclaus, D. Kast, K. P. Lieb, C. Teich, M. Weiszflog, T. Härtlein, C. Ender, F. Köck, D. Schwalm, I. P. Johnstone, J. Reif, R. Schwengner, R. Peusquens, A. Dewald, J. Eberth, H. G. Thomas, M. Górska, and H. Grawe, Phys. Rev. C **60**, 014309 (1999).
[29] M. Grecescu, A. Nilsson, and L. Harms-Ringdahl, Nucl. Phys. A **212**, 429 (1973).
[30] C. Broude *et al.*, Z. Phys. A **336**, 133 (1990).
[31] H. A. Roth, S. E. Arnell, D. Foltescu, O. Skeppstedt, J. Blomqvist, A. Nilsson, T. Kuroyanagi, S. Mitarai, and J. Nyberg, Phys. Rev. C **50**, 1330 (1994).
[32] M. Hausmann, A. Jungclaus, E. Galindo, K. P. Lieb, O. Yordanov, I. P. Johnstone, R. Schwengner, A. Dewald, A. Fitzler, O. Möller, G. de Angelis, A. Gadea, T. Martinez, D. R. Napoli, and C. Ur, Phys. Rev. C **68**, 024309 (2003).
[33] W. Schneider, K. Gonsior, and C. Günther, Nucl. Phys. A **249**, 103 (1975).
[34] W. Andrejtscheff, L. Kostov, L. Kostova, P. Petkov, M. Senba, N. Tsoupas, Z. Ding, and C. Tuniz, Nucl. Phys. A **445**, 515 (1985).
[35] C. M. Baglin, Nucl. Data Sheets **112**, 1163 (2011).
[36] C. M. Baglin, Nucl. Data Sheets **114**, 1293 (2013).
[37] O. Häusser *et al.*, Nucl. Phys. A **293**, 248 (1977).
[38] C. Lederer *et al.*, Nucl. Phys. A **169**, 449 (1971).
[39] B. Brown, O. Häusser, T. Faestermann, D. Ward, H. Andrews, and D. Horn, Nucl. Phys. A **306**, 242 (1978).
[40] T. Kibédi *et al.*, Nucl. Instrum. Methods Phys. Res., Sect. A **589**, 202 (2008).
[41] B. Brown and W. Rae, Nucl. Data Sheets **120**, 115 (2014).
[42] O. Kavatsyuk *et al.*, Eur. Phys. J. A **31**, 319 (2007).
[43] H. Grawe *et al.*, Phys. Lett. B **820**, 136591 (2021).

4 | Manuscript I: Lifetime measurement in ^{95}Rh and ^{95}Ru: Investigation of seniority conservation in the $N = 50$ isotones

Lifetime measurements in ^{95}Rh and ^{95}Ru: Investigation of seniority conservation in the $N = 50$ isotones

M. Ley,* J. Jolie, A. Esmaylzadeh, C. Fransen, A. Blazhev, A. Pfeil, J. Fischer, D. Al Daas, R. Burggraf, A. Bohn, S. Dantanarayana, M. Droste, F. Dunkel, A. Karaka, C.-D. Lakenbrink, and F. von Spee
Institut für Kernphysik, Universität zu Köln, Zülpicher Str. 77, D-50937 Köln, Germany

P. Van Isacker
Grand Accélérateur National d'Ions Lourds, CEA/DRF–CNRS/IN2P3, Bvd Henri Becquerel, F-14076 Caen, France
(Dated: June 27, 2025)

Excited states in ^{95}Rh and ^{95}Ru have been populated in fusion-evaporation reactions and their lifetimes have been measured using the fast-timing technique with a setup consisting of LaBr scintillators and high-purity germanium detectors. The resulting lifetimes are used to calculate reduced quadrupole transition probabilities and discussed within the context of seniority conservation in the $1\pi g_{9/2}$ orbital. In contrast to the latest experimental findings, the new experimental data indicate that seniority symmetry is partially conserved in the mid-shell nucleus ^{95}Rh.

I. INTRODUCTION

The concept of seniority plays an important role in understanding nuclear structure, particularly in semi-magic nuclei, where pairing forces dominate and seniority remains approximately conserved. The number of nucleons not coupled into pairs with total angular momentum $J = 0$ is called the quantum number of seniority υ. The conservation of seniority is associated with selection rules that lead to characteristic patterns of the quadrupole transition probabilities and to the formation of seniority isomers. Seniority is strictly conserved only in shells where $j \leq 7/2$ but can be partially conserved for $j > 7/2$. Especially the case of the $j = 9/2$ orbital became subject of recent experimental studies regarding the conservation of seniority [1–8]. In the semi-magic $N = 50$ nuclei between ^{90}Zr and ^{100}Sn the proton configurations are expected to be largely confined to the $g_{9/2}$ orbital, making it an ideal testing ground for the study of seniority conservation. The unique properties of the $g_{9/2}$ orbital, such as its relatively high angular momentum and the resulting complexity of its coupling schemes, make the question of seniority mixing relevant especially for the case of four or six valence protons [9]. In recent experiments [4, 5, 8] an increased quadrupole transition strength for the $4_1^+ \rightarrow 2_1^+$ transition in ^{94}Ru was measured showing deviations from the pure seniority scheme that can be caused by seniority mixing.

A particularly intriguing situation arises at mid-shell, corresponding to a half-filled $g_{9/2}$ orbital with five valence protons. Due to seniority selection rules most of the states theoretically would not mix. The only exception is mixing between the ground state with seniority $\upsilon = 1$ and one excited $J = 9/2$ state with $\upsilon = 5$, but the mixing is expected to be negligible small since the energy difference between them is rather large [9]. Recently, the lifetimes of the $13/2_1^+$ and $17/2_1^+$ states in ^{95}Rh have been measured for the first time [7]. The resulting transition probabilities indicate a very abrupt breakdown of seniority in the mid-shell. This would require theory to make major revision of the nucleon–nucleon interactions in theoretical models or the inclusion of three-body forces [7]. Because these lifetimes have such a large impact on the interpretation of the underlying physics in this region, a further experiment was conducted to verify the previous findings.

II. EXPERIMENT

The states in the nuclei of interest were populated in fusion-evaporation reactions using a 5.5 mg/cm^2 thick target of highly enriched (99.93%) ^{92}Mo and a 36 MeV ^{6}Li beam provided by the Cologne 10 MV FN Tandem accelerator with an average current of 1 pnA over a period of two weeks. The main reaction channel at the given energy is ^{92}Mo(^{6}Li, $2n$p)^{95}Ru with an estimated reaction cross section of 677 mbarn [10]. The states in ^{95}Rh were populated via the ^{92}Mo(^{6}Li, $3n$)^{95}Rh reaction with an estimated reaction cross section of 63 mbarn [10]. Analog to previous experiments [4, 6], the experiment was conducted using the HORUS spectrometer [11] in the fast-timing configuration. The detector setup included ten cerium-doped lanthanum bromide detectors and eight high-purity germanium detectors (hereafter referred to as LaBr and Ge). Six of the LaBr detectors were equipped with bismuth germanium oxide (BGO) anti-Compton shields for active shielding. Lead sheaths were used to shield the remaining LaBr detectors passively against scattered γ rays. The LaBr detector signals were processed using a 500 MHz digitizer [12], implementing online interpolation constant fraction discrimination (CFD) to achieve timestamp information with precision down to picoseconds. Suitable CFD parameters for fast-timing applications were taken from Ref. [13].

The lifetimes were determined using the fast-timing

* Corresponding author: mley@ikp.uni-koeln.de

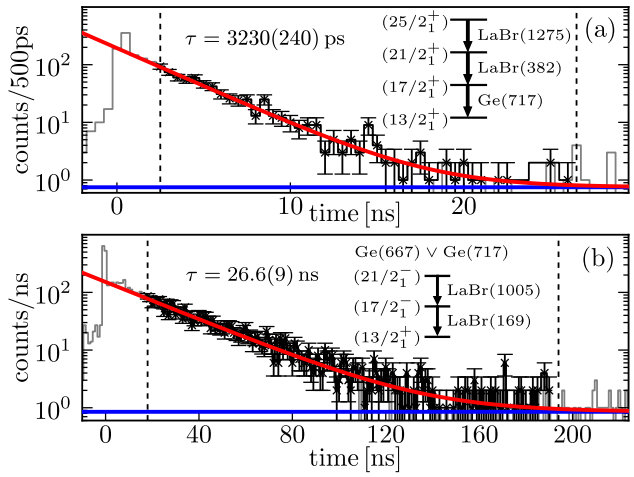

FIG. 1. Time spectra used for the measurement of the lifetime of the $21/2_1^+$ state (a) and for the lifetime of the $17/2_1^-$ state (b) in ^{95}Rh. The fit is shown in red and the level of the value for the random distributed background offset in blue. The fit interval is indicated using the dashed lines. The reduced level schemes show information on the used gates. More details are given in the text.

technique, which is a method based on the direct measurement of the time difference between the population and depopulation of an excited state. In this case, the time difference between the feeding and decaying γ rays is measured. Using the setup above described the measurement of lifetimes down to the range of some picoseconds is possible [13, 14]. For a more detailed description of the fast-timing method in general please refer to Refs. [13–16]. The analysis procedure using a setup similar to the one used in this work can be found in Refs. [4, 6]. Lifetimes much longer than the time resolution of the detector setup, can simply be obtained by fitting the exponential tail of the time distribution, which is shown in Fig. 1. The term for the level of the randomly distributed background was set to a constant value, which was determined by integration and also as a parameter from the fit, leading to consistent results. States with shorter lifetimes are analyzed using the centroid-shift method [17], where the lifetime is determined from the first moment of the time distribution.

The centroid of a time-difference spectrum of a particular feeding-decay cascade consists of the lifetime and the energy-dependent γ-γ time walk (TW).

$$C = \tau + TW(E_{\text{feeder}}, E_{\text{decay}})\,, \tag{1}$$

$$TW(E_{\text{feeder}}, E_{\text{decay}}) = TW(E_{\text{feeder}}) - TW(E_{\text{decay}})\,. \tag{2}$$

Because the time walk is specific to each detector setup and the used CFD settings, it has to be calibrated for each experiment by measuring well-known calibration standards. To achieve an optimal coverage of energies, three sources were measured before and after the experiment. For the mid-energy range a ^{152}Eu source was used. A ^{226}Ra source was used to cover energies between 609-1510 keV and for the low energies a ^{133}Ba source was used. The recently published values for lifetimes in ^{214}Po and ^{152}Gd were used within the calibration procedure [18–20].

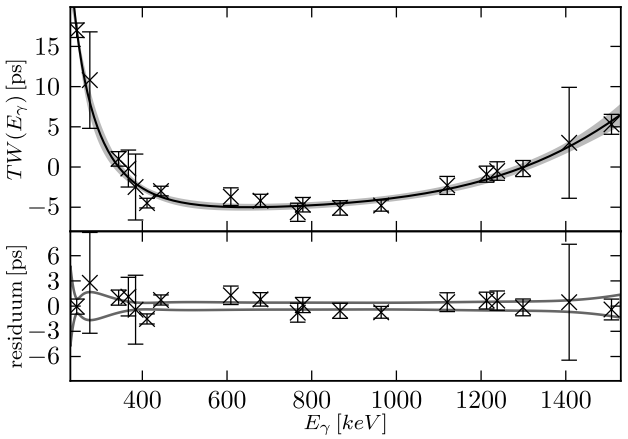

FIG. 2. Calibration of the mean time-walk characteristic of the detector setup. Data points are generated using ^{152}Eu, ^{133}Ba and ^{226}Ra sources. The upper panel shows the fit of Eq. 3 in the region between 244-1510 keV. The fit residual and the 1σ uncertainty interval is shown in the lower panel.

Figure 2 shows the combined time walk and the residuum from the fit of the equation

$$TW(E_\gamma) = \frac{a}{\sqrt{\mathrm{E}_\gamma + \mathrm{b}}} + E_\gamma^2\, c + E_\gamma\, d + e \tag{3}$$

to the data from the source measurements in the range from 244 to 1510 keV. In this range, the maximal time walk is less than 20 ps.

III. ANALYSIS

The primary goal of the experiment was the measurement of lifetimes of excited states in ^{95}Rh. The procedure using the centroid-shift method is explained in detail in the following section for the measurement of the first excited $13/2^+$ state in ^{95}Rh. The analysis of further states measured using the centroid-shift method was performed analogously, if not explicitly marked otherwise in Table I.

A. ^{95}Rh

The analysis was done using a threefold multiplicity condition with exactly two LaBr and one Ge detector signals within a coincidence window of 600 ns. For the analysis using the centroid-shift method, an additional coincidence window of 4 ns explicit for the LaBr-LaBr timing was required. This is essential for the background correction procedure, because the amount of random co-

TABLE I. Summary of the measured mean lifetimes of states J^π in ^{95}Rh, ^{95}Ru, ^{92}Mo, ^{93}Tc and ^{94}Ru along information on the applied gates, P/B ratios of feeder and decay transitions and the known literature values. The italic numbers in the table are used to emphasize adopted values.

nucleus	state J^π	E_{state} keV	cascade keV−keV	Ge gate keV	P/B feeder−decay	τ_{expt} ps	$\tau_{adopted}$ ps	$\tau_{literature}$ ps
^{95}Rh	$13/2_1^+$	1351	717−1351	382, 1275, 1005 [a]	2.70(7)−8.5(2)	−0.1(39)	*≤4*	36(15) [7]
	$17/2_1^+$	2068	382−717 169−717	1275 1005	3.63(13)−3.17(11) 9.7(2)−4.15(8)	140(9) 134(5)	*135(4)* [b]	≤ 26 [7]
	$(21/2_1^+)$	2449	1275−382	717	0.82(4)−1.43(5)	3230(240) [c]	*3230(240)*	3660(320) [21–23]
	$(17/2_1^-)$	2236	1005−169	717, 667 [a]	1.57(3)−4.12(7)	26.6(9)×10^3 [c]	*26.6(9)*×10^3	27.1(14)×10^3 [24, 25]
	$(21/2_1^-)$	3241	667−1005	717, 169 [a]	2.25(5)−1.04(3)	11(5)	*11(5)*	6.6(3) [22]
^{95}Ru	$7/2_1^+$	942	410−942	255 [d], 677 [a]	1.78(3)−2.16(4)	1(6)	*≤7*	—
	$9/2_1^+$	1352	677−1352	255 [d]	26.7(2)−22.19(13)	0(1)	*≤3*	—
	$13/2_1^+$	2030	464−677	281, 283	0.57(4)−1.38(3)	20(20)	*≤40*	—
	$17/2_1^+$	2284	255−677	255 [d]	5.92(2)−6.51(2)	10.25(11)×10^3 [c]	*10.25(11)*×10^3	12.0(14)×10^3 [26] 4.4(4)×10^3 [27]
	$21/2_1^+$	2538	1292−255	255 [d]	2.73(7)−7.52(8)	$11.7^{+0.7}_{-0.4}\times10^3$ [c]	$11.7^{+0.7}_{-0.4}\times10^3$	14.5(2)×10^3 [27]
^{92}Mo	4_1^+	2283	330−773	1510	13.33(9)−34.9(4)	23.5(18)	*23.5(18)*	22.5(11) [6] 35.5(6) [8]
^{93}Tc	$13/2_1^+$	1435	750−1435	350	2.7(2)−3.1(2)	−3(8)	*≤8*	≤4 [4]
	$17/2_1^+$	2185	350−750	1435	4.5(2)−5.1(3)	34(9)	*34(9)*	28(1), 39(7) [4, 28]
^{94}Ru	4_1^+	2187	311−756	1431	19.4(3)−31.1(5)	66(3)	*66(3)*	66(2) [4] 32(11) [5] 87(8) [8]

[a] Matrices with multiple Ge gates have been added to increase the statistic.
[b] Weighted average.
[c] Determined by fitting the exponential slope.
[d] Note that this transition is a coincident doublet in ^{95}Ru.

incidences, which occur within the large 600 ns window might lead to incorrect peak-to-background (P/B) ratios.

In Fig. 3, partial level schemes are displayed for ^{95}Rh and ^{95}Ru, showing the transitions that were used within the analysis. The lifetime of the $13/2_1^+$ state in ^{95}Rh was measured using LaBr gates on the $17/2_1^+ \rightarrow 13/2_1^+ \rightarrow 9/2_{gs}^+$ 717−1351 keV cascade combined with a cleaning Ge gate on a suitable coincident transition namely the 382, 1275 and 1005 keV transitions. Because the $9/2_1^+ \rightarrow 5/2_{gs}^+$ transition in ^{95}Ru has an energy of 1352 keV, the main challenge in measuring the $13/2_1^+$ state in ^{95}Rh was to ensure the absence of ^{95}Ru contamination. Figure 4 (a) shows the full projection of a γ-γ matrix with Ge-Ge events. It can be seen that the spectrum is largely dominated by transitions from ^{95}Ru. Figure 4 (b), (c) and (d) show the effect of setting Ge gates on the 382, 1275 and 1005 keV transitions to select for ^{95}Rh. Note that the spectrum coincident to the Compton background in the proximity of the respective gates was subtracted. The remaining spectra show almost exclusively transitions from ^{95}Rh. Therefore we can conclude that the three gates on the 382, 1275 and 1005 keV transitions are suitable to separate ^{95}Rh from ^{95}Ru and that remaining peaks from ^{95}Ru in the LaBr spectra, like shown in Fig. 5 (a), are the result of the coincident Compton background under the peaks. Because the energy resolution of the LaBr detectors is not sufficient enough to separate

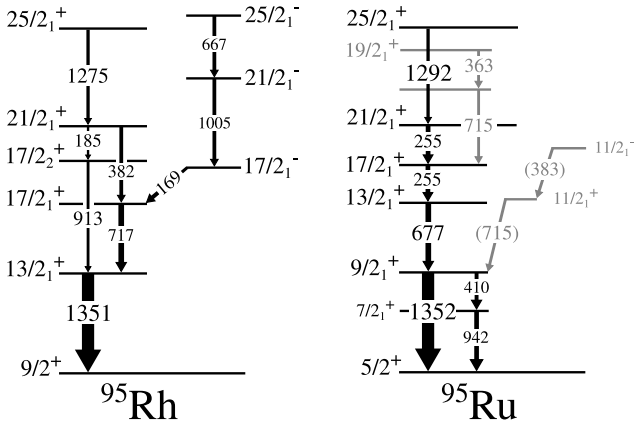

FIG. 3. Reduced level schemes for ^{95}Rh and ^{95}Ru, showing the transitions used for the analysis. Data shown in this figure was taken from Ref. [21]. The transitions shown in grey are the ones only observed in Refs. [27, 29] and the brackets mark the transitions that have been reassigned to belong to ^{95}Rh in the course of this work.

the 1351 and 1352 keV transition, Ge-Ge-LaBr events were used to have the advantage of the much better energy resolution of the resulting Ge spectrum after using a LaBr gate on 717 keV and Ge gates on the 382, 1275 or 1005 keV transitions. In Fig. 6 (b) the resulting spectrum is compared to the spectrum obtained when using a Ge gate on the 255 keV doublet from ^{95}Ru. The expected shift of 1 keV indicates the separation between ^{95}Rh and ^{95}Ru.

Because it is not possible to simply subtract the coincident Compton background when using the centroid-shift method, the influence of the Compton background beneath feeder and decay transitions was corrected using a standard background correction procedure, as described in Ref. [20]. To obtain the pure peak-versus-peak centroid C_{PP} in the procedure the uncorrected centroid C_{expt}, the respective peak-to-background ratios $P/B(E)$ and the interpolated centroids of the Compton background under the peaks C_{BG} are used. The Compton background C_{BG} is not measurable directly, but can be estimated via interpolation of the time response in the proximity of feeder and decay peaks. This is shown for both transitions in Fig. 5. Using Eqs. (4)-(6) one obtains the peak-versus-peak centroid C_{PP}.

$$C_{\mathrm{PP}} = C_{\mathrm{expt}} + \tilde{t}_{\mathrm{cor}}\,, \tag{4}$$

$$\tilde{t}_{\mathrm{cor}} = \frac{P/B(E_d)\,t_{\mathrm{cor}}(E_f) + P/B(E_f)\,t_{\mathrm{cor}}(E_d)}{P/B(E_f) + P/B(E_d)}\,, \tag{5}$$

$$t_{\mathrm{cor}}(E) = \frac{C_{\mathrm{expt}} - C_{\mathrm{BG}}(E)}{P/B(E)}\,, \tag{6}$$

Here E_f and E_d are the energies of feeder and decay transition. The resulting time spectrum after gating on feeder and decay transitions and on the 382, 1275 or 1005 keV transitions with the Ge detectors is shown in Fig. 7 (a) along the uncorrected centroid $\mathrm{C_{expt}}$, the corrected centroid $\mathrm{C_{PP}}$, and the time walk value TW for the feeder-decay combination. The resulting lifetime is $\tau = -0.1(39)$ ps from which we adopt an upper limit of $\tau \leq 4$ ps.

Because the contamination from the ^{95}Ru is rather complex, the following part is intended to prove the validity of the previous analysis for the lifetime of the $13/2^+$ state in ^{95}Rh. Reference [27] reports a $11/2^-_1 \rightarrow 11/2^+_1 \rightarrow 9/2^+_1 \rightarrow 5/2^+_{\mathrm{gs}}$ cascade in ^{95}Ru with the energies 383−715−1352 keV which would make the measurement of the $13/2^+$ state in ^{95}Rh impossible using the 382 keV transition for the Ge gate. The placement of the 383 and 715 keV transition in the level scheme is marked as uncertain in the nuclear data sheets [21]. Since the transitions were observed in a similar experiment using the reaction ^{92}Mo(^{6}Li, $p2n$)^{95}Ru @ 34 MeV and after gating on the 1352 keV ground-state transition we tried to reproduce their findings and came to the conclusion, that the 383 keV transition reported in Ref. [27] is most likely contamination from the ^{92}Mo(^{6}Li, $3n$)^{95}Rh reaction channel and can be identified with the 382 keV transition in ^{95}Rh. In Fig. 4 (b) the projection of the γ-γ matrix from Ge-Ge events is displayed after gating on the 382 keV transition and subtraction of the coincident background. The resulting spectrum shows only transitions from ^{95}Rh and no evidence for the 410 or 942 keV transitions, which would be expected if the 383 keV transition originates from ^{95}Ru, as reported in Ref. [27]. Additionally, in the inset of Fig. 4 (b) the 1 keV shift with respect to the spectrum after gating on the 255 keV peak in ^{95}Ru is displayed, showing the difference between the 1351 and 1352 keV transitions. In Fig. 8 (b) and (c) no remaining 383 keV transition is visible after gating on the 410 or 942 keV transitions, which further emphasizes the hypothesis that this transition has to be reassigned and most likely belongs to ^{95}Rh. Figure 8 (a) shows the projection after gating on the 715/717 keV transition resulting in a spectrum dominated by peaks from ^{95}Rh, again the 1 keV shift in the inset, and the 677 keV $13/2^+_1 \rightarrow 9/2^+_1$ transition from ^{95}Ru, which contradicts the placement of the 715 keV transition in Ref. [27]. Furthermore, when gating on the combined peak of 1351 and 1352 keV a similar intensity for the 715/717 keV peak as reported in Ref. [27] was obtained. Therefore, it was concluded that the 383 keV and most of the 715 keV peak's intensity reported in Ref. [27] originates from the ^{95}Rh.

In Ref. [29], a 715 keV transition is assigned as feeder transition for the $17/2^+_1$ state in ^{95}Ru. This assignment was confirmed in this work using gates on the 363, 255 and 677 keV transitions. However, the influence on the lifetime measurement of the $13/2^+_1$ state is negligible, because the Ge gates on the 382, 1275 and 1005 keV transitions separate ^{95}Rh from ^{95}Ru as already shown in Fig 4. As a further argument, Fig. 6 (a) shows a comparison between the resulting spectra using a Ge gate

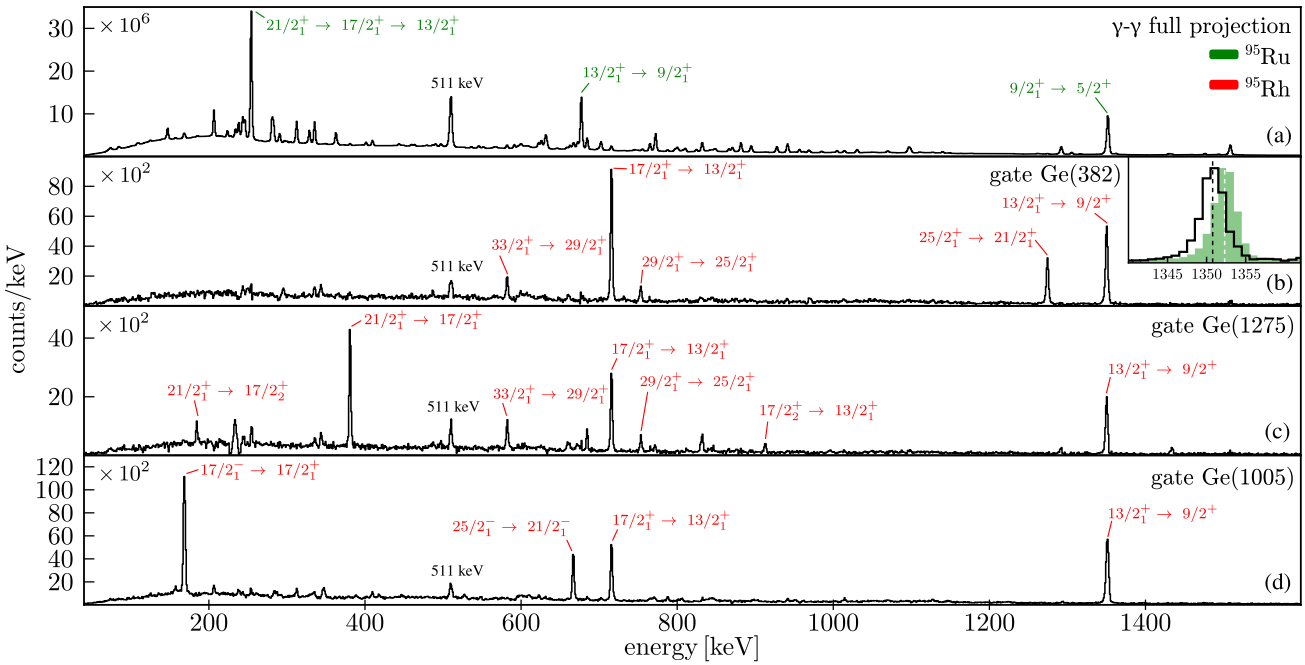

FIG. 4. Projections of a γ-γ matrix from Ge-Ge events to show the effect of Ge gates used to separate ^{95}Rh from ^{95}Ru. A full projection of the γ-γ matrix is shown in (a) where no gate was applied. In (b), (c) and (d) the effect of selective gates on the 382, 1275 and 1005 keV transitions from ^{95}Rh are shown. The inset in (b) displays a comparison between the resulting Ge spectra after using Ge gates on the 382 keV transition (black) and on the 255 keV doublet (green), showing the difference between the 1351 and 1352 keV transitions from ^{95}Rh and ^{95}Ru respectively. Note that the coincidence background was subtracted and the green spectrum in the inset of (b) was scaled for better clarity.

on the 255 keV transition in ^{95}Ru (green) versus a gate on 382 keV in ^{95}Rh (black), each in combination with a LaBr gate on the 1351/1352 keV peak. The green spectrum can be seen here as a worst-case estimate for the contamination from the 715 keV transition. Hence, it can be concluded that the actual amount will be much lower and therefore negligible. Note that the spectra are normalized to the same level of background. Finally, we would like to point out that due to the long lifetime of the $17/2^+_1$ state in ^{95}Ru a contamination with the 715 keV transition would cause the measured value to be longer and therefore the actual lifetime of the $13/2^+_1$ state in ^{95}Rh would be even smaller if there was such kind of contamination.

The lifetime determination of the $17/2^+_1$ state in ^{95}Rh was less complicated, because it was possible to avoid using a gate on the 1351 keV transition. Furthermore, it was possible to measure the lifetime using two different feeder transitions. Because the time walk for the feeder-decay combinations differs, systematic uncertainties of the time walk are minimized. Figure 9 shows the resulting time spectra after gating on the feeder-decay transitions 169−717 keV (a) and 382−717 keV (b) as well as Ge gates on suitable transitions. A slope component is clearly visible on the delayed sides of both time spectra. The results overlap within the uncertainty interval of 1σ and are listed in Table I. Because they are obtained from two strictly independent data subsets, the weighted average of 135(4) ps is taken as adopted value. It was also possible to measure the lifetime of the $21/2^-_1$ state in ^{95}Rh using the 667−1005 keV cascade. The resulting lifetime is 11(5) ps which is consistent with the literature value of 6.6(3) ps [22]. The lifetimes of the $21/2^+_1$ and $17/2^-_1$ states in ^{95}Rh are rather long and therefore are obtained by fitting the exponential tails. In Fig. 1 this is shown for both states leading to lifetimes that confirm the respective literature values (see Table I).

B. ^{95}Ru

The analysis of the ^{95}Ru data was conducted analogously to the analysis of the ^{95}Rh data. Figure 7 (b) shows the resulting time distribution after using LaBr gates on the 677-1352 keV cascade and a Ge gate on the 255 keV doublet. Due to the higher cross section, a large amount of data was generated, which reduced the statistical uncertainties. The resulting value for the lifetime of the $9/2^+_1$ state is 0(1) ps. Because this value is at the very limit of the method, an upper limit of 3 ps is taken as adopted value, which represents an uncertainty of 3σ. Analogously, upper limits were determined for the lifetimes of the $7/2^+_1$ and $13/2^+_1$ states, which are listed in Table I.

The analysis for the $21/2^+_1$ and $17/2^+_1$ state, was more complicated due to the 255 keV doublet. It was possible

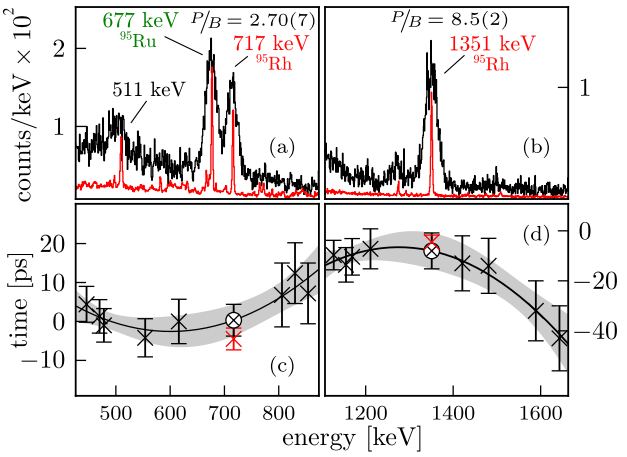

FIG. 5. The background correction procedure for the analysis of the first excited $13/2^+$ state in ^{95}Rh. (a) Resulting Ge and LaBr spectra after gating on the 1351 keV decay transition. (b) Respective spectra after gating on the 717 keV feeder transition. The LaBr spectra are shown in black and corresponding gated Ge spectra for monitoring in red. The Ge spectra have been scaled for better clarity. Time response of the Compton background in the proximity of the feeder transition with respect to the decay (c) and vice versa (d). Data from the respective background interpolation (black); the uncorrected centroid C_{expt} is shown in red, and the interpolated centroid C_{BG} at the energie of interest is marked with the symbol ⊗.

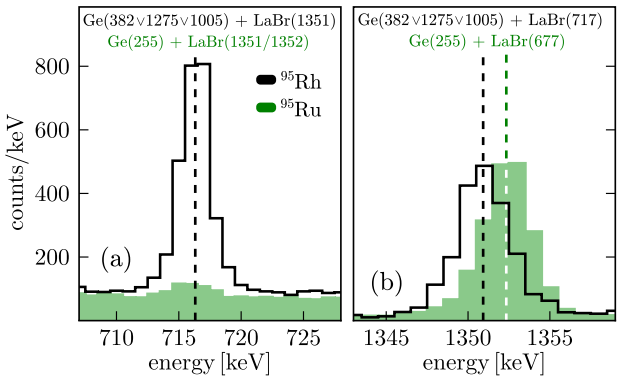

FIG. 6. Comparison for gates selective for ^{95}Rh versus ^{95}Ru. Events with the multiplicity of exactly two Ge and one LaBr were used. The green spectra show the effect of using gates to select for ^{95}Ru. The gate information is shown in the figures in green. In black the resulting spectra are shown after using gates to select for ^{95}Rh which are Ge(382 ∨ 1275 ∨ 1005) + LaBr(1351) for (a) and Ge(382 ∨ 1275 ∨ 1005) + LaBr(717) for (b). The green spectra are scaled to match the same level of background for better clarity. For more information see text.

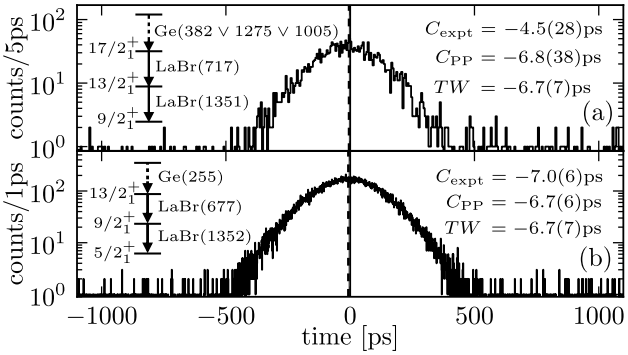

FIG. 7. The resulting time distributions generated to measure the lifetimes of (a) the $13/2^+_1$ in ^{95}Rh and (b) the $9/2^+_1$ state in ^{95}Ru. The reduced level schemes show information on the applied gates and the dashed lines indicate the respective centroid. The total statistic of the time distribution in (a) amounts to 2580 counts and in (b) 56200 counts.

to determine the lifetimes using two different approaches. In Ref. [27] both states were measured simultaneously using a pulsed beam and by fitting the equation

$$f(t) = A_0 + (A_1/\tau_1)e^{-t/\tau_1} + (A_2/\tau_2)e^{-t/\tau_2} + [A_1/(\tau_1-\tau_2)](e^{-t/\tau_1} - e^{-t/\tau_2}) \quad (7)$$

to the spectrum of the differences from both 255 keV transitions with respect to the pulse. The first approach used in this work was similar to the one from Ref. [27] but instead of using a pulse as reference signal, the 1292 keV transition was used as start signal. The time-difference spectrum in Fig. 10 (b) shows the time differences between the 1292 keV feeder transition and both 255 keV transitions. For this purpose, events of exactly one Ge and two LaBr hits within a time window of 1 μs were used. A LaBr gate was used on the 1292 keV transition and the second LaBr gate as well as the Ge gate on the 255 keV doublet.s The resulting time spectrum looks similar to the one in Ref. [27]. The fit and the results for the lifetimes are shown in Fig. 10 (b), where τ_a and τ_b refer to the lifetimes of the $21/2^+_1$ and $17/2^+_1$ states, respectively.

It was also possible to determine both lifetimes in a different way. First, the lifetime of the $13/2^+_1$ state was measured using LaBr gates on the 255-677 keV cascade and an additional Ge gate on the 255 keV transition. Because the lifetime of the $13/2^+_1$ state was measured to be smaller than 40 ps contributions from the $17/2^+_1 \rightarrow 13/2^+_1 \rightarrow 9/2^+_1$ cascade will be only in the prompt part of the time distribution. The resulting spectrum is shown in Fig. 10 (a). The obtained lifetime of the $17/2^+_1$ state is $\tau = 10.25(11)$ ns which is in agreement with the result $\tau_b = 8.6(19)$ ns from the fit of Eq. 7 in Fig. 10 (b). To obtain also the lifetime of the $21/2^+_1$ state, the Eq. 7 was again fitted to the data from Fig. 10 (b) but with the lifetime from the previous slope fit as a constant for $\tau_b \equiv 10.25$ ns. To include the uncertainty of the constant τ_b a Monte Carlo ansatz was used. The fit was performed 10^6 times were the value for the constant τ_b was randomly chosen with a probability normal distributed around 10.25 ns and σ of 0.11 ns for each fit. The distribution of the results for the lifetime is shown in Fig. 10 (c)

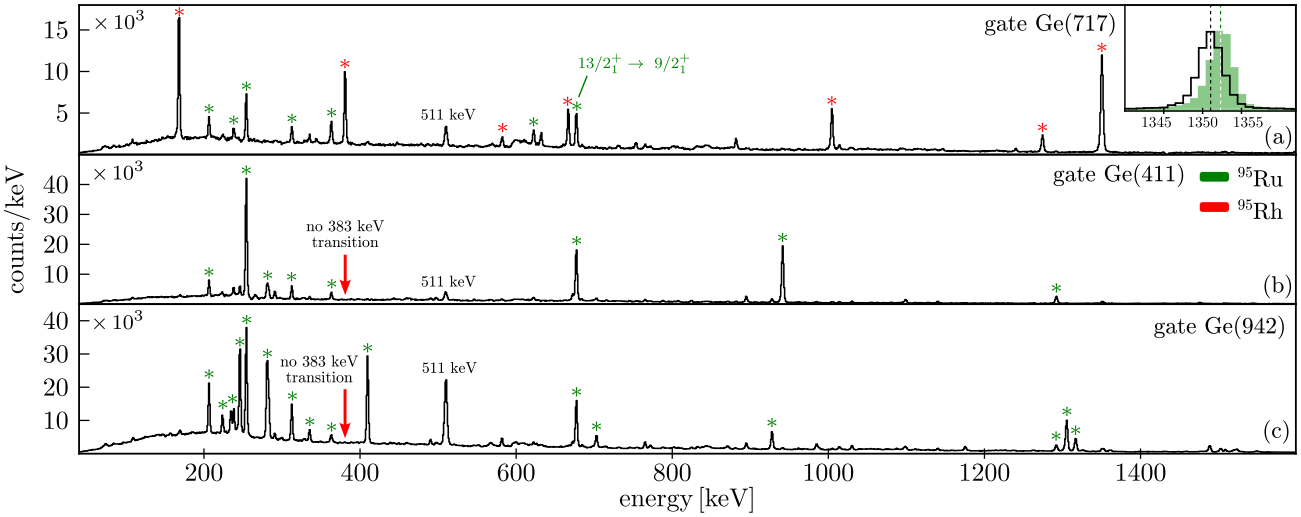

FIG. 8. Projections of γ-γ matrix from Ge-Ge events to clarify the uncertain assignment of the 383 and 715 keV transitions from Ref. [27]. The resulting projection after gating on the 717/715 keV peak is displayed in (a) showing predominantly transitions from ^{95}Rh. The inset in (a) shows the proximity of the region at the 1351 and 1352 keV transitions, in black after gating on the 717 keV transition and in green after gating on the 255 keV doublet. In (b) and (c) the projections after gating on the 410 and 942 keV transitions respectively are shown. In both cases no 383 keV transition was observed.

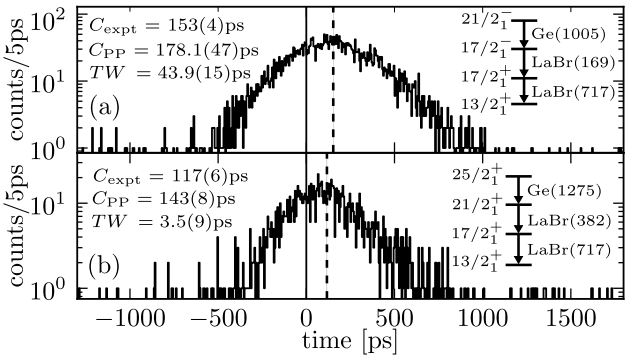

FIG. 9. The resulting time distributions used to measure the lifetime of the $17/2_1^+$ state in ^{95}Rh. The reduced level schemes show information on the applied gates and the dashed lines indicate the respective centroid.

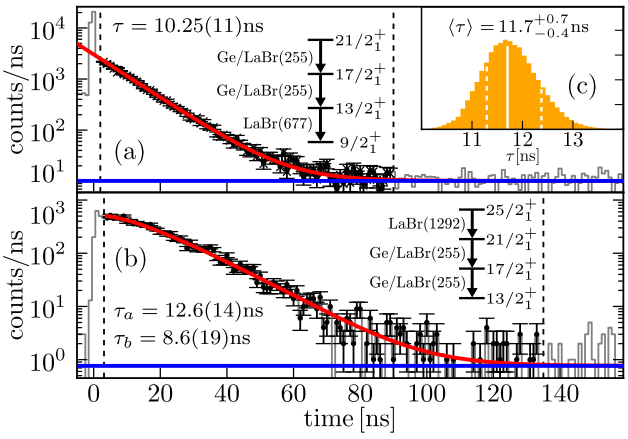

FIG. 10. Time spectra used for the measurement of the lifetimes of the $17/2_1^+$ and $21/2_+^+$ state in ^{95}Ru. The fit of the exponential tail to measure the lifetime of the $17/2_1^+$ state is shown in (a). The fit of Eq. 7 to measure both lifetimes at once is shown in (b). The inlay (c) displays the distribution of results for the determination of the lifetime from the $21/2_+^+$ state using a Monte Carlo method. More details are given in the text.

and the obtained median lifetime was $\langle\tau\rangle = 11.7^{+0.7}_{-0.4}$ ns. This value is also in agreement with the previous result $\tau_a = 12.6(14)$ ns from the fit in Fig. 10 (b). Both methods lead to consistent values for the lifetimes of the $21/2_1^+$ and $17/2_1^+$ state. The results from the later method are taken as adopted values because the fit in Fig. 10 (a) is independent from the lifetime of the $21/2_1^+$ state and consequently the fit for the determination of the second lifetime has less free parameters.

C. ^{92}Mo, ^{93}Tc and ^{94}Ru

Due to further reaction side channels it was possible to analyse some of the by-products to re-measure lifetimes of excited states in ^{92}Mo, ^{93}Tc and ^{94}Ru in order to verify the results of previous measurements [4, 6] on these nuclei. The data for ^{92}Mo and ^{94}Ru was high in statistic and the Ge gate alone was sufficient to select only the respective nucleus of interest, which also results in the very high P/B ratios. The ^{93}Tc nucleus was less populated but still sufficient for the analysis. The results are listed in Table I and support the previous findings from [4, 6].

IV. DISCUSSION

The measured lifetimes are used to calculate the reduced transition probabilities $B(\sigma\lambda)$ for the known transitions in ^{95}Rh and ^{95}Ru. The transition energies and branching ratios were taken from Ref. [21] and the respective total conversion coefficients were calculated using the program BrIcc [30]. The results are listed in Table II alongside literature values and theoretical values from a single-j approximation, with state-dependent effective charges derived from ^{92}Mo [6]. Figure 11 shows a systematic overview of currently known experimental values for reduced quadrupole transition probabilities for the $N = 50$ isotones with valence protons in the $g_{9/2}$ orbital. Results from this work as well as the combined results from Refs. [4, 6] are shown in red. Since the focus of the discussion is on ^{95}Rh, the experimental findings from Ref. [7] on the $B(E2)$ values of the $17/2^+_1 \rightarrow 13/2^+_1 \rightarrow 9/2^+_{gs}$ cascade in ^{95}Rh are emphasised in green, while further experimental data from Refs. [23, 31–55] and the remaining data from Ref. [7] is shown in blue. The characteristic pattern associated with the conservation of seniority would become extremal at mid-shell, which would be the five particle/hole system for the $g_{9/2}$ orbital. For the isotones with $N = 50$ the mid-shell corresponds to the nucleus ^{95}Rh. For the seniority-changing ground-state transition ($\Delta\upsilon = 2$) one would expect the $B(E2)$ transition strength to have a maximum at mid-shell. The upper limit for the lifetime of the $13/2^+_1$ state in ^{95}Rh leads to a lower limit of ≥ 45 e^{2}fm^4 for the reduced transition probability, in agreement with the theory, and indicates that seniority might be partially conserved for the mid-shell case. The lifetime measurement from Ref. [7] on the other hand, finds a lifetime of 36(15) ps for the $13/2^+_1$ state, which results in a strongly suppressed ground-state transition with a small $B(E2)$ value of only $5.0^{+3.6}_{-1.6}$ e^{2}fm^4. As pointed out in Ref. [7] this inhibited transition strength would mean a sudden break of seniority symmetry at mid-shell that cannot be explained by calculations employing standard interactions and would maybe require to include also three-body forces within theoretical calculations.

Interestingly, this deviation continues when considering the results for the $17/2^+_1$ state. The lifetime measured in Ref. [7] is an upper limit of ≤ 26 ps, which leads to a lower limit of ≥ 167 e^{2}fm^4 for the reduced transition probability of the seniority conserving ($\Delta\upsilon = 0$) $17/2^+_1 \rightarrow 13/2^+_1$ transition. This is also conflicting with theoretical calculations. If seniority is conserved along the $g_{9/2}$ orbital one would expect the $\Delta\upsilon = 0$ transitions to be hindered towards mid-shell. The new result of 135(4) ps for the lifetime of the $17/2^+_1$ state, leads to a reduced transition probability of 32(1) e^{2}fm^4 for the $17/2^+_1 \rightarrow 13/2^+_1$ transition. In contrast to the lower limit from Ref. [7], this fits well within the observed trend shown in Fig. 11 and would also support the assumption that seniority is, at least, partially conserved in the mid-shell nucleus ^{95}Rh. The lifetime of the $21/2^+_1$ state was already well-known and thus does not provide new insight, but just a confirmation. Unfortunately, the statistics were not sufficient to also measure the lifetime of the second excited $17/2^+_2$ state.

However, the single-j approximation still significantly underestimates the transition probability of the $17/2^+_1 \rightarrow 13/2^+_1$ transition. This could indicate that states with different seniority actually mix. Analogous to the previous case of ^{94}Ru in Refs. [4, 6], the analytical approach of the single-j approximation can be used to derive admixtures (α, β) for a the composition of states with different seniority to reproduce the experimental findings. Because the energy difference between the $17/2^+_1$ and $17/2^+_2$ state is small compared to the one between the $13/2^+_1$ and $13/2^+_2$ state, only mixing of the $17/2^+$ $\upsilon = 3$ and $\upsilon = 5$ states was considered. The yrast $17/2^+$ state can be expanded as follows:

$$|17/2^+_1\rangle = \alpha|17/2^+_{\upsilon=3}\rangle + \beta|17/2^+_{\upsilon=5}\rangle, \tag{8}$$

where the admixtures α and β have to satisfy the normalization condition $\alpha^2 + \beta^2 = 1$. The admixtures (α, β) are adjusted to minimize a summed χ^2 function that represents the deviation between the calculated and experimental $B(E2)$ values of the $21/2^+_1 \rightarrow 17/2^+_1 \rightarrow 13/2^+_1$ cascade. The resulting admixtures $(\alpha, \beta) = (0.895(3), 0.446(6))$ reproduce the experimental findings, where the uncertainty for α is obtained from $\chi^2 + 1$ and the uncertainty of β is linked to the one from α via the normalization condition. This is also confirmed when minimizing the χ^2 for the transitions independently, yielding results for the admixtures that agree with the results when minimizing for the whole cascade. The uncertainty of the admixtures allows also to derive uncertainty intervals for the $B(E2)$ values with optimized admixtures (α, β) using a Monte Carlo ansatz. The resulting values are $B(E2; 21/2^+_1 \rightarrow 17/2^+_1) = 26.2(9)$ e^{2}fm^4 and $B(E2; 17/2^+_1 \rightarrow 13/2^+_1) = 32(1)$ e^{2}fm^4.

V. CONCLUSION

Lifetimes of excited states in ^{95}Rh and ^{95}Ru have been measured and used to calculate reduced quadrupole transition probabilities. The data for the mid-shell nucleus ^{95}Rh is compared with the results of a single-j approximation using state-dependent effective charges derived from the two nucleon system ^{92}Mo from Ref. [6] as well as with other experimental findings from Ref. [7] and discussed with regard to the question of seniority conservation in the $g_{9/2}$ orbital. While the results from Ref. [7] indicate a drastic violation of seniority symmetry for the mid-shell nucleus ^{95}Rh, the re-measured lifetimes of the $13/2^+_1$ and $17/2^+_1$ states lead to the opposite conclusion of a partial conservation of seniority. Because the experiment from Ref. [7] and this work came to very different results, leading to fundamentally contradictory conclusions about the physical interpretation, it would be important

TABLE II. Reduced transition probabilities $B(\sigma\lambda)$ calculated from the, in this work, adopted experimental values. Theoretical predictions from the single-j approximation using a one-body transition operator with constant effective charge $T_1(E2)$ or state-dependent effective charges $T_1'(E2)$ are taken from Ref. [6]. All $B(\sigma\lambda)$ values are given in e^2fm^4.

nucleus	transition $J_i^{\pi_i} \to J_f^{\pi_f}$	E_γ keV	$\sigma\lambda$	$B(\sigma\lambda; J_i^{\pi_i} \to J_f^{\pi_f})$ this work	$B(\sigma\lambda; J_i^{\pi_i} \to J_i^{\pi_f})$ literature	$B(\sigma\lambda; J_i^{\pi_i} \to J_f^{\pi_f})$ single-j $T_1(E2) \mid T_1'(E2)$
^{95}Rh	$13/2_1^+ \to 9/2_{gs}^+$	1351	E2	≥ 45	$5.0^{+3.6}_{-1.6}$ [7]	137 | 174(3)
	$17/2_1^+ \to 13/2_1^+$	717	E2	32(1)	≥ 167 [7]	0 | $0.87^{+0.22}_{-0.19}$
	$21/2_1^+ \to 17/2_1^+$	382 [a]	E2	27(2)	24(2) [21–23]	0 | 1.0(2)
	$21/2_1^+ \to 17/2_2^+$	185 [a]	E2	128(10)	113(13) [21–23]	138 | 176(3)
	$21/2_1^- \to 17/2_1^-$	1005	E2	71^{+56}_{-22}	120(25) [22]	—
^{95}Ru	$9/2_1^+ \to 5/2_{gs}^+$	1352	E2	≥ 60	—	—
	$13/2_1^+ \to 9/2_1^+$	677	E2	≥ 140 [b]	—	—
	$17/2_1^+ \to 13/2_1^+$	255	E2	71.0(8)	165(15) [21, 27]	—
	$21/2_1^+ \to 17/2_1^+$	255	E2	62(3)	50.0(13) [21, 27]	—

[a] The branching ratio is taken from Ref. [21].
[b] The 2029 keV transition to the ground state was neglected for the calculation.

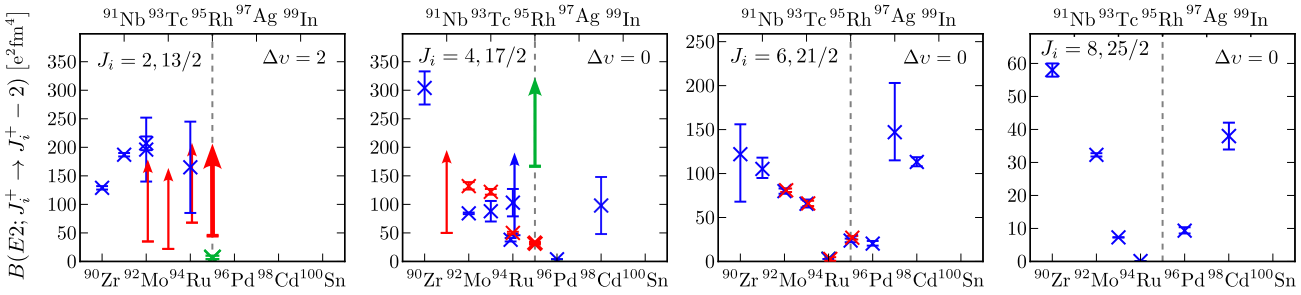

FIG. 11. Evolution of the reduced electric quadrupole transition probabilities $B(E2)$ along the $\pi g_{9/2}$ orbital. The data shown in red is taken from Refs. [4, 6] as well as the results for ^{95}Rh from this work. The data shown in blue is taken from Refs. [23, 31–55] and the green data from Ref. [7].

to have the lifetimes confirmed by another independent experiment.

VI. ACKNOWLEDGEMENT

We acknowledge the Deutsche Forschungsgemeinschaft (DFG) for the upgrade of the used germanium detectors under grant INST 216/988-1 FUGG. M.L. acknowledges the financial support of the DFG under grant JOL 391/18-2. A.E. acknowledges the support by the DFG under grant number JO 391/20-1. J.J acknowledges support by GANIL for an extended stay there. Support of the University of Cologne in operating the Tandem accelerator is acknowledged.

[1] V. Karayonchev *et al.*, Phys. Rev. C **99**, 024326 (2019).
[2] V. Karayonchev *et al.*, Phys. Rev. C **106**, 044321 (2022).
[3] H. Mach *et al.*, Phys. Rev. C **95**, 014313 (2017).
[4] M. Ley *et al.*, Phys. Rev. C **110**, 034320 (2024).
[5] B. Das *et al.*, Phys. Rev. C **105**, L031304 (2022).
[6] M. Ley *et al.*, Phys. Rev. C **108**, 064313 (2023).
[7] B. Das *et al.*, Phys. Rev. Res. **6**, L022038 (2024).
[8] R. M. Pérez-Vidal *et al.*, Phys. Rev. Lett. **129**, 112501 (2022).
[9] P. Van Isacker, Eur. Phys. J. Spec. Top. **233**, 921 (2024).
[10] F. Pühlhofer, Nucl. Phys. A **280**, 267 (1977).
[11] L. Netterdon *et al.*, Nucl. Instrum. Methods Phys. Res. A **754**, 94 (2014).
[12] S.p.A. CAEN, *User manual UM2792 V1730/VX1730 and V1725/VX1725* (2021).
[13] A. Harter *et al.*, Nucl. Instrum. Methods Phys. Res. A **1053**, 168356 (2023).
[14] J.-M. Régis *et al.*, Nucl. Instrum. Methods Phys. Res. A **622**, 83 (2010).
[15] J.-M. Régis *et al.*, Nucl. Instrum. Methods Phys. Res. A **726**, 191 (2013).
[16] J.-M. Régis *et al.*, Nucl. Instrum. Methods Phys. Res. A **897**, 38 (2018).
[17] Z. Bay, Phys. Rev. **77**, 419 (1950).
[18] A. Esmaylzadeh *et al.*, Phys. Rev. C **110**, 034324 (2024).
[19] L. Knafla *et al.*, Nucl. Instrum. Methods Phys. Res. A **1052**, 168279 (2023).
[20] J.-M. Régis *et al.*, Nucl. Instrum. Methods Phys. Res. A **955**, 163258 (2020).
[21] S. Basu, G. Mukherjee, and A. Sonzogni, Nuclear Data Sheets **111**, 2555 (2010).
[22] E. Nolte, G. Korschinek, and U. Heim, Z. Phys. A **298**, 191 (1980).
[23] A. Jungclaus *et al.*, Nucl. Phys. A **637**, 346 (1998).
[24] H. Grawe, H. H. Bertschat, and H. Haas, Hyperfine Interactions **15**, 65 (1983).
[25] E. Nolte, G. Korschinek, and U. Heim, Z. Phys. A **298**, 191 (1980).
[26] C. Lederer, J. Jaklevic, and J. Hollander, Nucl. Phys. A **169**, 489 (1971).
[27] P. Chowdhury *et al.*, Phys. Rev. C **32**, 1238 (1985).
[28] C. Broude *et al.*, Z. Phys. A **336** (1990), 10.1007/BF01290613.
[29] S. S. Ghugre *et al.*, Phys. Rev. C **50**, 1346 (1994).
[30] T. Kibédi *et al.*, Nucl. Instrum. Methods Phys. Res. A **589**, 202 (2008).
[31] G. Zhang *et al.*, Physics Letters B **863**, 139378 (2025).
[32] A. Yaneva *et al.*, Acta Phys. Pol. B Proc. Suppl. **16**, 4 (2023).
[33] D. Alber *et al.*, Zeitschrift für Physik A Atomic Nuclei **332**, 129 (1989).
[34] H. Grawe and H. Haas, Physics Letters B **120**, 63 (1983).
[35] W. F. Piel *et al.*, Phys. Rev. C **28**, 209 (1983).
[36] D. Abriola and A. Sonzogni, Nuclear Data Sheets **109**, 2501 (2008).
[37] J. Park *et al.*, Phys. Rev. C **96**, 044311 (2017).
[38] A. Blazhev *et al.*, Phys. Rev. C **69**, 064304 (2004).
[39] J. Chen and B. Singh, Nuclear Data Sheets **164**, 1 (2020).
[40] M. Lipoglavšek *et al.*, Phys. Rev. C **72**, 061304 (2005).
[41] O. Häusser *et al.*, Nucl. Phys. A **293**, 248 (1977).
[42] H. A. Roth *et al.*, Phys. Rev. C **50**, 1330 (1994).
[43] C. M. Baglin, Nuclear Data Sheets **112**, 1163 (2011).
[44] W. Schneider, K. Gonsior, and C. Günther, Nucl. Phys. A **249**, 103 (1975).
[45] K. Löbner, Nucl. Phys. **58**, 49 (1964).
[46] S. Basu and E. Mccutchan, Nuclear Data Sheets **165**, 1 (2020).
[47] W. Andrejtscheff *et al.*, Nucl. Phys. A **445**, 515 (1985).
[48] S. Cochavi, J. M. McDonald, and D. B. Fossan, Phys. Rev. C **3**, 1352 (1971).
[49] C. Lederer, J. Jaklevic, and J. Hollander, Nucl. Phys. A **169**, 449 (1971).
[50] C. M. Baglin, Nuclear Data Sheets **113**, 2187 (2012).
[51] M. Hausmann *et al.*, Phys. Rev. C **68**, 024309 (2003).
[52] D. Abriola and A. Sonzogni, Nuclear Data Sheets **107**, 2423 (2006).
[53] G. Jakob *et al.*, Phys. Lett. B **494**, 187 (2000).
[54] W. Beens, *Lifetimes of excited states in nuclei with mass number around A = 88 by means of the Doppler shift attenuation method*, Tech. Rep. (Vrije Universiteit, Amsterdam (Netherlands), 1973).
[55] M. Grecescu, A. Nilsson, and L. Harms-Ringdahl, Nucl. Phys. A **212**, 429 (1973).

5 | Summary and Conclusion

Within the scope of this thesis, the results of three experimental campaigns with the goal of measuring lifetimes of low-lying excited states in the $N = 50$ isotones ^{91}Nb, ^{92}Mo, ^{93}Tc, ^{94}Ru, and ^{95}Rh are presented. The lifetimes were obtained by employing the well established γ-γ fast-timing technique using a hybrid setup of LaBr and HPGe detectors installed at the HORUS spectrometer of the Institute for Nuclear Physics in Cologne. This resulted in three partial studies, which are summarized in the following. The obtained $B(E2)$ values are discussed with regard to seniority conservation in the $\pi 1g_{9/2}$ shell. The experimental data are compared with theoretical predictions based on a single-j approach, making use of an analytical relation between the n and $n+1$ valence nucleon system. The precise measurement of the $B(E2; 4_1^+ \rightarrow 2_1^+)$ strength from the two valence particle system ^{92}Mo allowed the determination of state-dependent effective charges, which are used within the single-j calculation to enhance the predictions for ^{93}Tc, ^{94}Ru, and ^{95}Rh.

Lifetime measurements in ^{92}Mo: Investigation of seniority conservation in the $N = 50$ isotones

In a first experimental campaign, lifetimes of excited states in ^{92}Mo were measured in two independent fast-timing experiments and two independent reactions. The lifetimes of the 4_1^+, 6_1^+, 8_1^+, and 5_1^- states have been measured with increased precision. The lifetime of the 9_1^- state was measured for the first time. An upper limit for the lifetime of the 2_1^+ state has been measured, which is in agreement with the current literature value from Ref. [4], and an upper limit for the lifetime of the 7_1^- state has been measured for the first time. In particular, the lifetime of the 4_1^+ state was determined with high precision.

Experimental $B(E2)$ strengths were extracted from the measured lifetimes. The complete set of experimental $B(E2)$ values from the $8_1^+ \rightarrow 6_1^+ \rightarrow 4_1^+ \rightarrow 2_1^+ \rightarrow 0_{\text{gs}}^+$ cascade was used to derive state-dependent effective charges, which are used within a single-j calculation for $j = 9/2$. When comparing the results from the single-j calculation to the known experimental $B(E2; 4_1^+ \rightarrow 2_1^+)$ values in ^{94}Ru, a notable discrepancy was observed. Both literature values 38(3) and 103(24) e^2fm^4 from Refs. [4, 5], respectively, are significantly higher than the results from the single-j calculation with 12 e^2fm^4 using a constant effective charge and 7.8(7) e^2fm^4 for state-dependent effective charges. The deviation between single-j prediction and the respective experimental value can be quantitatively resolved for both cases by introducing an ad hoc mixing between the $v = 2$ and $v = 4$ states. The admixtures for this mixing have been determined by minimizing the χ^2 with respect to the experimental data. Including the mixing allowed both experimental values

for the $B(E2; 4_1^+ \rightarrow 2_1^+)$ strength in ^{94}Ru to be accurately reproduced using state-dependent effective charges. This work laid the foundation for the following two studies measuring lifetimes of excited states in the nuclei ^{93}Tc, ^{94}Ru, and ^{95}Rh.

Lifetime measurement in ^{94}Ru and ^{93}Tc to investigate seniority conservation in the $N = 50$ isotones

The follow-up to the previous work on ^{92}Mo, was to study further nuclei in the $\pi 1g_{9/2}$ shell above ^{92}Mo. Therefore, lifetimes of excited states in the nuclei ^{93}Tc, ^{94}Ru, as well as an upper limit in ^{91}Nb have been measured within the second experimental campaign. The lifetimes of the 4_1^+, 6_1^+, 5_1^-, 9_1^-, and 11_1^- states in ^{94}Ru have been measured as well as upper limits for the 2_1^+, 10_1^+, and 7_1^- states. The lifetimes of the 7_1^- and 9_1^- states in ^{94}Ru were previously unknown. The upper limits for the lifetimes of the 2_1^+ and 10_1^+ state match the literature values [4, 96]. The lifetime of the 6_1^+ state agrees with the literature value and was measured with increased precision. The lifetime of the 11_1^- state matches the literature values within 2σ. The re-measured lifetime of the 5_1^- state differs significantly from the literature value in Ref. [96] measured using the RDDS technique. The re-measured lifetime of the 4_1^+ state in ^{94}Ru is intermediate to the values reported in Refs. [4, 5]. In ^{93}Tc, lifetimes for the $17/2_1^+$ and $21/2_1^+$ states have been measured. Upper limits for the lifetimes of the $11/2_1^+$, $13/2_1^+$, and $21/2_1^-$ states have been determined. The lifetime of the $17/2_1^+$ state agrees with the literature value within 2σ. The re-measured lifetime of the $21/2_1^+$ state matches the literature value. For the $21/2_1^-$ state the upper limit is consistent with the previously known limit. The precision of the upper limit for the $13/2_1^+$ state is significantly enhanced. The upper limit for the $11/2_1^+$ was measured for the first time. In ^{91}Nb, the upper limit of the $17/2_1^+$ was measured with more precision than the previously known literature value.

The measured lifetimes have been used to obtain reduced transition probabilities, which are compared with theoretical predictions based on a single-j approximation using state-dependent effective charges derived from the newly measured $B(E2)$ strenths in ^{92}Mo [7], as well as with shell-model calculations performed in the $\pi(2p_{1/2}, 1g_{9/2})$ model space. For ^{93}Tc, the theoretical calculations show good agreement with the experimental data. Because the lifetimes of the $11/2_1^+$, $13/2_1^+$, and $21/2_1^+$ states are below the sensitivity of the used fast-timing technique, only lower limits for the $B(E2)$ strengths are obtained, limiting the conclusions that can be drawn. In ^{94}Ru, the lifetime of the 4_1^+ state was measured with high statistical precision and a large peak-to-background ratio, leading to high confidence in the new experimental value. The shell-model calculation in the $\pi(2p_{1/2}, 1g_{9/2})$ model space, as well as the single-j approximation, do not reproduce the increased experimental value of the $B(E2; 4_1^+ \rightarrow 2_1^+)$ transition strength. To account for the discrepancy, the previously discussed ad hoc mixing of the 4^+ and 6^+ states with seniorities $v = 2$ and $v = 4$ was applied using the newly measured $B(E2)$ strengths and the literature data. It was not possible to simultaneously reproduce the $B(E2)$ strengths of both the

$4_1^+ \rightarrow 2_1^+$ and $6_1^+ \rightarrow 4_1^+$ transitions using this ansatz. This work builds upon previous research on the two-valence-nucleon system ^{92}Mo, extending the investigation by providing experimental data to test the single-j predictions for the three and four nucleon systems ^{93}Tc and ^{94}Ru.

Lifetime measurement in ^{95}Rh and ^{95}Ru: Investigation of seniority conservation in the $N = 50$ isotones

To also study the interesting case of the $\pi 1g_{9/2}$ mid-shell nucleus, a further experimental campaign was conducted to measure lifetimes of excited states in ^{95}Rh. The lifetimes of the $17/2_1^+$, $21/2_1^+$, $17/2_1^-$, and $21/2_1^-$ states were measured and an upper limit for the lifetime of the $13/2_1^+$ state was determined. Given the vast amount of data for ^{95}Ru within the recorded data set, lifetimes of the $17/2_1^+$ and $21/2_1^+$ states in ^{95}Ru have been measured, as well as upper limits for the lifetimes of the $7/2_1^+$, $9/2_1^+$, and $13/2_1^+$ states. Furthermore, it was possible to reproduce relevant results from the previous work [7, 8], leading to a high degree of confidence in the findings.

The measured lifetimes have been used to obtain values for the $B(E2)$ strength. The newly measured data for ^{95}Rh is discussed in the context of partial conservation of seniority. It is compared with the previously known literature and with the results of the single-j prediction from Ref. [7]. In contrast to the findings in Ref. [9], the lower limit for the $B(E2)$ strength of the $\Delta v = 2$ ground state transition $13/2_1^+ \rightarrow 9/2_{\text{gs}}^+$ and the $B(E2)$ value for the $\Delta v = 0$ transition $17/2_1^+ \rightarrow 13/2_1^+$ are not in conflict with the expected seniority pattern. However, deviations from the pure seniority pattern are obtained for the $17/2_1^+ \rightarrow 13/2_1^+$ transition, which theoretically should be suppressed even further. To explain this deviations ad hoc mixing between the $17/2^+$ states with seniority $v = 3$ and $v = 5$ was assumed. Admixtures that reproduce the experimental $B(E2)$ have been determined. The study of the mid-shell nucleus ^{95}Rh was particularly significant, as deviations from pure seniority become immediately apparent in this case.

Systematic of $B(E2)$ Strength in the $\pi 1g_{9/2}$ Orbital

Figure 8 shows an overview of the current literature values on experimental $B(E2)$ strengths for the $4_1^+ \rightarrow 2_1^+ \rightarrow 0_{\text{gs}}^+$ transitions in the even-even and $17/2_1^+ \rightarrow 13/2_1^+ \rightarrow 9/2_{\text{gs}}^+$ transitions in the odd-even nuclei. As shown in the extended version of this figure in the previous Chapter 4, the results for the $B(E2; 6_1^+ \rightarrow 4_1^+)$ and $B(E2; 21/2_1^+ \rightarrow 17/2_1^+)$ strengths confirm the literature values and are therefore not further discussed here. The red data was determined within the scope of this thesis, data from Ref. [9] is shown in green and other experimental data is shown in blue. In Fig. 8(a) the systematic trend for the $B(E2)$ strengths of the $\Delta v = 2$ ground state transitions is shown. Because these lifetimes are below the sensitivity of the applied fast-timing technique, only upper limits for lifetimes have been determined, leading to lower limits for the $B(E2)$ values. However, it can be seen that the trend likely corresponds to the pattern expected

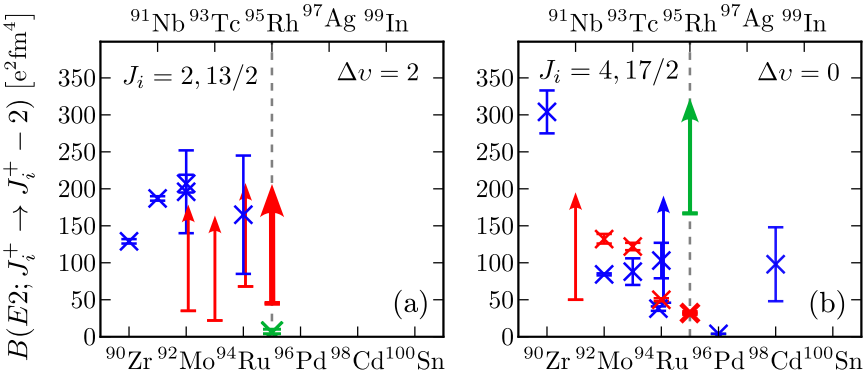

Figure 8: Experimental data showing the evolution of reduced quadrupole transition probabilities $B(E2)$ along the $\pi 1g_{9/2}$ shell. Data that was measured within the scope of this thesis is shown in red, data from Ref. [9] is shown in green and other experimental data [54] is shown in blue (a) The systematic of the $\Delta v = 2$ ground state transitions $B(E2; 2_1^+ \rightarrow 0_{\text{gs}}^+)$. (b) The systematic trend for the $B(E2; 4_1^+ \rightarrow 2_1^+)$ values, that do not change seniority $\Delta v = 0$. The figure is part of an extended version shown in the previous Chapter 4.

for the case $\Delta v = 2$, which is shown schematically in Fig. 1(c). The green data point from Ref. [9] on the other hand would imply, that the 1351 keV $13/2_1^+ \rightarrow 9/2_{\text{gs}}^+$ ground state transition is largely suppressed in the mid-shell nucleus ^{95}Rh, which is a significant deviation from the expected pattern. So far, no corresponding $B(E2)$ values have been determined for the upper half of the $\pi 1g_{9/2}$ orbital above ^{95}Rh.

Figure. 8 (b) shows the systematic trend for the $B(E2)$ strength of the $\Delta v = 0$ transitions between the lowest states of the respective $v = 2$ or $v = 3$ multiplet. The trend in the data shows that the transition probability is inhibited towards the middle of the $\pi 1g_{9/2}$ orbital, leading to the expected pattern for the $\Delta v = 0$ case. The lower limit for the strength $B(E2)$ from Ref. [9] would imply a distinctly different behavior with an abruptly increased transition probability in the mid-shell nucleus ^{95}Rh. The lower limit of $\geq$167 e^{2}fm^4, corresponding to $\geq$6.5 W.u., approaches the range typically associated with the onset of moderate collectivity. As pointed out in Ref. [9], reproducing this increased $B(E2; 17/2_1^+ \rightarrow 13/2_1^+)$ and the above mentioned hindered $B(E2; 13/2_1^+ \rightarrow 9/2_{\text{gs}}^+)$ transition strengths within shell-model calculations using standard effective two-body interactions proves to be extremely challenging. Since the findings from Ref. [9] are fundamentally different to the results of this work, it would be important to have the lifetimes confirmed by another independent experiment. However, the result for $B(E2; 17/2_1^+ \rightarrow 13/2_1^+)$ from this work 32(1) e^{2}fm^4, is also significantly higher when considering that this transition should be close to zero when assuming a pure single-j system with conserved seniority. Such a deviation is also observed for the $B(E2; 21/2_1^+ \rightarrow 17/2_1^+)$ transition with a value of 27(2) e^{2}fm^4. To explain the deviation, mixing between the $17/2^+$ states with $v = 3$ and $v = 5$ is assumed, although at the mid-shell case $(j = 9/2)^5$ mixing between states with $\Delta v = 2$ should not be possible due to the $\Delta v = \pm 4$ seniority mixing rule and would therefore require extra model-space configurations aside from the pure $\pi 1g_{9/2}$. Mixing of $13/2^+$ and $21/2^+$ states with different seniority has been

neglected since the energy gap between the respective states is significantly larger compared to the one between the $17/2^+$ states. The admixture coefficients (α, β) that reproduce the experimental $B(E2)$ strength of the $21/2_1^+ \rightarrow 17/2_1^+ \rightarrow 13/2_1^+$ cascade have been determined to be $(\alpha, \beta) = (0.895(3), 0.446(6))$. In ^{93}Tc, the re-measured $B(E2; 17/2_1^+ \rightarrow 13/2_1^+)$ strength from this work is slightly increased with respect to the literature value from Ref. [97]. The increased value can be reproduced within the single-j analysis using state-dependent effective charges. There are currently three experimental values for the $B(E2; 4_1^+ \rightarrow 2_1^+)$ strength in ^{94}Ru, that do not overlap within the uncertainties [4, 5, 8]. During this work, it was possible to confirm our result from [8] in a second fast-timing experiment presented in Chapter 4. However, it would be important to have a further independent experiment to clarify the issue. Similar to the situation in ^{95}Rh, the increased $B(E2; 4_1^+ \rightarrow 2_1^+)$ strength in ^{94}Ru is not reproduced by the single-j approach and also not within shell-model calculations in a $\pi(2p_{1/2}, 1g_{9/2})$ model space using SR88MHJM interaction [8, 98]. The solution adopted in Ref. [3] is reducing the model space below $N = 50$ to the $\nu 1g_{9/2}$ orbital and adding $N = Z = 50$ cross-shell excitations. Although leading to an increased $B(E2; 4_1^+ \rightarrow 2_1^+)$ strength, the predictions for $B(E2; 2_1^+ \rightarrow 0_{\text{gs}}^+)$ and $B(E2; 6_1^+ \rightarrow 4_1^+)$ deteriorates significantly, as also pointed out in Ref. [4]. Another ansatz to explain the deviations is given in Ref. [32], which studied the $(j = 9/2)^{\pm 4}$ systems in the $\pi 1g_{9/2}$ orbital with a partial seniority conservation, related to the existence of the uniquely defined $\upsilon = 4$ states. It was shown that the diminishing $B(E2; 8_1^+ \rightarrow 6_1^+)$ strength in ^{94}Ru can be mostly understood as the cancellation between few terms induced by the seniority-non-conserving interaction in the $j = 9/2$ system [32]. Furthermore, it was shown that the influence of the neighboring orbitals $(p_{1/2}, p_{3/2}, f_{5/2})$ can lead to significant mixture between the $\upsilon = 2$ and the uniquely defined $\upsilon = 4$ states [20, 32, 34]. The seniority $\upsilon = 2$ and $\upsilon = 4$ configurations can interfere either constructively or destructively. This would explain the slightly increased $B(E2; 4_1^+ \rightarrow 2_1^+)$ strength in ^{94}Ru as result of constructive interference and the hindered $B(E2; 4_1^+ \rightarrow 2_1^+)$ strength in ^{96}Pd as result of destructive interference of the $\upsilon = 2$ and $\upsilon = 4$ configurations.

In summary, it can be stated that the overall picture resulting from the newly measured data and the literature values for the $B(E2)$ strengths in the $N = 50$ isotones is ambiguous to a certain extent. The picture of a complete breakdown of seniority in ^{94}Ru and ^{95}Rh could not be confirmed in this work. Instead, the $B(E2)$ pattern suggests that seniority appears to be conserved to a certain degree. However, there are relevant deviations from the ideal pattern, which can be explained by seniority mixing. The origin of this mixing might be attributed to the influence of the neighboring $2p_{1/2}$, $2p_{3/2}$, and $1f_{5/2}$ orbitals.

6 | Outlook

In this chapter current projects and ideas for future experiments are discussed to further study seniority conservation on different parts of the nuclear chart. Some of the experiments have already been conducted, with ongoing analysis, while others are presented as raw plans. For the purpose of simplicity, only experiments using the instruments available at the Institute for Nuclear Physics in Cologne are discussed. In addition, potential innovations regarding the optimization of the institute's fast-timing setup are discussed, which could be relevant for future applications.

Further Studies in the $N = 50$ Isotones

Additional attempts have already been made to measure further lifetimes in the $N = 50$ isotones. Because the lifetimes for the lowest-lying states are usually very short, only upper limits were determined due to the limitations of the applied fast-timing method. Following the example from Ref. [39], an attempt was made to populate the low-lying states in ^{93}Tc or ^{94}Ru using transfer reactions. Unfortunately, no significant signs of proton transfer reaction channels were observed during the test experiments using a ^{92}Mo target and an ^{16}O or ^{19}F beam. Further investigations of even more proton-rich $N = 50$ isotones beyond ^{95}Rh appear to be rather challenging using stable beam experiments. The ^{96}Pd nucleus could theoretically be produced using the institute's Tandem accelerator and the fusion-evaporation reaction ^{96}Ru(^{3}He, $3n$)^{96}Pd. However, several challenges and circumstances suggest that the success of such an experiment is rather unlikely. Both target material and beam are relatively rare and therefore expensive. The current duoplasmatron source for the He-beam is known to be unreliable. The estimated reaction cross section at 25 MeV is only approximately 10 mb which is much lower than the cross-section of the ^{92}Mo(^{6}Li, $3n$)^{95}Rh that was used in the last experiment, where 12 days of beam time were required to collect sufficient statistic. Many other reaction channels will dominate the collected data as it was the case in the ^{95}Rh experiment. The critical angular momentum $L_{\text{crit.}}$ is estimated at $9\hbar$, which would be just enough to populate the states of interest within the reaction. The lifetimes of the first excited 4^+, 6^+, and 8^+ states have been measured already in RIB experiments [6, 67], while the lifetime of the first excited 2^+ is very likely too short to be measured using the fast-timing method. The experiment would therefore primarily verify literature values but would not yield any completely new information. In summary, it must therefore be said that such an experiment would not be advisable.

Semi-Magic Nuclei in the Proximity of ^{208}Pb

One region that is accessible with the resources available at the institute is the $N = 126$ isotones above ^{208}Pb. As already mentioned in this work, the situation is rather similar there. The $\pi 1h_{9/2}$ orbital is well isolated due to the shell closure at $Z = 82$. Many lifetimes of the low-lying states have already been measured recently [38, 39, 52, 53], but the data are still incomplete. In February 2025 a fast-timing experiment was conducted in Cologne to measure lifetimes of excited states in ^{212}Rn, using the ^{209}Bi(^{6}Li, $3n$)^{212}Rn fusion-evaporation reaction. The analysis has not been finalized yet, but it is expected that there will be a revision of the current lifetime of the 4_1^+ state, and a new upper limit for the lifetime of the 2_1^+ state [99]. The mid-shell nucleus in the $\pi 1h_{9/2}$ orbital is ^{213}Fr, which was already measured in December 2018 using the fusion-evaporation reaction ^{206}Pb(^{11}B,$4n$)^{213}Fr @ 56 MeV and an analog fast-timing setup. Unfortunately, the results have not been published yet [100]. The experiment could easily be repeated using a modern digital fast-timing setup.

Non Semi-Magic Nuclei in the Proximity of ^{208}Pb

In the vicinity of ^{208}Pb, the 8_1^+ seniority isomers are also found in non semi-magic nuclei with neutron holes below the $N = 126$ shell closure. The 8_1^+ states in the even-even nuclei in the Po-Rn-Ra isotonic chains with $122 \leq \mathrm{N} \leq 126$ are isomers with wave functions dominated by the $\pi 1h_{9/2}$ configuration and the respective $B(E2)$ follow a typical seniority-like pattern [48]. The substantial shell gap between proton and neutron orbitals probably prevents proton-neutron interactions that would destroy seniority [19, 48]. A transition from single-particle excitations to collectivity is expected to emerge around N =118−120 [19]. However, recent studies in ^{204}Po and ^{206}Po showed increased $B(E2; 4_1^+ \rightarrow 2_1^+)$ values, indicating that the 4_1^+ states in both nuclei are of collective nature [51, 101]. In order to investigate this onset of collectivity in Rn isotopes as well, a series of experiments has been conducted over the recent years. The lifetimes of the low-lying excited states in the isotopic chain ^{206}Rn, ^{208}Rn, ^{210}Rn, and ^{214}Rn were measured using analog and digital fast-timing setups. The data has already been fully analyzed and a manuscript is in preparation.

Further Developments for the Fast-Timing Setup in Cologne

The experiments presented in this paper were all measured using the HORUS spectrometer at the Institute for Nuclear Physics in Cologne. In 2023, the new γ-ray spectrometer CATHEDRAL (Coincidence Array at the Tandem accelerator for High-Efficiency Doppler-Recoil And LaBr fast-timing measurements) [102] was commissioned at the institute. The spectrometer has mounts for up to 33 detectors and is optimized for RDDS experiments with detector rings at angles of 0°, 30°, 55°, 90°, 125°, and 150° with respect to the beam axis. Since no Doppler shift can be

observed at an angle of 90°, the positions in the 90° ring can be equipped with up to 8 LaBr detectors, which enables the simultaneous measurement of lifetimes using both fast-timing and RDDS techniques. This is a great advantage, as both methods overlap in their sensitivity range and thus can be used for cross-checking. Also the methods have some complementary advantages and disadvantages. For example, the RDDS method suffers from undesired feeding, whereas the fast-timing method can be strongly influenced due to coincident Compton background under the peaks. To avoid the disturbing influence of scattered γ rays, the LaBr in the 90° ring have been passively shielded against each other using lead sheathings [83, 102]. This reduces the amount of Compton-scattered γ rays from entering the detector and thus minimizes time-correlated inter-detector scattering. However, to significantly improve the peak-to-Compton ratio, the use of active anti-Compton detectors with an anti-coincidence logic are required [90]. The bulky HORUS BGO shield are not suited to be used within the new CATHEDRAL spectrometer. Furthermore, they were primarily build for large volume HPGe detectors and are not optimized for the usage with the $1.5" \times 1.5"$ LaBr detectors. The progress on silicon photomultipliers (SiPMs) allowes to use them instead of large photomultiplier tubes for a compact designed BGO anti Compton detector, optimized for the use with $1.5" \times 1.5"$ LaBr detectors at the CATHEDRAL spectrometer. Furthermore, the time resolution of SiPM arrays in combination with LaBr scintillators becomes increasingly competitive to the use of PMTs [103]. In terms of energy resolution and linearity they perform already better than classical PMTs [103]. Changing to SiPM for the LaBr detector array at the CATHEDRAL spectrometer would be another task for the future and may improve the fast-timing method at the institute.

Bibliography

[1] R. F. Casten. Nuclear Structure from a Simple Perspective. Oxford University Press, 2001.

[2] A. Arima, T. Ohtsuka, F. Iachello and I. Talmi. "Collective nuclear states as symmetric couplings of proton and neutron excitations." *Phys. Lett. B* 66.3 (1977), 205–208.

[3] H. Mach, A. Korgul, M. Górska, H. Grawe, I. Matea, M. Stănoiu, L. M. Fraile, Y. E. Penionzkevich, F. D. O. Santos, D. Verney, S. Lukyanov, B. Cederwall, A. Covello, Z. Dlouhý, B. Fogelberg, G. De France, A. Gargano, G. Georgiev, R. Grzywacz, A. F. Lisetskiy, J. Mrazek, F. Nowacki, W. A. Płóciennik, Z. Podolyák, S. Ray, E. Ruchowska, M.-G. Saint-Laurent, M. Sawicka, C. Stodel and O. Tarasov. "Ultrafast-timing lifetime measurements in ^{94}Ru and ^{96}Pd: Breakdown of the seniority scheme in $N = 50$ isotones." *Phys. Rev. C* 95 (2017), 014313.

[4] R. M. Pérez-Vidal, A. Gadea, C. Domingo-Pardo, A. Gargano, J. J. Valiente-Dobón, E. Clément, A. Lemasson, L. Coraggio, M. Siciliano, S. Szilner, M. Bast, T. Braunroth, J. Collado, A. Corina, A. Dewald, M. Doncel, J. Dudouet, G. de France, C. Fransen, V. González, T. Hüyük, B. Jacquot, P. R. John, A. Jungclaus, Y. H. Kim, A. Korichi, M. Labiche, S. Lenzi, H. Li, J. Ljungvall, A. López-Martens, D. Mengoni, C. Michelagnoli, C. Müller-Gatermann, D. R. Napoli, A. Navin, B. Quintana, D. Ramos, M. Rejmund, E. Sanchis, J. Simpson, O. Stezowski, D. Wilmsen, M. Zielińska, A. J. Boston, D. Barrientos, P. Bednarczyk, G. Benzoni, B. Birkenbach, H. C. Boston, A. Bracco, B. Cederwall, D. M. Cullen, F. Didierjean, J. Eberth, A. Gottardo, J. Goupil, L. J. Harkness-Brennan, H. Hess, D. S. Judson, A. Kaşkaş, W. Korten, S. Leoni, R. Menegazzo, B. Million, J. Nyberg, Z. Podolyak, A. Pullia, D. Ralet, F. Recchia, P. Reiter, K. Rezynkina, M. D. Salsac, M. Şenyiğit, D. Sohler, C. Theisen and D. Verney. "Evidence of Partial Seniority Conservation in the $\pi g_{9/2}$ Shell for the $N = 50$ Isotones." *Phys. Rev. Lett.* 129 (2022), 112501.

[5] B. Das, B. Cederwall, C. Qi, M. Górska, P. H. Regan, Ö. Aktas, H. M. Albers, A. Banerjee, M. M. R. Chishti, J. Gerl, N. Hubbard, S. Jazrawi, J. Jolie, A. K. Mistry, M. Polettini, A. Yaneva, S. Alhomaidhi, J. Zhao, T. Arici, S. Bagchi, G. Benzoni, P. Boutachkov, T. Davinson, T. Dickel, E. Haettner, O. Hall, C. Hornung, J. P. Hucka, P. R. John, I. Kojouharov, R. Knöbel, D. Kostyleva, N. Kuzminchuk, I. Mukha, W. R. Plass, B. S. Nara Singh, J. Vasiljević, S. Pietri, Z. Podolyák, M. Rudigier, H. Rösch, E. Sahin, H. Schaffner, C. Scheidenberger, F. Schirru, A. Sharma, R. Shearman, Y. Tanaka, J. Vesić, H. Weick, H. J. Wollersheim, U. Ahmed, A. Algora, C. Appleton, J. Benito, A. Blazhev, A. Bracco, A. M. Bruce, M. Brunet, R. Canavan, A. Esmaylzadeh, L. M. Fraile, G. Häfner, H. Heggen, D. Kahl, V. Karayonchev, R. Kern, A. Korgul, G. Kosir, N. Kurz, R. Lozeva, M. Mikolajczuk, P. Napiralla, R. Page, C. M. Petrache, N. Pietralla, J.-M. Régis, P. Ruotsalainen, L. Sexton, V. Sanchez-Temble, M. Si, J. Vilhena, V. Werner, J. Wiederhold, W. Witt, P. J. Woods and G. Zimba. "Nature of seniority symmetry breaking in the semimagic nucleus ^{94}Ru." *Phys. Rev. C* 105 (2022), L031304.

[6] A. Yaneva, S. Jazrawi, B. Das, M. Mikolajczuk, M. Górska, P. Regan, B. Cederwall, J. Jolie, G. Benzoni, H. Albers, et al. "Fast-timing Measurement in ^{96}Pd: Improved Accuracy for the Lifetime of the 4_1^+ State." *Acta Phys. Pol. B Proc. Suppl.* 16.4 (2023), A30.

[7] M. Ley, L. Knafla, J. Jolie, A. Esmaylzadeh, A. Harter, A. Blazhev, C. Fransen, A. Pfeil, J.-M. Régis and P. Van Isacker. "Lifetime measurements in ^{92}Mo: Investigation of seniority conservation in the $N = 50$ isotones." *Phys. Rev. C* 108 (2023), 064313.

[8] M. Ley, J. Jolie, L. Knafla, A. Blazhev, A. Esmaylzadeh, C. Fransen, A. Pfeil, J.-M. Régis and P. Van Isacker. "Lifetime measurement in ^{94}Ru and ^{93}Tc to investigate seniority conservation in the $N = 50$ isotones." *Phys. Rev. C* 110 (2024), 034320.

[9] B. Das, B. Cederwall, C. Qi, M. Górska, P. H. Regan, Ö. Aktas, H. M. Albers, A. Banerjee, M. M. R. Chishti, J. Gerl, N. Hubbard, S. Jazrawi, J. Jolie, A. K. Mistry, F. Nowacki, M. Polettini, A. Yaneva, U. Ahmed, S. Alhomaidhi, A. Algora, C. Appleton, T. Arici, S. Bagchi, G. Benzoni, J. Benito, A. Blazhev, P. Boutachkov, A. Bracco, A. M. Bruce, M. Brunet, R. Canavan, T. Davinson, T. Dickel, A. Esmaylzadeh, L. M. Fraile, E. Haettner, O. Hall, G. Häfner, H. Heggen, C. Hornung, J. P. Hucka, P. R. John, D. Kahl, V. Karayonchev, R. Kern, R. Knöbel, A. Korgul, G. Kosir, I. Kojouharov, D. Kostyleva, N. Kuzminchuk, N. Kurz, R. Liotta, R. Lozeva, M. Mikolajczuk, I. Mukha, P. Napiralla, R. Page, C. M. Petrache, N. Pietralla, S. Pietri, W. R. Plaß, Z. Podolyák, J.-M. Régis, M. Rudigier, H. Rösch, P. Ruotsalainen, E. Sahin, V. Sánchez-Tembleque, H. Schaffner, C. Scheidenberger, F. Schirru, L. Sexton, B. S. N. Singh, A. Sharma, R. Shearman, M. Si, Y. K. Tanaka, J. Vasiljević, J. Vesić, J. Vilhena, H. Weick, H. J. Wollersheim, V. Werner, J. Wiederhold, W. Witt, P. J. Woods, G. Zimba and J. Zhao. "Broken seniority symmetry in the semimagic proton mid-shell nucleus ^{95}Rh." *Phys. Rev. Res.* 6 (2024), L022038.

[10] G. Zhang, M. Polettini, D. Mengoni, G. Benzoni, Z. Huang, M. Górska, A. Blazhev, L. Fraile, A. Gargano, G. De Gregorio, F. Nowacki, G. Aggez, U. Ahmed, O. Aktas, M. Al-Aqeel, B. Alayed, H. Albers, A. Algora, S. Alhomaidhi, F. Amjad, C. Appleton, T. Arıcı, M. Armstrong, B. Arnés, A. Astier, M. Balogh, A. Banerjee, D. Bazzacco, J. Benito Garcìa, S. Bottoni, P. Boutachkov, A. Bracco, A. Bruce, D. Brugnara, C. Bruno, F. Camera, B. Cederwall, M. Cicerchia, M. Chishti, A. Corsi, M. Cortes, D. Cox, F. Crespi, B. Das, T. Davidson, G. de Angelis, T. Dickel, M. Doncel, A. Ertoprak, A. Esmaylzadeh, L. Gaffney, F. Galtarossa, E. Gamba, J. Garbe, D. Genna, J. Gerl, A. Goasduff, A. Gottardo, A. Gozzelino, T. Grahn, J. Ha, E. Haettner, O. Hall, L. Harkness-Brennan, H. Heggen, C. Hornung, Y. Hrabar, S. Hu, N. Hubbard, K. Ide, A. Illana, S. Jazrawi, P. John, J. Jolie, C. Jones, D. Joss, D. Judson, V. Karayonchev, E. Kazantseva, R. Kern, G. Kiss, L. Knafla, R. Knöbel, I. Kojouharov, A. Korgul, W. Korten, P. Koseoglou, D. Kostyleva, T. Kurtukian-Nieto, G. Kosir, N. Kurz, I. Kuti, M. Labiche, S. Lenzi, S. Leoni, G.-S. Li, Z. Liu, M. Llanos Expósito, R. Lozeva, J. Lu, M. Luoma, G. Mantovani, T. Marchi, M. Mazzocco, R. Menegazzo, T. Mertzimekis, M. Mikolajczuk, B. Million, A. Mistry, I. Mukha, E. Nacher, D. Napoli, B. Nara Singh, S. Orrigo, R. Page, P. Papadakis, G. Pasqualato, J. Pellumaj, S. Pelonis, R. Peréz Vidal, C. Petrache, J. Petrovic, N. Pietralla, S. Pietri, S. Pigliapoco, Z. Podolyák, C. Porzio, A. Raggio, F. Recchia, P. Regan, J. Régis, P. Reiter, K. Rezynkina, E. Rocco, J. Rodriguez Murias, H. Rösch, P. Roy, B. Rubio, M. Rudigier, P. Ruotsalainen, E. Sahin, L. Sarmiento, M.-M. Satrazani, H. Schaffner, C. Scheidenberger, L. Sexton, A. Sharma, M. Siciliano, J. Simpson, J. Smallcombe, P. Söderström, D. Sohler, A. Sood, F. Soramel, B.-H. Sun, H. Sun, A. Sveiczer, N. Szegedi, Y. Tanaka, J. Valiente-Dobón, P. Vasileiou, J. Vesic, M. von Tresckow, L. Waring, H. Watanabe, H. Weick, V. Werner, J. Wiederhold, O. Wieland, K. Wimmer, H.-J. Wollersheim, P. Woods, J. Wu, A. Yaneva, I. Zanon, J. Zhao, H. Zhang, G. Zhang, K. Zheng, L. Zhu, R. Zidarova, S. Ziliani and A. Zyriliou. "Approaching ^{100}Sn: Structural evolution in ^{98,100}Cd via lifetime measurements." *Phys. Lett. B* 863 (2025), 139378.

[11] A. Dewald, O. Möller and P. Petkov. "Developing the Recoil Distance Doppler-Shift technique towards a versatile tool for lifetime measurements of excited nuclear states." *Prog. Part. Nucl. Phys.* 67.3 (2012), 786–839.

[12] J.-M. Régis, G. Pascovici, J. Jolie and M. Rudigier. "The mirror symmetric centroid difference method for picosecond lifetime measurements via γ-γ coincidences using very fast $LaBr_3$(Ce) scintillator detectors." *Nucl. Instrum. Methods Phys. Res. A* 622.1 (2010), 83–92.

[13] A. Harter, M. Weinert, L. Knafla, J.-M. Régis, A. Esmaylzadeh, M. Ley and J. Jolie. "Systematic investigation of time walk and time resolution characteristics of CAEN digitizers V1730 and V1751 for application to fast-timing lifetime measurement." *Nucl. Instrum. Methods Phys. Res. A* 1053 (2023), 168356.

[14] S. Jazrawi, A. Yaneva, M. Polettini, B. Das, P. Regan, M. Górska, B. Cederwall, J. Jolie, H. Albers, M. Chishti, A. Banerjee, N. Hubbard, A. Mistry, M. Rudigier, G. Benzoni, J. Gerl, A. Bruce, Z. Podolyák, B. Nara Singh, G. Zhang, S. Alhomaidhi, C. Appleton, T. Arici, A. Blazhev, T. Davinson, A. Esmaylzadeh, L. Fraile, G. Häfner, O. Hall, P. John, V. Karayonchev, I. Koujoharov, N. Kurz, M. Mikolajczuk, N. Pietralla, S. Pietri, J. Regis, E. Sahin, L. Sexton, H. Schaffner, C. Scheidenberger, A. Sharma, J. Vesic, H. Weick, V. Werner, R. Lozeva and M. Si. "Commissioning the FAst TIMing array (FATIMA) at FAIR Phase-0: Half-lives of excited states in the $N = 50$ isotones ^{96}Pd and ^{94}Ru." *Rad. Phys. Chem.* 200 (2022), 110234.

[15] G. Racah. "Theory of Complex Spectra. III." *Phys. Rev.* 63 (1943), 367–382.

[16] G. Racah. "Farkas Memorial Volume." *Research Council of Israel, Jerusalem* (1952).

[17] B. H. Flowers. "Studies in jj-coupling. I. Classification of nuclear and atomic states." *Proc. R. Soc. Lond. A Math. Phys. Sci* 212 (1952), 248–263.

[18] B. Maheshwari and K. Nomura. "Overview of Seniority Isomers." *Symmetry* 14.12 (2022).

[19] J. J. Ressler, R. F. Casten, N. V. Zamfir, C. W. Beausang, R. B. Cakirli, H. Ai, H. Amro, M. A. Caprio, A. A. Hecht, A. Heinz, S. D. Langdown, E. A. McCutchan, D. A. Meyer, C. Plettner, P. H. Regan, M. J. S. Sciacchitano and A. D. Yamamoto. "Transition from the seniority regime to collective motion." *Phys. Rev. C* 69 (2004), 034317.

[20] A. Escuderos and L. Zamick. "Seniority conservation and seniority violation in the $g_{9/2}$ shell." *Phys. Rev. C* 73 (2006), 044302.

[21] N. Zamfir and R. Casten. "Empirical global anharmonic vibrator spectra and the IBA model." *Phys. Lett. B* 341.1 (1994), 1–5.

[22] A. De-Shalit and I. Talmi. "Nuclear Shell Theory." *Academic* (1963).

[23] I. Talmi. Simple Models of Complex Nuclei. 1st. Routledge, 1993.

[24] P. Van Isacker. "Seniority isomers and particle−hole conjugation." *Eur. Phys. J. Spec Top.* 233.5 (2024), 921–932.

[25] J. Park, R. Krücken, D. Lubos, R. Gernhäuser, M. Lewitowicz, S. Nishimura, D. S. Ahn, H. Baba, B. Blank, A. Blazhev, P. Boutachkov, F. Browne, I. Čelikovi ć, G. de France, P. Doornenbal, T. Faestermann, Y. Fang, N. Fukuda, J. Giovinazzo, N. Goel, M. Górska, H. Grawe, S. Ilieva, N. Inabe, T. Isobe, A. Jungclaus, D. Kameda, G. D. Kim, Y.-K. Kim, I. Kojouharov, T. Kubo, N. Kurz, G. Lorusso, K. Moschner, D. Murai, I. Nishizuka, Z.

Patel, M. M. Rajabali, S. Rice, H. Sakurai, H. Schaffner, Y. Shimizu, L. Sinclair, P.-A. Söderström, K. Steiger, T. Sumikama, H. Suzuki, H. Takeda, Z. Wang, H. Watanabe, J. Wu and Z. Y. Xu. "Properties of γ-decaying isomers and isomeric ratios in the ^{100}Sn region." *Phys. Rev. C* 96 (2017), 044311.

[26] G. Racah and I. Talmi. "The pairing property of nuclear interactions." *Physica* 18.12 (1952), 1097–1100.

[27] C. Schwartz and A. de-Shalit. "Many-Particle Configurations in a Central Field." *Phys. Rev.* 94 (1954), 1257–1266.

[28] P. Van Isacker. "Partial conservation of seniority in nuclei." *Int. J. Mod. Phys. E* 20.02 (2011), 191–198.

[29] C. Zener. "Non-adiabatic Crossing of Energy Levels." *Proc. R. Soc. London A* 137.833 (1932), 696–702.

[30] L. D. Landau. "A theory of energy transfer II." *Phys. Z. Sowjetunion* 2.46 (1932), 19.

[31] H. Grawe. "Shell Modelfrom a Practitioner's Point of View." *The Euroschool Lectures on Physics with Exotic Beams, Vol. I.* Ed. by J. Al-Khalili and E. Roeckl. Springer Berlin Heidelberg, 2004, pp. 33–75.

[32] C. Qi. "Partial conservation of seniority and its unexpected influence on E2 transitions in $g_{9/2}$ nuclei." *Phys. Lett. B* 773 (2017), 616–619.

[33] Y. Qian and C. Qi. "Partial seniority conservation and solvability of single-j systems." *Phys. Rev. C* 98 (2018), 061303(R).

[34] P. Van Isacker and S. Heinze. "Partial Conservation of Seniority and Nuclear Isomerism." *Phys. Rev. Lett.* 100 (2008), 052501.

[35] Y. Alhassid and A. Leviatan. "Partial dynamical symmetry." *J. Phys. A: Math. Theor.* 25.23 (1992), L1265.

[36] A. Leviatan. "Partial dynamical symmetries." *Prog. Part. Nucl. Phys.* 66.1 (2011), 93–143.

[37] E. Galindo, M. Hausmann, A. Jungclaus, K. P. Lieb, O. Yordanov, I. P. Johnstone, R. Schwengner, A. Dewald, A. Fitzler, O. Möller, G. de Angelis, A. Gadea, T. Martinez, D. R. Napoli and C. A. Ur. "Transition strengths between particle hole excitations in ^{95}Ru." *Phys. Rev. C* 69 (2004), 024304.

[38] V. Karayonchev, A. Blazhev, A. Esmaylzadeh, J. Jolie, M. Dannhoff, F. Diel, F. Dunkel, C. Fransen, L. M. Gerhard, R.-B. Gerst, L. Knafla, L. Kornwebel, C. Müller-Gatermann, J.-M. Régis, N. Warr, K. O. Zell, M. Stoyanova and P. Van Isacker. "Lifetimes in ^{211}At and their implications for the nuclear structure above ^{208}Pb." *Phys. Rev. C* 99 (2019), 024326.

[39] V. Karayonchev, A. Blazhev, J. Jolie, A. Dewald, A. Esmaylzadeh, C. Fransen, G. Häfner, L. Knafla, C. Müller-Gatermann, G. Rainovski, J.-M. Régis, K. Schomacker and P. Van Isacker. "New aspects of the low-energy structure of ^{211}At." *Phys. Rev. C* 106 (2022), 044321.

[40] A. I. Morales, G. Benzoni, H. Watanabe, G. De Angelis, S. Nishimura, L. Coraggio, A. Gargano, N. Itaco, T. Otsuka, Y. Tsunoda, et al. "Is seniority a partial dynamic symmetry in the first $\nu g_{9/2}$ shell?" *Phys. Lett. B* 781 (2018), 706–712.

[41] R. D. Lawson. Theory of the nuclear shell model. Oxford: Clarendon Press, 1980.

[42] J. Valiente-Dobón, A. Gottardo, G. Benzoni, A. Gadea, S. Lunardi, A. Algora, G. de Angelis, D. Bazzacco, J. Benlliure, P. Boutachkov, A. Bracco, A. Bruce, F. Camera, E. Casarejos, M. Cortés, F. Crespi, A. Corsi, C. Domingo-Pardo, M. Doncel, T. Engert, H. Geissel, J. Gerl, A. Goasduff, N. Goel, M. Górska, J. Grebosz, E. Gregor, T. Habermann, S. Klupp, I. Kojouharov, N. Kurz, S. Lenzi, S. Leoni, S. Mandal, R. Menegazzo, D. Mengoni, B. Million, A. Morales, D. Napoli, F. Naqvi, C. Nociforo, M. Pfützner, S. Pietri, Z. Podolyák, A. Prochazka, F. Recchia, P. Regan, D. Rudolph, E. Sahin, H. Schaffner, A. Sharma, B. Sitar, D. Siwal, P. Strmen, I. Szarka, C. Ur, P. Walker, H. Weick, O. Wieland, H.-J. Wollersheim and P. Van Isacker. "Manifestation of the Berry phase in the atomic nucleus ^{213}Pb." *Phys. Lett. B* 816 (2021), 136183.

[43] M. V. Berry. "Quantal phase factors accompanying adiabatic changes." *Proc. R. Soc. London A* 392.1802 (1984), 45–57.

[44] M. S. Basunia. "Full evaluation for ^{210}Pb." *Nucl. Data Sheets* 121 (2014), 561.

[45] K. Auranen and E. McCutchan. "Nuclear Data Sheets for $A = 212$." *Nucl. Data Sheets* 168 (2020), 117–267.

[46] S. Zhu and E. McCutchan. "Nuclear Data Sheets for $A = 214$." *Nucl. Data Sheets* 175 (2021), 1–149.

[47] S.-C. Wu. "Nuclear Data Sheets for $A = 216$." *Nucl. Data Sheets* 108.5 (2007), 1057–1092.

[48] J. J. Ressler, C. W. Beausang, H. Ai, H. Amro, M. A. Caprio, R. F. Casten, A. A. Hecht, S. D. Langdown, E. A. McCutchan, D. A. Meyer, P. H. Regan, M. J. S. Sciacchitano, A. Yamamoto and N. V. Zamfir. "Isomer decay tagging in the heavy nuclei: ^{210}Ra and ^{209}Ra." *Phys. Rev. C* 69 (2004), 034331.

[49] K. Heyde, J. Jolie, J. Moreau, J. Ryckebusch, M. Waroquier, P. Van Duppen, M. Huyse and J. Wood. "A shell-model description of 0^+ intruder states in even-even nuclei." *Nucl. Phys. A* 466.2 (1987), 189–226.

[50] T. Grahn, J. Pakarinen, L. Jokiniemi, M. Albers, K. Auranen, C. Bauer, C. Bernards, A. Blazhev, P. A. Butler, S. Bönig, A. Damyanova, T. D. Coster, H. D. Witte, J. Elseviers, L. P. Gaffney, M. Huyse, A. Herzáň, U. Jakobsson, R. Julin, N. Kesteloot, J. Konki, T. Kröll, L. Lewandowski, K. Moschner, P. Peura, M. Pfeiffer, D. Radeck, P. Rahkila, E. Rapisarda, P. Reiter, K. Reynders, M. Rudiger, M.-D. Salsac, S. Sambi, M. Scheck, M. Seidlitz, B. Siebeck, T. Steinbach, S. Stolze, J. Suhonen, P. Thoele, M. Thürauf, N. Warr, P. V. Duppen, M. Venhart, M. J. Vermeulen, V. Werner, M. Veselsky, A. Vogt, K. Wrzosek-Lipska and M. Zielińska. "Collective 2_1^+ excitations in ^{206}Po and ^{208,210}Rn." *Eur. Phys. J. A* 52.11 (2016), 340.

[51] M. Stoyanova, G. Rainovski, J. Jolie, N. Pietralla, A. Blazhev, M. Beckers, A. Dewald, M. Djongolov, A. Esmaylzadeh, C. Fransen, L. M. Gerhard, K. A. Gladnishki, S. Herb, P. R. John, V. Karayonchev, J. M. Keatings, R. Kern, L. Knafla, D. Kocheva, L. Kornwebel, T. Kröll, M. Ley, K. M. Mashtakov, C. Müller-Gatermann, J.-M. Régis, M. Scheck, K. Schomacker, J. Sinclair, P. Spagnoletti, C. Sürder, N. Warr, V. Werner and J. Wiederhold. "Lifetimes of the 4_1^+ states of ^{206}Po and ^{204}Po: A study of the transition from noncollective seniority-like mode to collectivity." *Phys. Rev. C* 100 (2019), 064304.

[52] D. Kocheva, G. Rainovski, J. Jolie, N. Pietralla, A. Blazhev, A. Astier, R. Altenkirch, S. Ansari, T. Braunroth, M. Cortés, et al. "A revised $B(E2; 2_1^+ \to 0_1^+)$ value in the semi-magic nucleus ^{210}Pb." *Eur. Phys. J. A* 53.9 (2017), 175.

[53] C. M. Nickel, V. Werner, G. Rainovski, P. R. John, M. Beckers, D. Bittner, A. Blazhev, A. Esmaylzadeh, C. Fransen, J. Garbe, L. Gerhard, K. Geusen, K. Gladnishki, A. Goldkuhle, K. E. Ide, J. Jolie, V. Karayonchev, R. Kern, E. Kleis, L. Klöckner, D. Kocheva, M. Ley, H. Mayr, N. Pietralla, F. von Spee, M. Steffan, T. Stetz and J. Wiederhold. "Revised $B(E2; 2_1^+ \to 0_1^+)$ value in the semi-magic nucleus ^{210}Pb." *arXiv preprint arXiv:2506.11316* (2025).

[54] National Nuclear Data Center (ENSDF and XUNDL). https://www.nndc.bnl.gov/ (2025).

[55] A. Gottardo, J. J. Valiente-Dobón, G. Benzoni, R. Nicolini, A. Gadea, S. Lunardi, P. Boutachkov, A. M. Bruce, M. Górska, J. Grebosz, S. Pietri, Z. Podolyák, M. Pfützner, P. H. Regan, H. Weick, J. Alcántara Núñez, A. Algora, N. Al-Dahan, G. de Angelis, Y. Ayyad, N. Alkhomashi, P. R. P. Allegro, D. Bazzacco, J. Benlliure, M. Bowry, A. Bracco, M. Bunce, F. Camera, E. Casarejos, M. L. Cortes, F. C. L. Crespi, A. Corsi, A. M. Denis Bacelar, A. Y. Deo, C. Domingo-Pardo, M. Doncel, Z. Dombradi, T. Engert, K. Eppinger, G. F. Farrelly, F. Farinon, E. Farnea, H. Geissel, J. Gerl, N. Goel, E. Gregor, T. Habermann, R. Hoischen, R. Janik, S. Klupp, I. Kojouharov, N. Kurz, S. M. Lenzi, S. Leoni, S. Mandal, R. Menegazzo, D. Mengoni, B. Million, A. I. Morales, D. R. Napoli, F. Naqvi, C. Nociforo, A. Prochazka, W. Prokopowicz, F. Recchia, R. V. Ribas, M. W. Reed, D. Rudolph, E. Sahin, H. Schaffner, A. Sharma, B. Sitar, D. Siwal, K. Steiger, P. Strmen, T. P. D. Swan, I. Szarka, C. A. Ur, P. M. Walker, O. Wieland, H.-J. Wollersheim, F. Nowacki, E. Maglione and A. P. Zuker. "New Isomers in the Full Seniority Scheme of Neutron-Rich Lead Isotopes: The Role of Effective Three-Body Forces." *Phys. Rev. Lett.* 109.16 (2012), 162502.

[56] G. Gürdal and E. McCutchan. "Nuclear Data Sheets for $A = 70$." *Nucl. Data Sheets* 136 (2016), 1–162.

[57] B. Singh, J. Chen and A. R. Farhan. "Nuclear Structure and Decay Data for $A = 76$ Isobars." *Nucl. Data Sheets* 194 (2024), 3–459.

[58] M. Sawicka, R. Grzywacz, I. Matea, H. Grawe, M. Pfützner, J. M. Daugas, M. Lewitowicz, D. L. Balabanski, F. Becker, G. Bélier, C. Bingham, C. Borcea, E. Bouchez, A. Buta, M. La Commara, E. Dragulescu, G. de France, G. Georgiev, J. Giovinazzo, M. Górska, F. Hammache, M. Hass, M. Hellström, F. Ibrahim, Z. Janas, H. Mach, P. Mayet, V. Méot, F. Negoita, G. Neyens, F. de Oliveira Santos, R. D. Page, O. Perru, Z. Podolyák, O. Roig, K. P. Rykaczewski, M. G. Saint-Laurent, J. E. Sauvestre, O. Sorlin, M. Stanoiu, I. Stefan, C. Stodel, C. Theisen, D. Verney and J. Żylicz. "Low energy levels in ^{72}Ni." *Phys. Rev. C* 68 (2003), 044304.

[59] C. J. Chiara, W. B. Walters, I. Stefanescu, M. Alcorta, M. P. Carpenter, B. Fornal, G. Gürdal, C. R. Hoffman, R. V. F. Janssens, B. P. Kay, F. G. Kondev, W. Królas, T. Lauritsen, C. J. Lister, E. A. McCutchan, T. Pawłat, A. M. Rogers, D. Seweryniak, N. Sharp, J. Wrzesiński and S. Zhu. "Seniority, collectivity, and $B(E2)$ enhancement in ^{72}Ni." *Phys. Rev. C* 84 (2011), 037304.

[60] H. Grawe, M. Gorska, C. Fahlander, M. Palacz, F. Nowacki, E. Caurier, J. Daugas, M. Lewitowicz, M. Sawicka, R. Grzywacz, et al. "Experimental approach towards shell structure at ^{100}Sn and ^{78}Ni." *Nucl. Phys. A* 704 (2002), 211–222.

[61] M. Sawicka, R. Grzywacz, I. Matea, H. Grawe, M. Pfützner, J. Daugas, M. Lewitowicz, D. Balabanski, F. Becker, G. Bélier, et al. "Low energy levels in ^{72}Ni." *Phys. Rev. C* 68.4 (2003), 044304.

[62] A. Lisetskiy, B. A. Brown, M. Horoi and H. Grawe. "New $T = 1$ effective interactions for the $f_{5/2}\ p_{3/2}\ p_{1/2}\ g_{9/2}$ model space: Implications for valence-mirror symmetry and seniority isomers." *Phys. Rev. C* 70.4 (2004), 044314.

[63] R. Wirowski, J. Yan, P. von Brentano, A. Dewald and A. Gelberg. "Valence mirror nuclei." *J. Phys. G: Nucl. Part.* 14.9 (1988), L195.

[64] H. Grawe, M. Górska, M. Lipoglavšek, J. Nyberg, R. Grzywacz, M. Lewitowicz, K. Rykaczewski, K. Maier and R. Schubart. "High spin spectroscopy of exotic nuclei." *Prog. Part. Nucl. Phys.* 38 (1997), 15–27.

[65] C. M. Baglin. "Nuclear Data Sheets for $A = 92$." *Nucl. Data Sheets* 113.10 (2012), 2187–2389.

[66] D. Abriola and A. Sonzogni. "Nuclear Data Sheets for $A = 94$." *Nucl. Data Sheets* 107.9 (2006), 2423–2578.

[67] D. Abriola and A. Sonzogni. "Nuclear Data Sheets for $A = 96$." *Nucl. Data Sheets* 109.11 (2008), 2501–2655.

[68] S. Basu, G. Mukherjee and A. Sonzogni. "Nuclear Data Sheets for $A = 95$." *Nucl. Data Sheets* 111.10 (2010), 2555–2737.

[69] E. Nolte, G. Korschinek and U. Heim. *Z. Phys. A* 298.3 (1980), 191–205.

[70] A. Jungclaus, D. Kast, K. Lieb, C. Teich, M. Weiszflog, T. Härtlein, C. Ender, F. Köck, D. Schwalm, J. Reif, R. Peusquens, A. Dewald, J. Eberth, H.-G. Thomas, M. Górska and H. Grawe. "Picosecond lifetime measurement of neutron core-excited states in the $N = 50$ nucleus ^{95}Rh." *Nucl. Phys. A* 637.3 (1998), 346–364.

[71] M. W. Kirson. "Oscillator parameters in nuclei." *Nuclear Physics A* 781.3 (2007), 350–362.

[72] J. Blomqvist and A. Molinari. "Collective 0^- vibrations in even spherical nuclei with tensor forces." *Nucl. Phys. A* 106.3 (1968), 545–569.

[73] P. Van Isacker. unpublished.

[74] P. Spagnoletti, G. S. Simpson, R. Carroll, J.-M. Régis, A. Blanc, M. Jentschel, U. Köster, P. Mutti, T. Soldner, G. de France, C. A. Ur, W. Urban, A. M. Bruce, F. Drouet, L. M. Fraile, L. P. Gaffney, D. G. Ghiță, S. Ilieva, J. Jolie, W. Korten, T. Kröll, C. Larijani, S. Lalkovski, R. Lică, H. Mach, N. Mărginean, V. Paziy, Z. Podolyák, P. H. Regan, M. Scheck, N. Saed-Samii, G. Thiamova, C. Townsley, A. Vancraeyenest, V. Vedia, A. Gargano and P. Van Isacker. "Half-life of the $15/2^+$ state of ^{135}I: A test of $E2$ seniority relations." *Phys. Rev. C* 95 (2017), 021302.

[75] H. Mach, R. Gill and M. Moszyński. "A method for picosecond lifetime measurements for neutron-rich nuclei: Outline of the method." *Nucl. Instrum. Methods Phys. Res. A* 280.1 (1989), 49–72.

[76] CAEN S.p.A. User manual UM2792 V1730/VX1730 and V1725/VX1725. 2021.

[77] Z. Bay. "Calculation of Decay Times from Coincidence Experiments." *Phys. Rev.* 77 (1950), 419–419.

[78] J.-M. Régis, H. Mach, G. Simpson, J. Jolie, G. Pascovici, N. Saed-Samii, N. Warr, A. Bruce, J. Degenkolb, L. Fraile, C. Fransen, D. Ghita, S. Kisyov, U. Koester, A. Korgul, S. Lalkovski, N. Mărginean, P. Mutti, B. Olaizola, Z. Podolyak, P. Regan, O. Roberts, M. Rudigier, L. Stroe, W. Urban and D. Wilmsen. "The generalized centroid difference

method for picosecond sensitive determination of lifetimes of nuclear excited states using large fast-timing arrays." *Nucl. Instrum. Methods Phys. Res. A* 726 (2013), 191–202.

[79] J.-M. Régis, M. Dannhoff and J. Jolie. "A simple procedure for γ-γ lifetime measurements using multi-element fast-timing arrays." *Nucl. Instrum. Methods Phys. Res. A* 897 (2018), 38–46.

[80] M. Martin. "Nuclear Data Sheets for $A = 152$." *Nucl. Data Sheets* 114.11 (2013), 1497–1847.

[81] L. Knafla, A. Harter, M. Ley, A. Esmaylzadeh, J.-M. Régis, D. Bittner, A. Blazhev, F. von Spee and J. Jolie. "Improving fast-timing time-walk calibration standards: Lifetime measurement of the 2_1^+ state in ^{152}Gd." *Nucl. Instrum. Methods Phys. Res. A* 1052 (2023), 168279.

[82] J.-M. Régis, A. Esmaylzadeh, J. Jolie, V. Karayonchev, L. Knafla, U. Köster, Y. Kim and E. Strub. "γ-γ fast timing at X-ray energies and investigation on various timing deviations." *Nucl. Instrum. Methods Phys. Res. A* 955 (2020), 163258.

[83] A. Esmaylzadeh, M. Ley, A. Blazhev, C. Fransen, J. Jolie, V. Karayonchev, L. Knafla, C.-D. Lakenbrink, A. Pfeil and F. von Spee. "Investigation of low-lying excited states in ^{214}Po and ^{214}Bi." *Phys. Rev. C* 110 (2024), 034324.

[84] F. Pühlhofer. "On the interpretation of evaporation residue mass distributions in heavy-ion induced fusion reactions." *Nucl. Phys. A* 280.1 (1977), 267–284.

[85] L. Netterdon, V. Derya, J. Endres, C. Fransen, A. Hennig, J. Mayer, C. Müller-Gatermann, A. Sauerwein, P. Scholz, M. Spieker and A. Zilges. "The γ-ray spectrometer HORUS and its applications for nuclear astrophysics." *Nucl. Instrum. Methods Phys. Res. A* 754 (2014), 94–100.

[86] A. Linnemann. "Das HORUS-Würfelspektrometer und Multiphononanregungen in ^{106}Cd." PhD thesis. Universität zu Köln, 2006.

[87] Hamamatsu Photonics K.K. photomultiplier tubes and assemblies. 2025.

[88] A. Harter, L. Knafla, G. Frießner, G. Häfner, J. Jolie, A. Blazhev, A. Dewald, F. Dunkel, A. Esmaylzadeh, C. Fransen, V. Karayonchev, K. Lawless, M. Ley, J.-M. Régis and K. O. Zell. "Lifetime measurements in the tungsten isotopes ^{176,178,180}W." *Phys. Rev. C* 106 (2022), 024326.

[89] J.-M. Régis, N. Saed-Samii, M. Rudigier, S. Ansari, M. Dannhoff, A. Esmaylzadeh, C. Fransen, R.-B. Gerst, J. Jolie, V. Karayonchev, C. Müller-Gatermann and S. Stegemann. "Reduced γ–γ time walk to below 50 ps using the multiplexed-start and multiplexed-stop fast-timing technique with $LaBr_3$(Ce) detectors." *Nucl. Instrum. Methods Phys. Res. A* 823 (2016), 72–82.

[90] J.-M. Régis, M. Dannhoff, J. Jolie, C. Müller-Gatermann and N. Saed-Samii. "On the time response of background obtained in γ-ray spectroscopy experiments using $LaBr_3$(Ce) detectors with different shielding." *Nucl. Instrum. Methods Phys. Res. A* 811 (2016), 42–48.

[91] CAEN S.p.A. User manual UM5960 CoMPASS. 2022.

[92] M. Weinert. "Investigation of Microscopic Structures in the Low-Energy Electric Dipole Response of ^{120}Sn using Consistent Experimental and Theoretical Observables and Digital

Signal Processing for Nuclear Physics Experiments." PhD thesis. Universität zu Köln, 2022.

[93] A. Harter. "Modernisations and digitalizations of fast timing techniques for γ-γ and e-γ timing and lifetime measurements in middle-heavy rare earths nuclei." PhD thesis. Universität zu Köln, 2023.

[94] A. Harter and N. Saed-Samii. ftSOCO - Fast timing Sorting Code. Version 1.0. 29. 2023.

[95] N. Saed-Samii and A. Harter. SOCO-v2 - Sorting Code Cologe. Version 1.0. 29. 2019.

[96] A. Jungclaus, D. Kast, K. P. Lieb, C. Teich, M. Weiszflog, T. Härtlein, C. Ender, F. Köck, D. Schwalm, I. P. Johnstone, J. Reif, R. Schwengner, R. Peusquens, A. Dewald, J. Eberth, H. G. Thomas, M. Górska and H. Grawe. "Lifetime study of particle-hole excitations in the semimagic nucleus ^{94}Ru." *Phys. Rev. C* 60 (1999), 014309.

[97] C. Broude, G. Goldring, M. Hass, N. Takahashi, S. Hofmann, F. Hessberger and V. Ninov. "Parity violation in the $17/2^-$ isomer of ^{93}Tc." *Z. Phys. A* 336 (1990), 133–138.

[98] O. Kavatsyuk et al. "Beta decay of ^{101}Sn." *Eur. Phys. J. A* 31.3 (2007), 319–325.

[99] M. Müller. personal communication. 2025.

[100] L. Kornwebel. "Fast-Timing Analysis of ^{213}Fr." Master's thesis. Universität zu Köln, 2019.

[101] V. Karayonchev, J. Jolie, D. Bittner, M. Beckers, A. Esmaylzadeh, J. Fischer, C. Fransen, J. Garbe, L. Knafla, C.-D. Lakenbrink and M. Ley. "Lifetime measurements in ^{206}Po with a shell-model interpretation." *Phys. Rev. C* 108 (2023), 054302.

[102] C. Fransen, C.-D. Lakenbrink, A. Esmaylzadeh, F. von Spee, M. Ley, J. Jolie and S. Thiel. "CATHEDRAL, a new spectrometer for lifetime measurements of excited states of atomic nuclei both with Doppler shift techniques and fast timing." (unpublished).

[103] C. Mihai, G. Pascovici, G. Ciocan, C. Costache, V. Karayonchev, A. Lungu, N. Mărginean, R. Mihai, C. Neacşu, J.-M. Régis, A. Turturica, S. Ujeniuc and A. Vasiliu. "Development of large area Silicon Photomultipliers arrays for γ-ray spectroscopy applications." *Nucl. Instrum. Methods Phys. Res. A* 953 (2020), 163263.

List of Figures

1 Schematic drawings to explain the concept of seniority 4
2 Partial nuclear chart for even-even nuclei 6
3 Spectra of identical nucleons in a $j = 9/2$ orbital 8
4 The region of the $N = 50$ isotones between ^{90}Zr and the doubly-magic ^{100}Sn . . . 10
5 Schematic drawings to explain the fast-timing method 13
6 Calibrated mean time-walk characteristic 14
7 The HORUS spectrometer in the fast-timing configuration 16

8 Experimental data showing the evolution of $B(E2)$ strengths in the $\pi 1g_{9/2}$ shell . 56

List of publications

Publications in refereed journals

[1] A. Esmaylzadeh, L. M. Gerhard, V. Karayonchev, J.-M. Régis, J. Jolie, M. Bast, A. Blazhev, T. Braunroth, M. Dannhoff, F. Dunkel, C. Fransen, G. Häfner, L. Knafla, M. Ley, C. Müller-Gatermann, K. Schomacker, N. Warr and K.-O. Zell.
Lifetime determination in ^{190,192,194,196}Hg via γ-γ fast-timing spectroscopy.
Phys. Rev. C 98 (2018), 014313.

[2] M. Stoyanova, G. Rainovski, J. Jolie, N. Pietralla, A. Blazhev, M. Beckers, A. Dewald, M. Djongolov, A. Esmaylzadeh, C. Fransen, L. M. Gerhard, K. A. Gladnishki, S. Herb, P. R. John, V. Karayonchev, J. M. Keatings, R. Kern, L. Knafla, D. Kocheva, L. Kornwebel, T. Kröll, M. Ley, K. M. Mashtakov, C. Müller-Gatermann, J.-M. Régis, M. Scheck, K. Schomacker, J. Sinclair, P. Spagnoletti, C. Sürder, N. Warr, V. Werner and J. Wiederhold.
Lifetimes of the 4_1^+ states of ^{206}Po and ^{204}Po: A study of the transition from noncollective seniority-like mode to collectivity.
Phys. Rev. C 100 (2019), 064304.

[3] M. Cholewa, M. Cappellazzo, M. Ley, D. Bittner, J. Jolie, K. Lee, M. Song, G.-C. Yi and P. Boutachkov.
In search of nano-materials with enhanced secondary electron emission for radiation detectors.
Scientific Reports 11.1 (2021), 10517.

[4] A. Esmaylzadeh, V. Karayonchev, K. Nomura, J. Jolie, M. Beckers, A. Blazhev, A. Dewald, C. Fransen, R.-B. Gerst, G. Häfner, A. Harter, L. Knafla, M. Ley, L. M. Robledo, R. Rodríguez-Guzmán and M. Rudigier.
Lifetime measurements to investigate γ softness and shape coexistence in ^{102}Mo.

Phys. Rev. C 104 (2021), 064314.

[5] L. Knafla, A. Esmaylzadeh, A. Harter, J. Jolie, U. Köster, M. Ley, C. Michelagnoli and J.-M. Régis.
Development of a new γ-γ angular correlation analysis method using a symmetric ring of clover detectors.
Nucl. Instrum. Methods Phys. Res. A 1042 (2022), 167463.

[6] A. Harter, L. Knafla, G. Frießner, G. Häfner, J. Jolie, A. Blazhev, A. Dewald, F. Dunkel, A. Esmaylzadeh, C. Fransen, V. Karayonchev, K. Lawless, M. Ley, J.-M. Régis and K. O. Zell.
Lifetime measurements in the tungsten isotopes ^{176,178,180}W.
Phys. Rev. C 106 (2022), 024326.

[7] D. Kumar, T. Bhattacharjee, S. S. Alam, S. Basak, L. Gerhard, L. Knafla, A. Esmaylzadeh, M. Ley, F. Dunkel, K. Schomaker, J. .-. Régis, J. Jolie, Y. H. Kim, U. Köster, G. S. Simpson and L. M. Fraile.
Lifetimes and transition probabilities for low-lying yrast levels in ^{130,132}Te.
Phys. Rev. C 106 (2022), 034306.

[8] A. Esmaylzadeh, A. Blazhev, K. Nomura, J. Jolie, M. Beckers, C. Fransen, R.-B. Gerst, A. Harter, V. Karayonchev, L. Knafla, M. Ley and F. von Spee.
Investigation of γ softness: Lifetime measurements in ^{104,106}Ru.
Phys. Rev. C 106 (2022), 064323.

[9] S. Bottoni, E. R. Gamba, G. De Gregorio, A. Gargano, S. Leoni, B. Fornal, N. Brancadori, G. Ciconali, F. C. L. Crespi, N. Cieplicka-Ory ńczak, Ł. W. Iskra, G. Colombi, Y. H. Kim, U. Köster, C. Michelagnoli, F. Dunkel, A. Esmaylzadeh, L. Gerhard, J. Jolie, L. Knafla, M. Ley, J.-M. Régis, K. Schomaker and M. Sferrazza.
Testing the predictive power of realistic shell model calculations via lifetime measurement of the $11/2^+$ state in ^{131}Sb.
Phys. Rev. C 107 (2023), 014322.

[10] A. Harter, M. Weinert, L. Knafla, J.-M. Régis, A. Esmaylzadeh, M. Ley and J. Jolie.
Systematic investigation of time walk and time resolution characteristics of CAEN digitizers V1730 and V1751 for application to fast-timing lifetime measurement.
Nucl. Instrum. Methods Phys. Res. A 1053 (2023), 168356.

[11] L. Knafla, A. Harter, M. Ley, A. Esmaylzadeh, J.-M. Régis, D. Bittner, A. Blazhev, F. von Spee and J. Jolie.
Improving fast-timing time-walk calibration standards: Lifetime measurement of the 2_1^+ state in ^{152}Gd.
Nucl. Instrum. Methods Phys. Res. A 1052 (2023), 168279.

[12] A. Pfeil, K. Nomura, N. Gavrielov, J.-M. Régis, U. Köster, Y. H. Kim, A. Esmaylzadeh, A. Harter, J. Jolie, L. Knafla, M. Ley and V. Karayonchev.
Lifetime measurements in ^{99}Nb and ^{99}Zr: Investigation of shape coexistence.
Phys. Rev. C 108 (2023), 034310.

[13] K. Stoychev, M. Djongolov, V. Karayonchev, G. Rainovski, M. Ley, J. Jolie, D. Bittner, A. Blazhev, F. Dunkel, A. Esmaylzadeh, C. Fransen, J. Garbe, L. M. Gerhard, R.-B. Gerst, K. Geusen, K. A. Gladnishki, G. Häfner, D. Kalaydjieva, L. Klöckner, L. Knafla, D. Kocheva, L. Kornwebel, C. Müller-Gatermann, E. Nikodem, J.-M. Régis, K. Schomacker and M. Stoyanova.
X-ray-γ fast-timing lifetime measurement of the 6_1^+ state in ^{206}Po.
Phys. Rev. C 108 (2023), 014316.

[14] V. Karayonchev, J. Jolie, D. Bittner, M. Beckers, A. Esmaylzadeh, J. Fischer, C. Fransen, J. Garbe, L. Knafla, C.-D. Lakenbrink and M. Ley.
Lifetime measurements in ^{206}Po with a shell-model interpretation.
Phys. Rev. C 108 (2023), 054302.

[15] E. R. Gamba, S. Bottoni, Ł. W. Iskra, C. Zavaglia, S. Leoni, B. Fornal, N. Cieplicka-Ory ńczak, G. Benzoni, G. Colombi, F. C. L. Crespi, A. Esmaylzadeh, M. Jentschel, J. Jolie, V. Karayonchev, Y. H. Kim, L. Knafla, U. Köster, M. Ley, N. M ărginean, R. M ărginean, C. Michelagnoli, M. Polettini, C. Porzio, J.-. Régis, D. Reygadas and A. Turturica.
Lifetime measurements in ^{96}Rb via fast-timing techniques: Investigating shape coexistence at $A \simeq 100$.
Phys. Rev. C 108 (2023), 064301.

[16] A. Harter, A. Esmaylzadeh, L. Knafla, C. Fransen, F. v. Spee, J. Jolie, M. Ley, V. Karayonchev, J. Fischer and A. Pfeil.

Lifetime measurements in low yrast states and spectroscopic peculiarities in ^{182}Os.
Phys. Rev. C 108 (2023), 024305.

[17] M. Ley, L. Knafla, J. Jolie, A. Esmaylzadeh, A. Harter, A. Blazhev, C. Fransen, A. Pfeil, J.-M. Régis and P. Van Isacker.
Erratum: Lifetime measurements in ^{92}Mo: Investigation of seniority conservation in the $N = 50$ isotones.
Phys. Rev. C 110 (2024), 059901.

[18] L. Knafla, K. Nomura, A. Esmaylzadeh, A. Harter, J. Jolie, V. Karayonchev, Y. H. Kim, U. Köster, M. Ley, C. Michelagnoli, A. Pfeil, J.-M. Régis and F. von Spee.
Investigating the prolate-to-oblate shape phase transition: Lifetime measurements and γ spectroscopy of the low-lying negative parity structure in ^{193}Os.
Phys. Rev. C 109 (2024), 014313.

[19] D. Kumar, A. Pal, S. Basak, T. Bhattacharjee, S. S. Alam, L. Gerhard, L. Knafla, A. Esmaylzadeh, M. Ley, F. Dunkel, K. Schomaker, J.-M. Régis, J. Jolie, Y. H. Kim and U. Köster.
Lifetime measurement for the $15/2_1^-$ and $13/2_1^-$ levels in ^{129}Sn.
Phys. Rev. C 109 (2024), 024304.

[20] M. Ley, J. Jolie, L. Knafla, A. Blazhev, A. Esmaylzadeh, C. Fransen, A. Pfeil, J.-M. Régis and P. Van Isacker.
Lifetime measurement in ^{94}Ru and ^{93}Tc to investigate seniority conservation in the $N = 50$ isotones.
Phys. Rev. C 110 (2024), 034320.

[21] A. Esmaylzadeh, M. Ley, A. Blazhev, C. Fransen, J. Jolie, V. Karayonchev, L. Knafla, C.-D. Lakenbrink, A. Pfeil and F. von Spee.
Investigation of low-lying excited states in ^{214}Po and ^{214}Bi.
Phys. Rev. C 110 (2024), 034324.

[22] F. Wu, C. Andreoiu, V. Karayonchev, C. M. Petrache, J.-M. Régis, A. Esmaylzadeh, C. Michelagnoli, M. Beuschlein, P. Spagnoletti, G. Colombi, J. M. Daugas, L. Domenichetti, P. E. Garrett, J. Jolie, M. Ley, S. Pannu and E. Taddei.
Evidence for shape coexistence in ^{120}Sn from the first 0_3^+ lifetime measurement.

Phys. Rev. C 111 (2025), L051307.

Publications in conference proceedings

[24] J.-M. Régis, A. Pfeil, J. Jolie, A. Esmaylzadeh, L. Knafla, M. Ley, A. Harter, V. Karayonchev, U. Köster, Y. H. Kim, N. Gavrielov and K. Nomura.
Shape transition and shape coexistence in odd-mass nuclei around ^{100}Zr.
Eur. Phys. J. Web Conf. 329 (2025), 01007.

[25] J. Jolie, V. Karayonchev, M. Ley, A. Blazhev, A. Esmaylzadeh, L. Knafla, A. Harter, J.-. Régis, D. Kocheva, G. Rainovski and P. Van Isacker.
Absolute electromagnetic transition rates in semi-magic $N = 50$ and 126 isotones as a test for $(\pi 9/2)^n$ single particle calculations.
Eur. Phys. J. Web Conf. 329 (2025), 01013.

Contribution to publications essential for this thesis

Publication I:
Lifetime measurements in ^{92}Mo: Investigation of seniority conservation in the $N = 50$ isotones

- M. Ley, L. Knafla, A. Esmaylzadeh, J. Jolie planned the experiment
- M. Ley, L. Knafla, A. Esmaylzadeh, C. Fransen, A. Harter, A. Pfeil installing the detector setup at the HORUS spectrometer
- A. Blazhev preparation of the targets
- M. Ley, L. Knafla, A. Esmaylzadeh, A. Harter, A. Pfeil carried out the experiment
- M. Ley performed the data analysis of the experiment
- P. Van Isacker performed the theoretical calculations
- J. Jolie, P. Van Isacker, providing guidance and reviewing drafts
- M. Ley, P. Van Isacker wrote the paper

Publication II:
Lifetime measurement in ^{94}Ru and ^{93}Tc to investigate seniority conservation in the $N = 50$ isotones

- M. Ley, L. Knafla, A. Esmaylzadeh, J. Jolie planned the experiment
- M. Ley, L. Knafla, A. Esmaylzadeh, C. Fransen, A. Pfeil installing the detector setup at the HORUS spectrometer
- A. Blazhev preparation of the targets
- M. Ley, L. Knafla, A. Esmaylzadeh, A. Pfeil carried out the experiment
- M. Ley performed the data analysis of the experiment
- A. Blazhev performed the shell-model calculations
- M. Ley performed the mixing calculation
- J. Jolie, P. Van Isacker, A. Blazhev providing guidance and reviewing drafts
- M. Ley wrote the paper

Manuscript I:
Lifetime measurement in ^{95}Rh and ^{95}Ru: Investigation of seniority conservation in the $N = 50$ isotones

- M. Ley, A. Esmaylzadeh, J. Jolie planned the experiment
- M. Ley, A. Esmaylzadeh, C. Fransen, A. Pfeil installing the detector setup at the HORUS spectrometer
- A. Blazhev preparation of the targets

- M. Ley, A. Esmaylzadeh, A. Pfeil, J Fischer, D. Al Daas, R. Burggraf, A. Bohn, S. Dantanarayana, M. Droste, F. Dunkel, A. Karaka, C.-D. Lakenbrink, F. von Spee carried out the experiment
- M. Ley performed the data analysis of the experiment
- J. Jolie, P. Van Isacker, A. Blazhev providing guidance and reviewing drafts
- M. Ley wrote the paper